EXPERIMENTAL AND NUMERICAL INVESTIGATION OF FLOW UNDER RADIAL GATES

A THESIS SUBMITTED TO
THE GRADUATE SCHOOL OF NATURAL AND APPLIED SCIENCES
OF
MIDDLE EAST TECHNICAL UNIVERSITY

BY

MAHMUT TANYERİ

IN PARTIAL FULFILLMENT OF THE REQUIREMENTS
FOR
THE DEGREE OF MASTER OF SCIENCE
IN
CIVIL ENGINEERING

AUGUST 2021

Approval of the thesis:

EXPERIMENTAL AND NUMERICAL INVESTIGATION OF FLOW UNDER RADIAL GATES

submitted by **MAHMUT TANYERİ** in partial fulfillment of the requirements for the degree of **Master of Science** in **Civil Engineering, Middle East Technical University** by,

Prof. Dr. Halil Kalıpçılar
Dean, Graduate School of **Natural and Applied Sciences** _________________

Prof. Dr. Ahmet Türer
Head of the Department, **Civil Engineering** _________________

Prof. Dr. Mete Köken
Supervisor, **Civil Engineering, METU** _________________

Prof. Dr. İsmail Aydın
Co-Supervisor, **Civil Engineering, METU** _________________

Examining Committee Members:

Assoc. Prof. Dr. Kerem Taştan
Civil Engineering, Gazi University _________________

Prof. Dr. Mete Köken
Civil Engineering, METU _________________

Prof. Dr. İsmail Aydın
Civil Engineering, METU _________________

Assoc. Prof. Dr. Melih Çalamak
Civil Engineering, METU _________________

Asst. Prof. Dr. Cüneyt Baykal
Civil Engineering, METU _________________

Date: 10.08.2021

I hereby declare that all information in this document has been obtained and presented in accordance with academic rules and ethical conduct. I also declare that, as required by these rules and conduct, I have fully cited and referenced all material and results that are not original to this work.

Name Last name : Mahmut Tanyeri

Signature :

ABSTRACT

EXPERIMENTAL AND NUMERICAL INVESTIGATION OF FLOW UNDER RADIAL GATES

Tanyeri, Mahmut
Master of Science, Civil Engineering
Supervisor: Prof. Dr. Mete Köken
Co-Supervisor: Prof. Dr. İsmail Aydın

August 2021, 87 pages

Radial gates are commonly used in spillways. At partial gate openings empirical equations, which were obtained from experimental work conducted in 60's, are used to calculate the discharge passing through. However, there are some discrepancies between the discharge values obtained from these equations and the ones from numerical calculations based on finite volume method and hydraulic models. It is aimed to put forward the source of these differences. For this purpose, experiments and numerical calculations were conducted for different gate configurations. By making use of the trends emerging from numerous numerical simulations, a novel discharge equation was derived at the end of the study. The proposed equation, which has one hydraulic and two geometric parameters, will allow designers to calculate the discharge easily without need of any tedious rating curves.

Keywords: Radial Gate, Spillway, Empirical Equations, Discharge Coefficient, Discharge Rating Curve

ÖZ

RADYAL KAPAKLARDAKİ AKIMIN SAYISAL VE DENEYSEL OLARAK İNCELENMESİ

Tanyeri, Mahmut
Yüksek Lisans, İnşaat Mühendisliği
Tez Yöneticisi: Prof. Dr. Mete Köken
Ortak Tez Yöneticisi: Prof. Dr. İsmail Aydın

Ağustos 2021, 87 sayfa

Radyal kapaklar dolusavaklarda sıklıkla kullanılmaktadır. Kısmi kapak açıklıklarında kapaktan geçen debi 60'lı yıllarda yapılan deneylerden elde edilen ampirik formüllerle hesaplanmaktadır. Lakin bu formüllerden elde edilen debi değerleri ile sonlu hacim yöntemine dayalı sayısal hesaplamalar ve hidrolik modellerden elde edilen değerler arasında farklılıklar olabilmektedir. Bu çalışmanın amacı bu farklılıkların kaynağının tespit edilmesidir. Bu amaç için farklı kapak konfigürasyonlarında deneysel ve sayısal çözümlemeler yapılmıştır. Çok sayıda sayısal simülasyondan ortaya çıkan eğilimlerden yararlanılarak çalışmanın sonunda yeni bir debi denklemi türetilmiştir. Bir hidrolik ve iki geometrik değişkenden oluşan önerilen denklem, tasarımcıların herhangi bir uğraştırıcı anahtar eğrisine ihtiyaç duymadan debiyi kolayca hesaplamalarını sağlayacaktır.

Anahtar Kelimeler: Radyal Kapak, Dolusavak, Ampirik Denklemler, Debi Katsayısı, Debi Anahtar Eğrisi

To my family

ACKNOWLEDGMENTS

I profoundly thank my supervisor Prof Dr. Mete Köken for suggesting me working on this attractive topic. This work has never been possible without guidance and technical support provided by him.

I am grateful to my co-supervisor Prof Dr. İsmail Aydın for improving my engineering perspective with his years of experience. His directions made me realize the details and research more.

I also specially thank Research Assistant Emre Haspolat for patiently helping me have done my experiments and for providing me documents necessary for conduction of this work.

TABLE OF CONTENTS

ABSTRACT v
ÖZ vi
ACKNOWLEDGMENTS viii
TABLE OF CONTENTS ix
LIST OF TABLES xii
LIST OF FIGURES xiv
LIST OF ABBREVIATIONS xvi
LIST OF SYMBOLS xvii
CHAPTERS
1 INTRODUCTION 1
1.1 Overview of Radial Gates 1
1.2 Definition of the Problem 2
1.3 Research Aims & Methodology 3
2 LITERATURE REVIEW 5
3 EXPERIMENTAL INVESTIGATION 13
3.1 Experimental Setup 13
3.1.1 Description of the Hydraulic Model 13
3.1.2 Measurement Devices 16
3.2 Data Collection 19
3.2.1 Procedure of the Experiments 19
3.2.2 Model-Based Errors 21
4 NUMERICAL INVESTIGATION 23

4.1 Simulation Software 23
4.2 Three-Dimensional Analysis 24
4.2.1 Description of the Numerical Model 24
4.2.2 Physics 25
4.2.3 Mesh Detail 26
4.2.4 Boundary and Initial Conditions 27
4.2.5 Duration of Simulations 30
4.2.6 Effect of Reservoir Configuration 31
4.3 Two-Dimensional Analysis 33
4.3.1 General Information on the 2D Models 33
4.3.2 Effect of Gate Position 34
4.3.3 Effect of Spillway Geometry 39
4.3.4 Grid Dependency 41
4.3.5 Model-Scale Effect 43
5 ANALYSIS OF RESULTS 49
5.1 Outline of the Numerical Data 49
5.2 Comparison of the Numerical and the Experimental Data 53
5.3 Derivation of New Discharge Equation 56
5.4 Error Percentages of the Suggested Equation 65
5.5 Geometric Derivation of Vertical Gate Opening 67
5.6 Comparison of Empirical Equations with the Novel Equation 69
6 CONCLUSIONS 75
REFERENCES 77
APPENDICES

A. Error Percentages of the Suggested Equation 79
B. Mesh Sensitivity Tables 80
C. Model-Scale Effect with Different Turbulence Models........................... 81
D. Relative Position of the Gate in Different Configurations....................... 84
E. Numerical Results for the Other Gate Positions 85

LIST OF TABLES

TABLES

Table 3.1 Some Salient Dimensions Related to the Setup 15
Table 3.2 Experiment Results at 5cm Gate Opening 20
Table 3.3 Experiment Results at 14cm Gate Opening 21
Table 4.1 Origin of Curvatures and Transition Point Locations (USACE, 1977) .. 40
Table 4.2 Station Coordinates of the Upstream Quadrant of the Alternative Design 40
Table 4.3 Model Discharges and Reynolds Numbers (d=12 cm) 46
Table 4.4 Prototype Discharges and Reynolds Numbers (d=360 cm) 46
Table 4.5 Model Discharges and Reynolds Numbers (d=5 cm) 47
Table 4.6 Prototype Discharges and Reynolds Numbers (d=150 cm) 47
Table 5.1 Discharge data of the 2D Numerical Solutions 50
Table 5.2 Discharge data of the 3D Numerical Solutions 51
Table 5.3 Radial Gate Factors for Different Gate Positions 58
Table 5.4 $(d/H_c)^{0.5}$ Values 59
Table 5.5 Recalculated Gate Factors for T1 Scenario 61
Table 5.6 Ratio of Gate Factors of T2&T3&T4 to Recalculated Gate Factors of T1 61
Table 5.7 X_s/H_c vs Average Ratio 63
Table 5.8 Average Errors at Different Gate Configurations 65
Table 5.9 Comparison of the Simulation Results of USACE Design with the Suggested Equation 66
Table 5.10 Constrains of the Suggested Equation 69
Table 5.11 Comparison Table for USBR (1960) 71
Table 5.12 Comparison Table for USACE (1977) 72
Table B.1 Discharge Variation Depending on Mesh Refinement (d=5 cm) 80
Table B.2 Discharge Variation Depending on Mesh Refinement (d=10 cm) 80
Table C.1 Model Discharges and Reynolds Numbers with LES (L_r=1/30) 81

Table C.2 Prototype Discharges and Reynolds Numbers with LES 81
Table C.3 Model Discharges and Reynolds Numbers with Laminar (L_r=1/30) 82
Table C.4 Prototype Discharges and Reynolds Numbers with Laminar 82
Table C.5 Model Discharges and Reynolds Numbers with RNG (L_r=1/100) 83
Table C.6 Protoype Discharges and Reynolds Numbers with RNG....................... 83

LIST OF FIGURES

FIGURES

Figure 1.1 Radial Gate of John H. Kerr Dam (Source: Wikipedia) 1
Figure 1.2 Descriptive Sketch of Radial-Gated Spillway 2
Figure 2.1 Discharge Coefficient Rating Curve Proposed by USBR (1960) 6
Figure 2.2 Design Chart to Estimate Discharge Coefficient by USACE (1977) (Adapted by USBR, 1987) 7
Figure 2.3 Linear Correlation for Obtaining Transition Head (Schohl, 2016).......... 9
Figure 2.4 Descriptive Sketch Demonstrating Tailwater Effect (Schohl, 2016)..... 10
Figure 2.5 Comparison of Discharge Coefficients by the Physical Models and USACE (1977) (Haktanır and Khalaf, 2020) 12
Figure 3.1 Spillway Plan of Lower Kaleköy Dam 13
Figure 3.2 Ogee-Shaped Crest Profile (USBR, 1987)... 14
Figure 3.3 General View of the Experimental Setup 17
Figure 3.4 Upstream View of the Radial Gated-Spillway....................................... 18
Figure 3.5 Side View of the Radial Gate During Operation 18
Figure 4.1 Components of the 3D Model (Radial-gated spillway, Piers, Reservoir) 25
Figure 4.2 Mesh Detail of the 3D Models 27
Figure 4.3 Initial and Boundary Conditions 29
Figure 4.4 A Sample of Simulation Durations and Volume Change in the Domain 30
Figure 4.5 Representation of Streamlines at t=0.90s.. 32
Figure 4.6 Representation of Streamlines at t=2.70s.. 32
Figure 4.7 Mesh Details of the 2D Numerical Model 34
Figure 4.8 Illustrative Sketch of Gate Positions and Dimensions 35
Figure 4.9 Discharge Variation Depending on Gate Position at d=14 cm 36
Figure 4.10 Discharge Variation Depending on Gate Position at d=9 cm 37
Figure 4.11 Discharge Variation Depending on Gate Position at d=4 cm 37

Figure 4.12 Velocity Magnitude Contours of T1, T2, T3 and T4 at the Design Head (d=10cm) ... 38
Figure 4.13 Upstream Crest Profile (USACE, 1977) ... 39
Figure 4.14 Crest Profiles According to USBR and USACE Design Criteria ... 40
Figure 4.15 Mesh Sensitivity Analysis at d=5 cm (T1 Case) ... 42
Figure 4.16 Mesh Sensitivity Analysis at d=10 cm (T1 Case) ... 42
Figure 4.17 Comparison of Model and Prototype Discharges (d=12 cm & T1 Case) ... 45
Figure 4.18 Comparison of Model and Prototype Discharges (d=5 cm & T1 Case) ... 45
Figure 5.1 2D Numerical Results for Original Gate Position (T3) ... 52
Figure 5.2 Comparison of the 2D and the 3D Numerical Results at d=7 cm ... 53
Figure 5.3 Comparison of the 2D and the 3D Numerical Results at d=10 cm ... 54
Figure 5.4 Comparison of the Numerical and the Experimental Results at d=5 cm 54
Figure 5.5 Comparison of the Numerical and the Experimental Results at d=14 cm ... 55
Figure 5.6 Descriptive Sketch ... 57
Figure 5.7 Gate Factors of T1 Configuration ... 59
Figure 5.8 Water Head vs Average Ratio Graph ... 62
Figure 5.9 X_s/H_c vs Average Ratio Graph ... 64
Figure 5.10 Comparison of USBR and the Suggested Equation ... 73
Figure 5.11 Comparison of USACE and the Suggested Equation ... 73
Figure C.1 Comparison of Model and Prototype Discharges with LES (L_r=1/30) 81
Figure C.2 Comparison of Model and Prototype Discharges with Laminar (L_r=1/30) ... 82
Figure C.3 Comparison of Model and Prototype Discharges with RNG (L_r=1/100) ... 83

LIST OF ABBREVIATIONS

METU	Middle East Technical University
USBR	United States Bureau of Reclamation
USACE	United States Army Corps of Engineers
DSI	State Hydraulic Works
CFD	Computational Fluid Dynamics
RNG	Renormalized Group
LES	Large Eddy Simulation
CAD	Computer-Aided Design
MAE	Mean Absolute Error
DSD	Design of Small Dams

LIST OF SYMBOLS

Q	Discharge (m^3/s)
Q_{cfd}	Numerically found discharge (m^3/s)
Q_{calc}	Discharge found by equation (m^3/s)
q	Unit discharge ($m^3/s/m$)
H	Effective head (m)
H_c	Head over crest (m)
H_d	Design head (m)
X_s	Horizontal distance between gate seat and crest (m)
D	Net gate opening (m)
d	Vertical gate opening (m)
R	Gate radius (m)
R_i	Radius of curvature (m)
C	Discharge coefficient
α	Gate angle (degree)
β	Gate lip angle (degree)
C_g	Gate factor
C_t	Correction due to gate position
R_e	Reynolds number
F_r	Froude number
L	Crest width (m)
L_{eff}	Effective crest length (m)
Z_{res}	Reservoir surface elevation (m)
Z_{cr}	Crest elevation (m)
Z_s	Gate seat elevation (m)

h_m Vertical distance between center of net gate opening and gate seat (m)

h' Elevation of center of net gate opening (m)

g Gravitational acceleration (m/s^2)

X_t Horizontal distance between crest and trunnion (m)

Y_t Vertical distance between crest and trunnion (m)

K A constant for determination of downstream quadrant

n A constant for determination of downstream quadrant

V Velocity (m/s)

D_h Hydraulic depth (m)

ν Kinematic viscosity (m^2/s)

N Number of bays

N_p Number of piers

K_a Contraction coefficient due to abutment

K_p Contraction coefficient due to pier

L_r Length scale ratio

A_r Area scale ratio

V_r Velocity scale ratio

CHAPTER 1

INTRODUCTION

1.1 Overview of Radial Gates

Radial gate (or tainter gate) is one of the extensively used overflow gate types to control flood release especially at high head dams. It consists of a steel curved leaf, supporting arms and pinned joints mounted on sidewalls of chute channel. The gate can be easily rotated around its pivot point at a desired angle to meet water need at the downstream or to regulate the upstream head.

Figure 1.1 Radial Gate of John H. Kerr Dam (Source: Wikipedia)

Radial gates have many advantages over other types. Their most remarkable property is requirement of less hoist power to move the gate. This is thanks to its arched shape which enables upstream water to exert lifting force to the gate, and thus it reduces energy consumption as well. Moreover, radial gates do not need slots, which sometimes cause operational problems since floating debris might be able to stack within them over time. Although there are several areas of their utilization, scope of this study is restricted to radial gates only accompanying to ogee-shaped spillways.

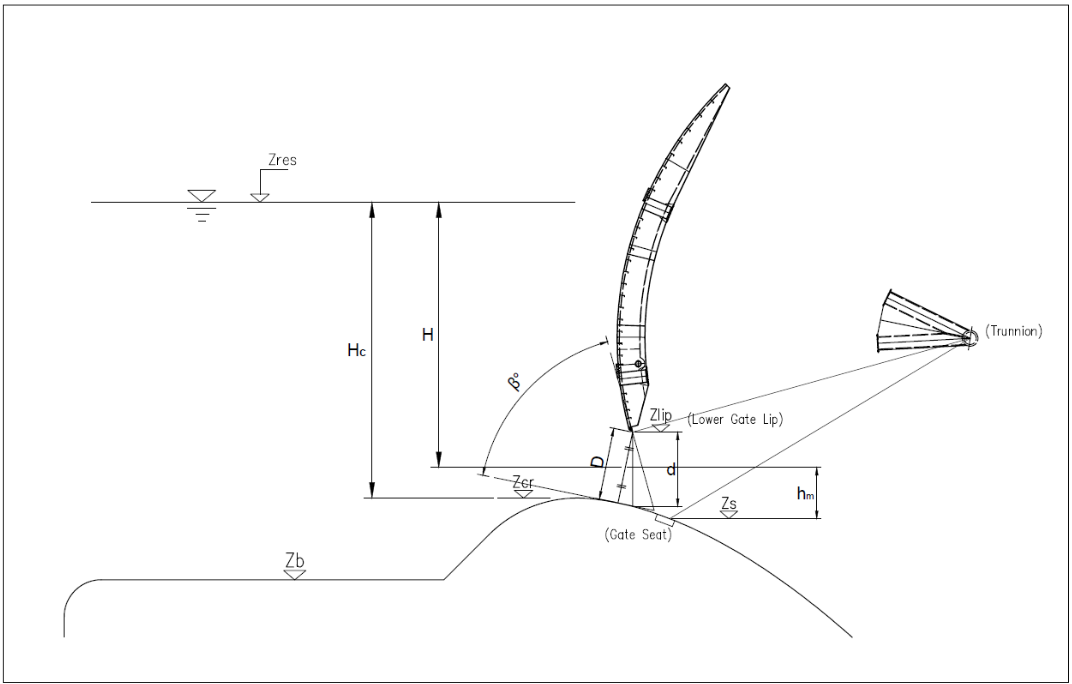

Figure 1.2 Descriptive Sketch of Radial-Gated Spillway

1.2 Definition of the Problem

When partially opened, flow passing under radial gate is influenced by various hydraulic and geometric factors. Therefore, precise estimation of discharge is a challenging issue. This problem is mainly caused by complexity of streamline behavior at the vicinity of the gate. Since the flow region contain highly curved streamlines, analytical solution on the rate of flow is not possible. For this reason, discharge had mostly been investigated on experimental models, where empirical relations were derived accordingly.

The discharge equations are developed on the basis of Bernoulli Equation, which is related to conversion of total energy on a streamline. Average velocity just under the gate can be deduced from the energy equation, and when it is multiplied with the net area of the gate opening, theoretical value of volume flow rate is obtained. However, in reality, cross-sectional area of issuing water jet contracts because streamlines are not perfectly able to follow sharp corners like bottom gate lip, and also friction result in slight decrease of theoretical velocity. On account of these effects an empirical correction factor, called discharge coefficient, is introduced to the equations to estimate the actual discharge (Tokyay, 2019).

As a case study, hydraulic calculations of the radial-gated spillway belonging to Lower Kaleköy Dam done by TEMELSU (2018), a private engineering company in Turkey, was examined. They did these calculations using the discharge coefficient rating curves provided in *'Design of Small Dams'*, a worldwide popular hydraulic design book. The discharge value computed based on these curves were compared with the results of a numerical model created on computational fluid dynamics (CFD) program. It was observed that there is explicit inconsistency between these results in case the gate is partly opened. In general, the proposed empirical equations underestimate the flow rate up to 20% in comparison of the simulations.

1.3 Research Aims & Methodology

There are mainly two aims of this study. The first aim is to investigate the reasons of disagreement between the mentioned empirical formulas and the numerical solutions, and the second one is to delve into which hydraulic and geometric parameters actually influences discharge under radial gates.

To begin with, the discharge value at predetermined gate openings were measured on the physical model of Lower Kaleköy Dam constructed in METU Hydraulics Laboratory. Data sets obtained from these experiments were then checked against the result of the numerical model to see whether they agree or not. After numerical results were verified in this way, different configurations such as gate position, spillway geometry of the numerical model were simulated provided that the original hydraulic conditions remain same. The analyzes were conducted at the model scale throughout the study. As a result of findings related to the mentioned effects, a novel discharge equation was formulated based on the numerical solutions. At the end, results obtained from old empirical formulas and the new formula were compared with the numerical solutions to observe their accuracy.

CHAPTER 2

LITERATURE REVIEW

There has been limited number of investigations regarding discharge capacity of radial gates used over ogee-shaped spillways. Researchers generally carried out experiments to measure volume flow rates and tried to correlate them with non-dimensional parameters related to weir geometry together with gate position. Since the dominant parameters were only peculiar to the experimental setups studied, various discharge equations and graphical solutions took their own place in the literature. However, reliability of these approaches to estimate discharge had significantly remained uncertain until the recent years.

The first noteworthy study took part in the first edition of *Design of Small Dams*, which was published by United States Bureau of Reclamation (USBR) in 1960. The authors associated characteristic of discharge under curved gates with orifice flow, and they presented an orifice flow equation with changeable discharge coefficient for the application of radial gates. According to USBR (1960), coefficient of discharge depends highly on upstream and downstream conditions since they have impact on contraction ratio of water jet and back pressure, respectively. Therefore, it was expressed with ratio of two independent parameters which are total head over the crest and vertical gate opening between the weir crest and the gate lip (See Figure 2.1, $d=H_1-H_2$). The formula on the figure is valid in configurations where gate seat, the point where the gate lip touches when fully closed, is located on weir crest: This approach does not take different gate positions into account. Also, effective crest length, L_{eff}, was used in the equation. It is often shorter than the net length since side contractions due to piers and abutments are taken into consideration. Calculation procedure of effective length is provided in the third edition of *Design of Small Dams (p.365)*.

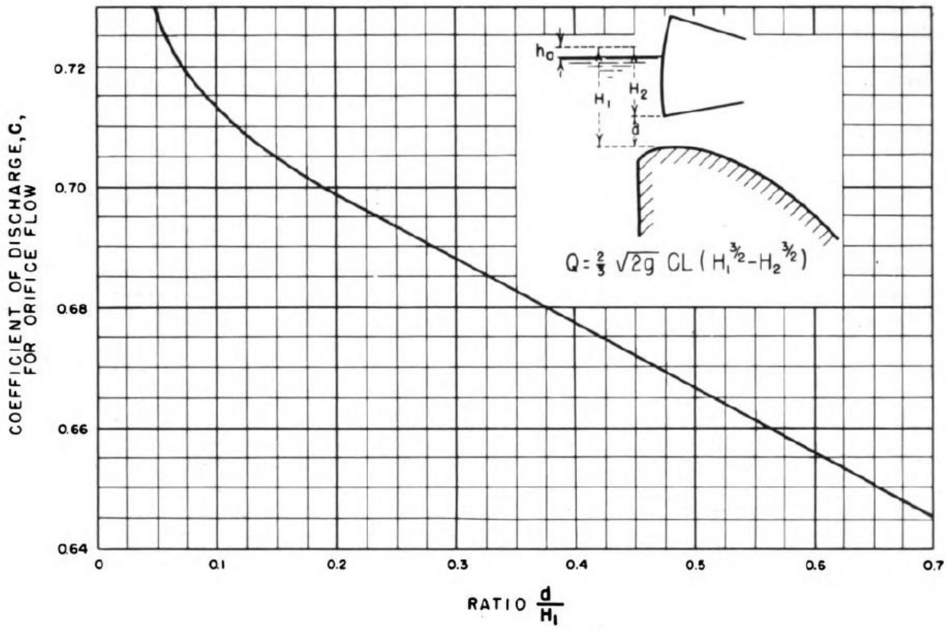

Figure 2.1 Discharge Coefficient Rating Curve Proposed by USBR (1960)

The subsequent approach for calculation of discharge value under radial gates was offered with a hydraulic design chart by United States Army Corps of Engineers (USACE) in 1977. They made discharge measurements on three actual dams located in United States and two models constructed in their laboratory. These prototypes and models had different gate seat positions so that its effect on rate of flow was able to be observed. As a result of the limited data collected, they formed calibration curves and developed a new equation. Its main difference from USBR (1960) is that the discharge coefficient was only linked to single parameter: lip angle, Θ, which is the angle between tangent line to the gate lip and tangent line to the point on crest surface at the smallest distance from the gate lip, as depicted in Figure 2.2. However, there are two different curves based on gate seat location with respect to spillway crest. Also, the discharge equation was slightly changed. Instead of using effective crest length, net crest length was preferred, and single energy head including approach velocity head was used in the formula. In this method, it requires a considerable effort to compute the lip angle and the net gate opening analytically; therefore, USACE provides set of additional design charts, named Charts 311-2,3,4 to find value of these variables. One disadvantage of this method is that these charts are applicable only if the crest geometry is designed according to the USACE standards.

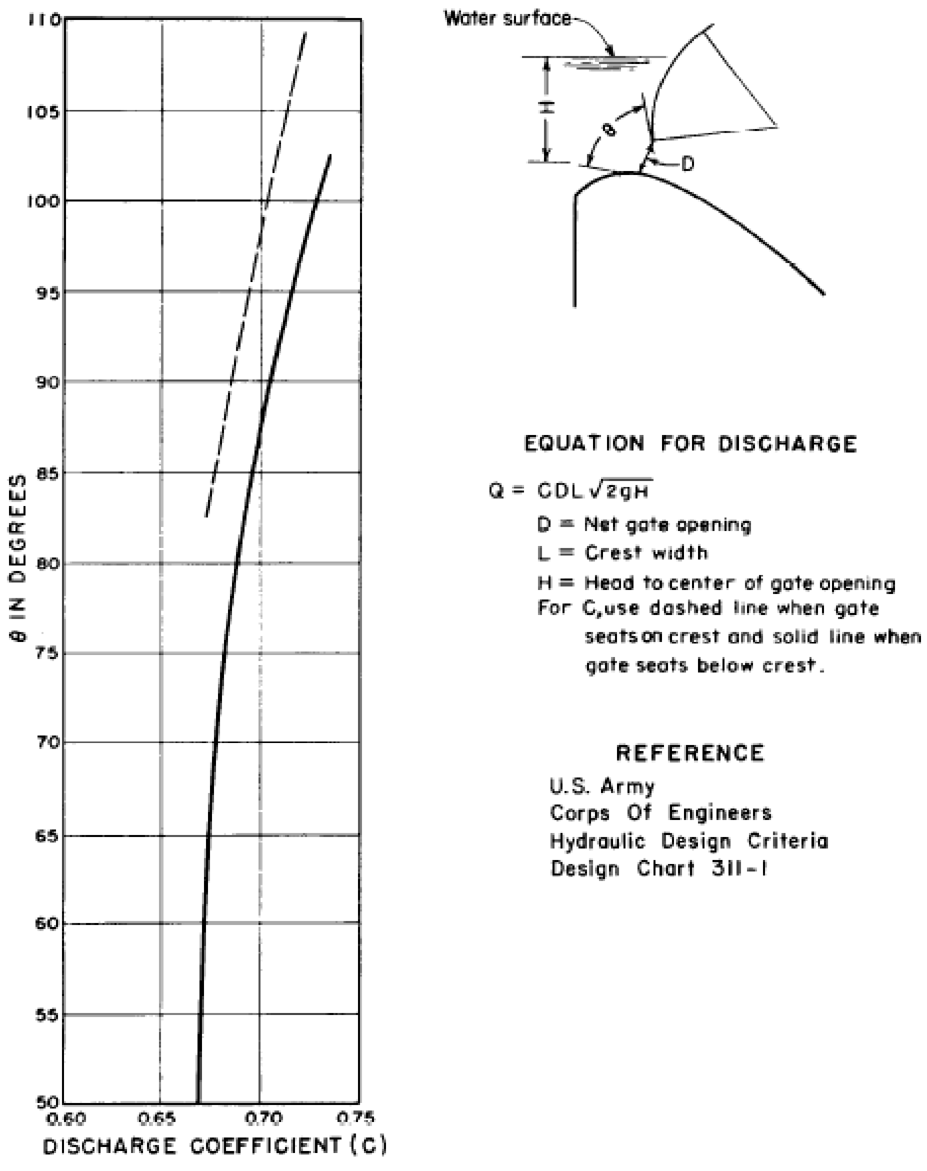

Figure 2.2 Design Chart to Estimate Discharge Coefficient by USACE (1977) (Adapted by USBR, 1987)

Sinniger and Hager (1989) defined discharge coefficient by combining two dimensionless parameters: ratio of effective head to design head and gate lip angle.

They were first to express discharge coefficient by a mathematical equation instead of graphical solution as following:

$$C_d = 0.908\left(1 - \frac{\beta}{277^{\circ}}\right)\left(\frac{H}{H_d}\right)^{0.12} \tag{2.1}$$

in which β is exactly same with Θ in degrees, and H_d is the design head. Even if the notation used by Sinniger and Hager (1989) is different, rest of the discharge equation on Figure 2.2 is the same and valid in their approach. It is commonly accepted that Equation 2.1 considerably improves the accuracy compared to the previous techniques.

Mazumdar and Roy (1997) tested reliability of formulae given by USBR (1960) and Sinniger and Hager (1989). For this, physical model of Salal Dam at 1/55 scale was constructed. Then, discharge data obtained from the model were compared with theoretical values of the equations. It was seen that there is a trend of increase in the error when head above the crest decreases, or gate opening gets smaller. To reduce the percentage error, a correction factor was developed for both equations as function of water head, H, and net gate opening, G:

$$C_p = \left(\frac{H}{H_d}\right)^{a}\left(\frac{G}{H_d}\right)^{b} \tag{2.2}$$

where a and b are some constants obtained by the least square fitting method. The values are different for the two methods and provided in the referred article. Moreover, Mazumdar and Roy (1997) stated that if the gate seat is shifted a bit downstream side of the weir, discharge capacity increases for the same water head and opening. It is more economical and reliable in terms of cavitation risk to design the gate slightly on the downstream side of the crest. For such configurations, discharge equation of USBR (1960) is not suitable, but that of Sinniger and Hager (1989) is applicable.

Until several years ago, studies related to radial gates had only been dealing with the case where water elevation at the upstream is sufficient enough to maintain an orifice type of flow. However, there are three types of flows needed to be considered. These are gated flow or orifice flow, free flow or non-orifice flow and transitional flow occurring in the midst of them. Gated discharge occurs when upstream head is high enough to submerge the gate while free discharge takes place in case upstream head falls to a stage which leads upper nappe of flow not able to contact the gate lip any longer.

Schohl (2016), in detail, investigated transition head where free flow starts to turn into orifice flow for the radial gates. For this purpose, model data pertaining to several dams constructed on rivers of Tennessee in U.S. were analyzed, and it was observed that there is a coherent relationship, close to linear, between two non-dimensional parameters.

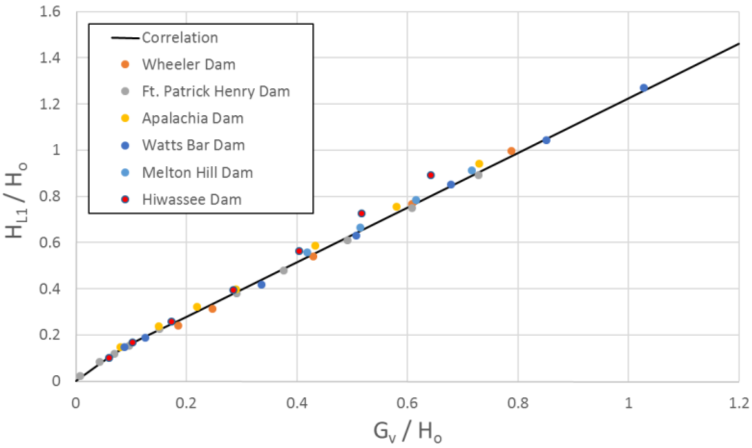

Figure 2.3 Linear Correlation for Obtaining Transition Head (Schohl, 2016)

In Figure 2.3, H_{L1} is transition head, H_o is design head over the crest, and G_v is vertical distance between the gate lip and the gate seat. This relationship was obtained when water level was kept rising from the elevation leading to free flow until the discharging jet first touches the gate lip. However, in practice, rising and falling water levels may not coincide with each other at a certain transition head due to the stability issues discussed by Mazumdar and Roy (1997). On the other hand, Hussain et al. (2014) remarked that the ratio of the water head on the crest to the net gate opening must be at least 1.5-1.7 in order to maintain the orifice flow.

Low head dams or weirs may be subjected to high tailwater levels during operation. In the literature, even though some sources offer tailwater effect on free flow, its effect on gated flow is not common. Schohl (2016) also did research on submergence effect on weirs with radial gates. By observing Tellico and Nickajack spillways with various tailwater and upstream heads, amount of decrease in discharge due to submergence was measured. Consequently, a correction factor was introduced to the equation suggested by USACE (1977). Actually, two separate equations were proposed according to level of submergence. In Figure 2.4, *S* represents the difference between height of tailwater and crest elevation based on any arbitrarily chosen datum. The equation used is changing depending on whether this value is greater or less than a specific transition value, which is determined from some conditional equations provided in the references.

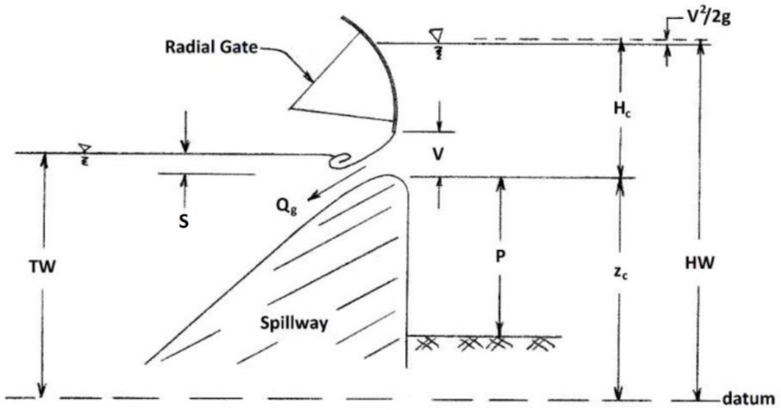

Figure 2.4 Descriptive Sketch Demonstrating Tailwater Effect (Schohl, 2016)

Shayan et al. (2017) conducted an extensive investigation concerning discharge capacity of radial gates at large dams. They collected numerous discharge data series belonging to 17 dams built in various regions of Iranian and compared the data with theoretical values of the first three methods aforementioned in this review. Average errors found indicated that old equations are not reliable to compute discharge precisely at all times. Especially in the transition zone, USACE (1977) makes very poor estimates (up to 25 percent error). For this reason, the authors decided to create a new equation based on their data series. Initially, a lot of dimensionless parameters were generated by applying Buckingham Π Theorem. These effective parameters involve geometrical variables such as gate lip angle, upstream weir slope, gate seat position, gate radius and so on. After performing statistical test (F-test), it was concluded that by far the most significant parameter is the ratio of vertical distance between upstream energy level and lower gate lip (corresponding to H_2 in Figure 2.1) to vertical distance from lower gate lip to apex of spillway (corresponding to V in Figure 2.4), followed by gate lip angle, β, with much less importance.

$$Q = Q^{*} N L \sqrt{g D^{3}} \tag{2.3}$$

$$Q^{*} = 0.752 \left(\frac{H_2}{V}\right)^{0.633-0.060\beta} + 0.323 \left(\frac{V}{H_o}\right)^{0.162} + 0.174 \tag{2.4}$$

In Equation 2.3, Q is the total discharge, and N is number of radial gates. The other quantities were defined previously. The authors claim that the suggested formula yields less than five percent error as long as the constraints provided in the article are satisfied. They persistently dwell on the fact that further investigations are needed in case multiple gates are operating at different openings since Equation 2.3 & 2.4 were derived when all gates have identical openings. Also, they stated that the effect of oblique approach flow on radial gates in estimation of discharge is unclear and should be studied. Shayan et al. (2017) also derived geometrical relations to find approximate values of β and D in different downstream crest profiles. Although USACE (1977) provides some design charts to calculate these values, they are not very practical for designers and only applicable for their standard crest shape.

Haktanır and Khalaf (2020) performed detailed analysis of experimental data of 22 radial-gated dam models at various scale provided by USBR, USACE and DSI (State Hydraulic Works). It was observed that results of neither USBR (1960) nor USACE (1977) solely agrees with empirical measurements at the desired level (Figure 2.5). They claimed that the discharge coefficient cannot be estimated by generalized approaches since so many different arrangements may exist, especially for approach channels. Hence, discharge equation should be specific to the spillway structure existing in a particular dam. To determine the discharge coefficient of USACE

(1977) accurately, a regression test considering both Θ and d/H_1, effective parameters suggested by USACE (1977) and USBR (1960) separately, should be performed according to Equation 2.5.

$$C = c_0 + c_1\theta + c_2\theta^2 + c_3\left(\frac{d}{H_1}\right) + c_4\left(\frac{d}{H_1}\right)^2 \quad (2.5)$$

where c_0, c_1, c_2 and c_3 are regression coefficients. The value of C in Equation 2.5 can only be obtained via a physical model of the related dam, which is not smaller than scale of 1/50 so that viscous effects are minimized. It is asserted that the proposed approach gives results among 95% confidence interval.

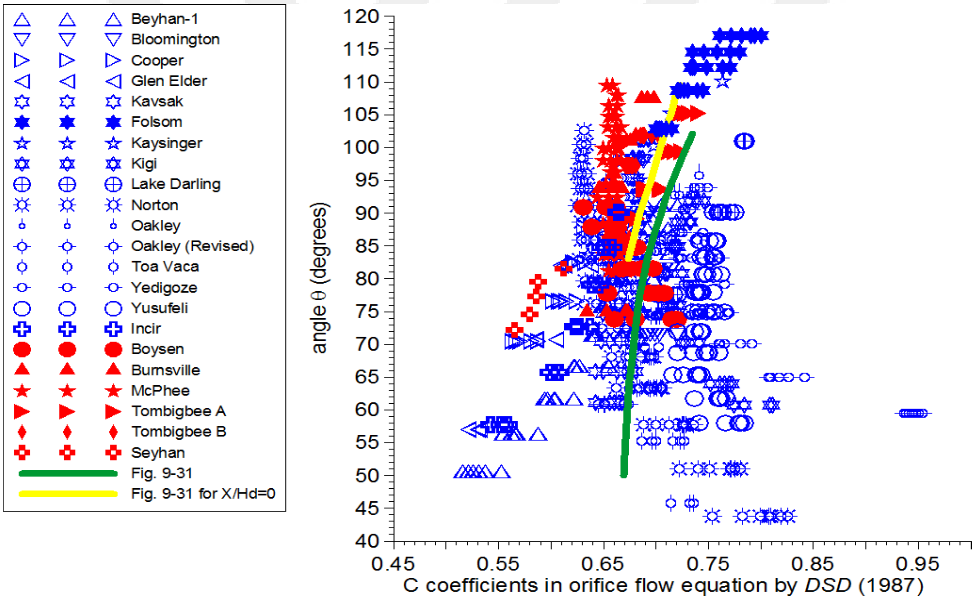

Figure 2.5 Comparison of Discharge Coefficients by the Physical Models and USACE (1977) (Haktanır and Khalaf, 2020)

It should be noted that the scale effects in the studied models are neglected in Figure 2.5, which somewhat accounts for the additional deviations from the generalized curves. Abbreviation DSD stands for *Design of Small Dams*. In the third edition of the book published in 1987, the authors replaced their discharge coefficient rating curve with that of USACE (1977).

CHAPTER 3

EXPERIMENTAL INVESTIGATION

3.1 Experimental Setup

3.1.1 Description of the Hydraulic Model

Spillway model of Lower Kaleköy Dam at 1/30 scale is investigated in this study. However, spillway arrangement of the hydraulic model is different than the prototype. The actual structure has four bays composed of three piers and two abutments as seen from Figure 3.1. On the other hand, the laboratory model has a single bay composed of two piers. Crest length in the prototype was designed to be 14 m whereas it is 30 cm in the model owing to geometical limitations in the reservoir outlet, which corresponds to 9 m in prototype scale.

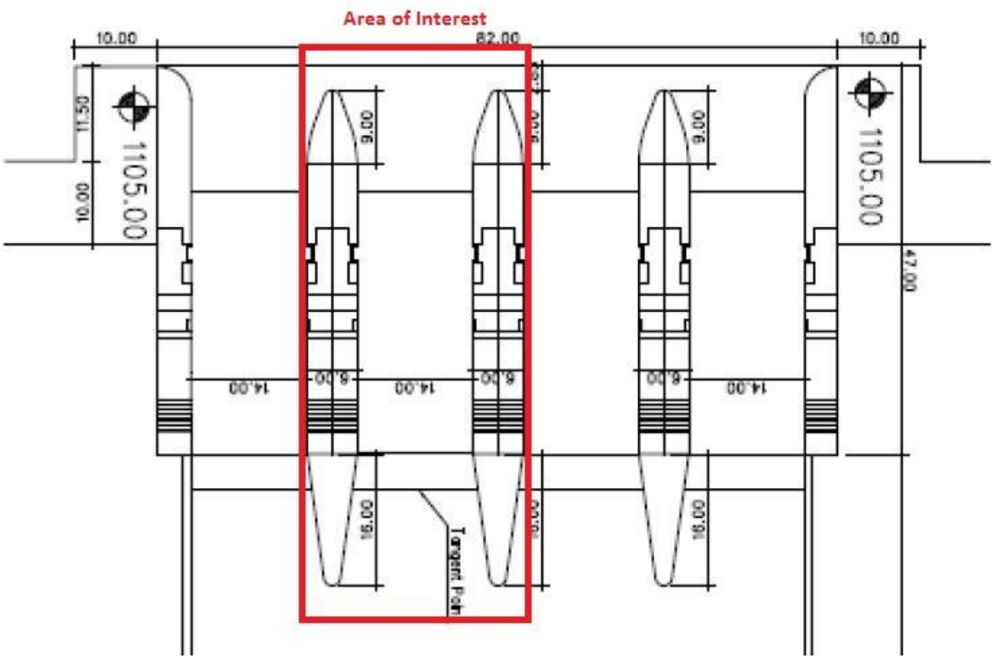

Figure 3.1 Spillway Plan of Lower Kaleköy Dam

Pointed-nosed piers are used in the prototype so are they in the model. According to *Design of Small Dams (1987)*, this pier type applies zero or little negative contraction to entraining flow to approach channel. The abutments are selected as rounded shape, whose headwalls are perpendicular to flow direction, but since the physical model does not contain abutments, they are not in the scope of this study. The spillway is ogee-shaped type and designed according to the USBR design criteria (Figure 3.2). Downstream face of the spillway is shaped by following equation:

$$\frac{y}{H_d} = -K\left(\frac{x}{H_d}\right)^n \tag{3.1}$$

in which *K* and *n* are constants which are function of ratio of approach velocity head to design head and upstream weir slope. The values are 0.512 and 1.752 for *K* and *n*, respectively. The origin is located at the crest point. The downstream curve is followed by discharge channel having constant slope and stilling basin at the end. Figure 3.2 is a depiction of crest profile for vertical upstream slopes, which has two different radius of curvatures denoted by R_1 and R_2 on upstream side. However, in our model, upstream face with inclination of 1:1 is preferred, which requires a single circle segment according to their design criteria (R_1=22.5 cm and R_2=∞ for the current model). Genaral view of this profile can be seen in Figure 1.2.

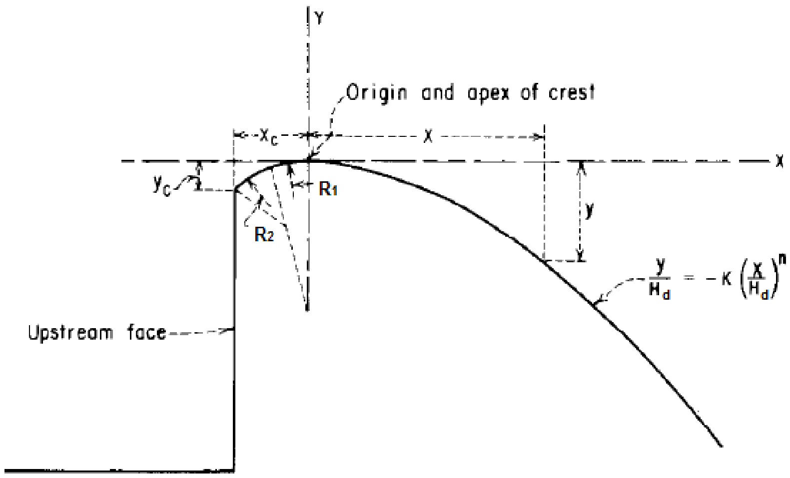

Figure 3.2 Ogee-Shaped Crest Profile (USBR, 1987)

Reservoir of the model is rectangular-shaped pool whose water capacity is almost 30m^3. The dimensions directly measured from the setup is given in Table 3.1. The spillway structure is placed at the middle of short side of the pool. Inlet pipe is connected to the other short side of the pool. This configuration allows symmetrical flow conditions to develop within the vicinity of the entrance channel.

Radial gate is placed slightly below downstream of the crest, which implies that the gate lip touches downstream face of the spillway when fully closed. The gate is pinned at the sidewalls of discharge channel. It can be rotated around its axis manually, and it is fixed with C-clamps.

Table 3.1 Some Salient Dimensions Related to the Setup

Resorvoir width	400 cm	Design Head	50 cm
Resorvoir depth	140 cm	Maximum Head	62 cm
Pier width	20 cm	Gate Radius	63 cm
Crest width	30 cm	Upstream Weir Slope	1H/1V
Weir Height	15 cm	Discharge Channel Slope	0.7H/1V

In a hydraulic model, it is essential to avoid excess viscous effect and surface tensions in order to get similiar physical behavior with the prototype. This is achieved by running the systems with adequate scale and also having smooth surfaces. For this, sidewalls and abutments are made of plexiglass, which is resistant to pressure and has almost zero roughness height, and the spillway is made of easily formable thin metal sheet.

The experimental setup works based on recirculation of water. Water is supplied by an inlet pipe from a large tank whose elevation is higher than the reservoir surface. Rate of flow is adjusted by a couple of valves installed on this pipe. Water respectively passes through pool, radial gate, chute channel, stilling basin and lastly elevated channel by a sill. Outflow from the system is poured into an underground reservoir. Then, it is again pumped to the elevated storage tank. This circulation continues until the experiment is terminated.

3.1.2 Measurement Devices

There are two devices responsible for measuring water stage in the reservoir and flow rate passing under the radial gate.

Manometer: Water surface elevation at millimetric precision is measured with simple U-type manometer. One end of the manometer is attached to center of the pool at the deepest point. It gives total upstream hydraulic head.

Electromagnetic flowmeter: It measures total inflow rate to the system, which must be same with outflow rate under the gate. It is connected to the pipe connecting the elevated storage tank and the reservoir of the model. The flowmeter is electrically operated, shows one decimal precision of a liter and is manufactured with a standard 0.5% error at flow speeds below 15 m/s (Q&T, 2019).

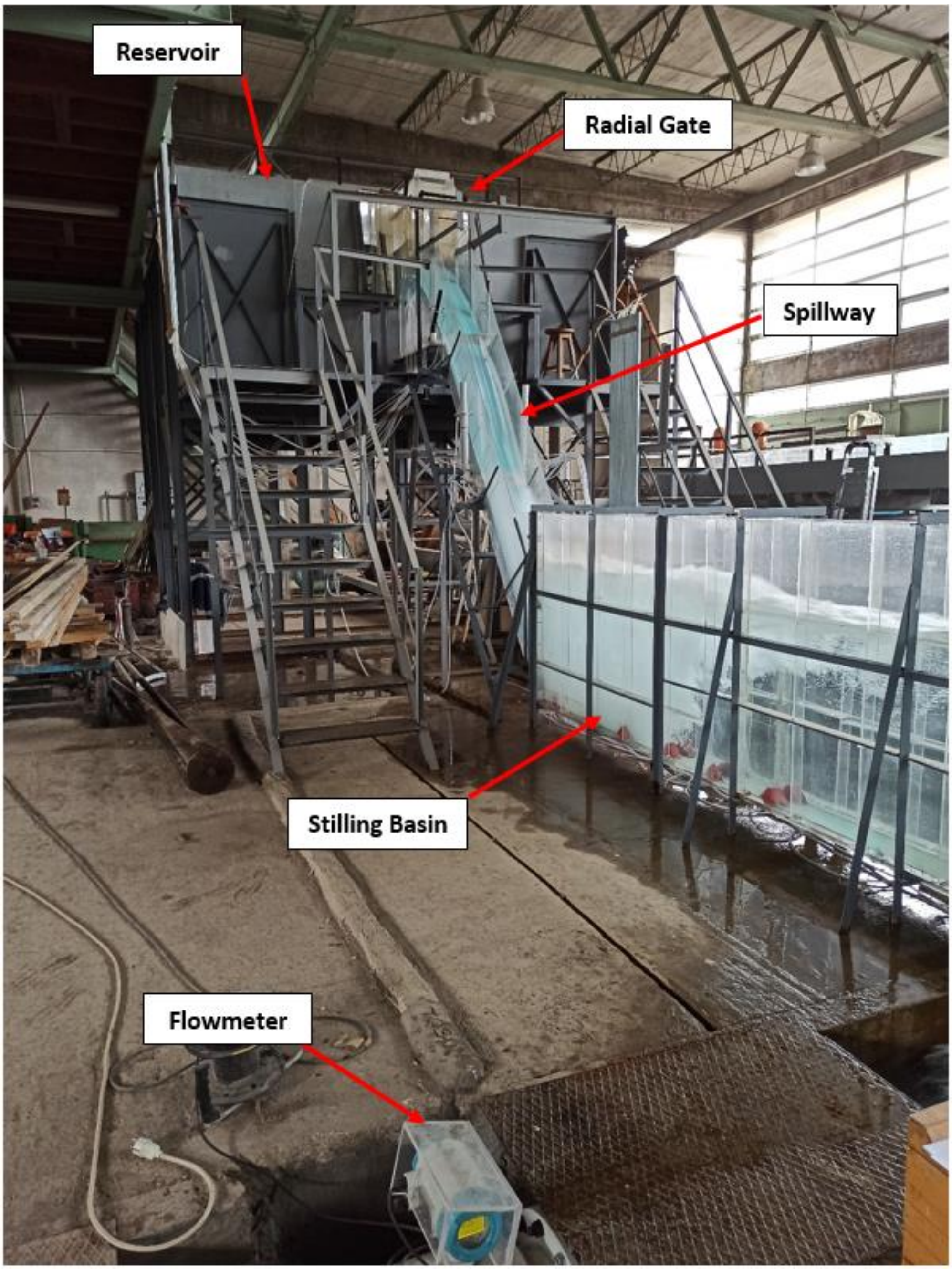

Figure 3.3 General View of the Experimental Setup

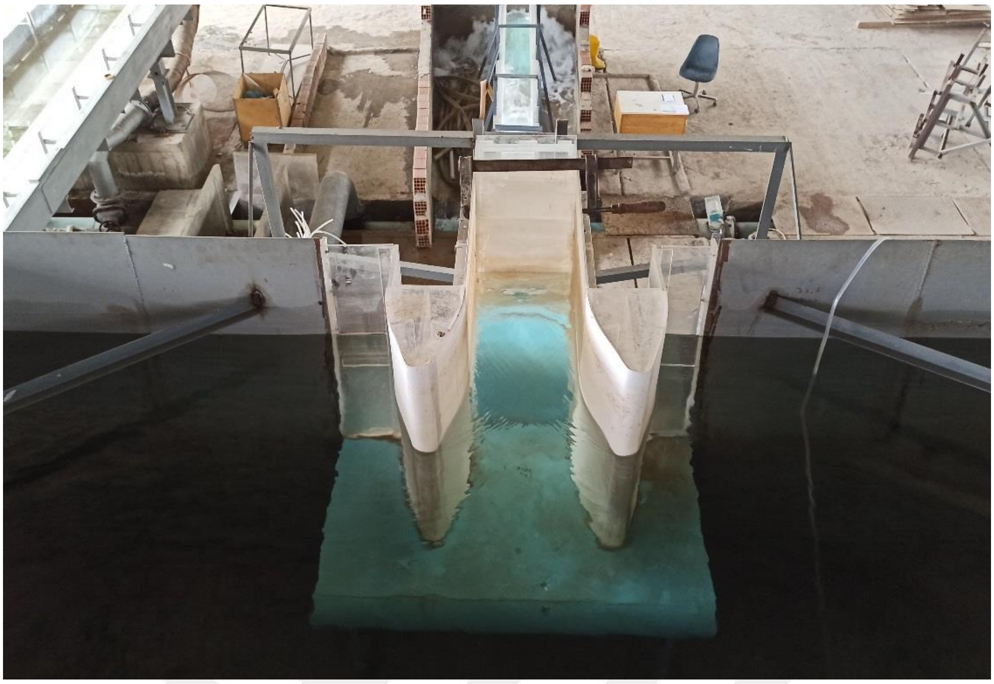

Figure 3.4 Upstream View of the Radial Gated-Spillway

Figure 3.5 Side View of the Radial Gate During Operation

3.2 Data Collection

3.2.1 Procedure of the Experiments

The basic aim of the experiments is to obtain stage-discharge relationship. Using this relationship, discharge coefficient can easily be found from continuity and energy equations. The procedure is simple to follow but requires relatively long time, average of 10 hours for a single set of experiment. Steps are as following:

1) Gate opening is adjusted to the desired value by hand manipulation, and its radial movement is restricted by a couple of C-clamps.
2) A plexiglass panel is inserted in front of the gate, and reservoir starts to be filled with water by opening the valve on the inlet pipe.
3) After reaching maximum water level, the panel is removed, and thus the system is allowed to discharge under the gate.
4) The valve is partly closed so that inflow from the inlet pipe does not overwhelm outflow from the gate.
5) A period of time is elapsed until the system reaches steady-state conditions, which means total inflow and outflow become exactly equal to each other. All the physical quantities such as velocity, pressure etc. in the system reach to a steady-state condition.
6) Discharge is read from the flowmeter and water stage is read from the manometer (Heads in manometer show water depth in the pool, not effective heads. Necessary manipulations are made in the calculation stage.)
7) The valve is again closed partially; thus, water surface begins to descend and reaches to a steady-state condition at a lower stage, and then new readings are taken. Duration needed in this this step is linked to the amount of gate opening. As the opening gets smaller, the system requires more time to evacuate residual water from the gate and vice versa. It takes approximately between 15 minutes to 2 hours to reach to the steady-state condition.

8) Previous step is iterated by gradually reducing valve opening until water jet seperates from the gate and turns into free flow.

In this study, discharge is investigated on the basis of vertical gate opening (*d*). It is defined as vertical distance between lower gate lip and spillway surface. There were 14 sets of experiments starting from 1 cm opening to 14 cm increased by one in advance. For this thesis, the experiments with two of them, 5 cm and 14 cm openings, were repeated to verify the previous data. Data sets belonging to 1 cm and 2 cm were dropped as consistent relationship between stage and discharge is not satisfied. The following tables show calculation of effective head, *H*, and head above the crest, H_c, from the raw data and corresponding discharges at 5 cm and 14 cm openings. Effective head is the height of water from reservoir surface to center of net gate opening (USACE, 1977).

Table 3.2 Experiment Results at 5cm Gate Opening

d (cm)	Z_{res} (cm)	Z_{cr} (cm)	Z_s (cm)	h_m (cm)	H_c (cm)	H (cm)	Q (lt/s)
5	134.4	71.6	67.93	3.90	62.8	62.57	40.5
5	123.3	71.6	67.93	3.90	51.7	51.47	36.1
5	113.5	71.6	67.93	3.90	41.9	41.67	31.8
5	105.9	71.6	67.93	3.90	34.3	34.07	28.4
5	99.4	71.6	67.93	3.90	27.8	27.57	25.2
5	93.6	71.6	67.93	3.90	22.0	21.77	21.9
5	88.9	71.6	67.93	3.90	17.3	17.07	19.1
5	85.5	71.6	67.93	3.90	13.9	13.67	16.8
5	83.0	71.6	67.93	3.90	11.4	11.17	14.9
5	81.8	71.6	67.93	3.90	10.2	9.97	14.0

In the table, Z_{res}, Z_{cr} and Z_s represent water surface elevation, crest elevation and gate seat elevation, respectively, and h_m is the vertical distance between center of net gate opening and gate seat, which is a parameter needed for calculating effective head ($H = Z_{res} - (Z_s + h_m)$).

Table 3.3 Experiment Results at 14cm Gate Opening

d (cm)	Z_{res} (cm)	Z_{cr} (cm)	Z_s (cm)	h_m (cm)	H_c (cm)	H (cm)	Q (lt/s)
14	132.7	71.6	67.93	9.59	61.1	55.18	100.6
14	127.2	71.6	67.93	9.59	55.6	49.68	95.1
14	124.1	71.6	67.93	9.59	52.5	46.58	91.3
14	119.6	71.6	67.93	9.59	48.0	42.08	86.2
14	114.2	71.6	67.93	9.59	42.6	36.68	79.5
14	109.7	71.6	67.93	9.59	38.1	32.18	74.5
14	106.4	71.6	67.93	9.59	34.8	28.88	69.7
14	102.4	71.6	67.93	9.59	30.8	24.88	64.7
14	100.3	71.6	67.93	9.59	28.7	22.78	61.4
14	98.3	71.6	67.93	9.59	26.7	20.78	58.5
14	96.5	71.6	67.93	9.59	24.9	18.98	56.3
14	95.2	71.6	67.93	9.59	23.6	17.68	54.3
14	93.9	71.6	67.93	9.59	22.3	16.38	53.2

3.2.2 Model-Based Errors

By nature of experiments, there is always possibility of having errors in the data. Errors may originate from observer as well as experimental setup itself. The followings are the main sources of probable errors as far as the current study is concerned:

***Air Bubbles in Manometer*:** Air bubbles can bring about overestimating water head. Therefore, manometer should be properly pressurized with water so that no air is entrapped within it. In our experiments, the manometer pipe was always checked before starting readings.

***Reading Error*:** If reading is taken from the manometer before reservoir water level becomes thoroughly stable, some errors emerge inevitably. Residual water not able to be discharged from the reservoir causes overestimated water head. Also, some small reading errors are possible due to observer.

Oscillation in Flowmeter**:** Due to instability of water head in the elevated storage tank during pump operation, the flowmeter cannot give a fixed discharge value, and depending on the number of setups operated in the laboratory, range of oscillation in the flowmeter increases. Therefore, average of maximum and minimum readings, which generally have a difference of a few liters, were recorded. This situation may lead to a little poor estimation of the discharge even if the radial gate setup is operated solely.

Adjustment of Gate Opening**:** Amount of gate opening is adjusted with the help of a ruler or tape measure. There might be errors at millimetric scale in opening, which may contribute to an undesired deviation in the discharge.

Leakage: In high water stages, it was observed that there exist consistent deviations from numerical results. This situation might arise from uncontrolled water leakage through the entrance channel seals and especially from the gate sides. The error gradually grows upon increase in the head since amount of leakage becomes more dominant from the gate sides. In all observations, at larger heads, discharge obtained from the experiments is slightly higher than the numerical results.

CHAPTER 4

NUMERICAL INVESTIGATION

4.1 Simulation Software

Today, computational fluid dynamics programs have become more favored with the advent of enhanced processors. A wide variety of flow types can be treated effectively by CFD programs. In this study, numerical analyzes were conducted via Flow-3D Software, which is user-friendly and well-reputed for dealing with free surface problems. The program executes the model based on finite volume methods. Control volume is represented with structured mesh containing rectangular blocks and cells, and the defined geometry is approximated as planes in each cell by calculating area and volume fractions (FAVOR^{TM} Method) to eliminate disadvantages of structured grids. Flow-3D solves three-dimensional non-hydrostatic Navier-Stokes equations among the adjacent cells and gives output of desired physical quantity such as velocity, discharge, pressure etc. at an interested point or region in the domain depending on time. It has an additional software, FlowSight, for post-processing of the model to meet visual expectations, to monitor streamlines, to create graphs and so on. Throughout the study, different versions of the program, v11.04, v11.1 and v11.2, were used. No computational difference was observed among them, but the more recent version has a better interface and an improved solver.

4.2 Three-Dimensional Analysis

4.2.1 Description of the Numerical Model

Numerical model was identically created with the laboratory model to be able to make direct discharge comparison between them. Stilling basin and great portion of downstream part of the chute channel was not considered in the numerical model since they are not in the scope of the discharge investigation. Bottom level of the model was determined as 25 cm below the crest point: All components with the inclusion of dead water volume below this datum plane were simply excluded from the solution.

Some dimensions of the components like the reservoir were directly measured from the laboratory model whereas more specific ones were adapted from the prototype drawings. Firstly, 2D drawings of the piers, the spillway and the radial gate were scaled to 1/30 and then converted to 3D solid objects on a CAD program. Next, a pool whose wall thickness is 10 mm was modelled and combined to the overflow solid structure to serve as a reservoir (Figure 4.1). After completion of the numerical model, some significant distances such as relative position of the piers or trunnion of the radial gate to the spillway apex were checked both in the numerical and the physical model to ensure their dimensional agreement.

In the same manner with the experiments, 12 different vertical openings of radial gate were arranged (from 3 cm until 14 cm). The openings were precisely measured on the CAD program by rotating the radial gate adequately. Corresponding solid models were separately generated and simulated on Flow-3D. However, in three-dimensional investigations, only five randomly selected openings, 5 cm, 7 cm, 10 cm, 12 cm and 14 cm, were simulated for the effective use of computer sources.

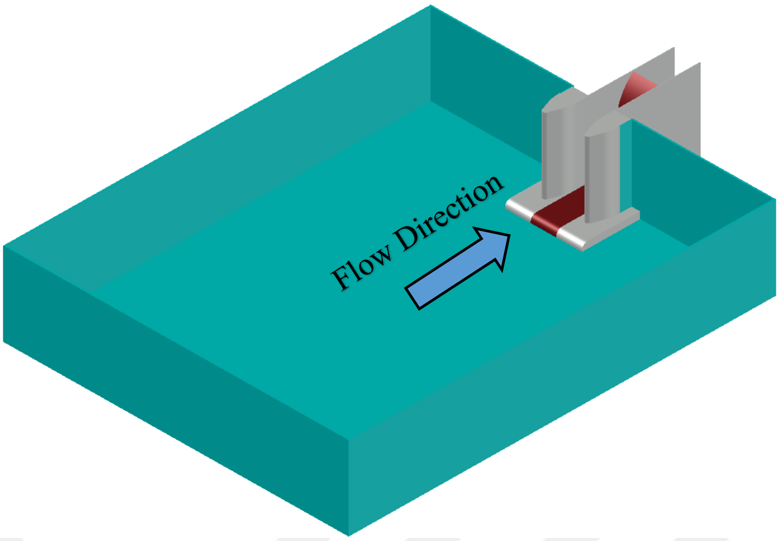

Figure 4.1 Components of the 3D Model (Radial-gated spillway, Piers, Reservoir)

4.2.2 Physics

At the very beginning, Flow-3D necessitates determination of physical rules to execute the model in accordance with the real case problem. The software offers a wide range of physical considerations depending on type of the problem. Since the current model involves free water surface, and the only aim is to measure volumetric flow rate, physical conditions existing in two tabs are enough to be assigned in the program. Names of these tabs are ‘viscosity and turbulence’ and ‘gravity and non-inertial reference frame’. The former one is regarding desired flow types such as ideal or viscous and appropriate turbulence models for the selected problem. In our case, viscous flow is selected, which allows development of shear forces between layers of fluids and no-slip boundaries. This flow type is much more realistic as it enables fluid rotation, and thus generation of vortices and eddies. As a turbulence model, Renormalized Group (RNG) with dynamical computation of maximum turbulent mixing length was selected, which is highly recommended by Flow-3D engineers for situations including open channel and weirs. Despite the presence of various turbulence models such as k-ε, k-ω, large eddy simulation etc. in the software, their effects were not individually addressed in this study. The latter one is responsible for magnitude and direction of gravitational acceleration. It was defined as 9.81 m/s^2 in downward direction (-z direction).

As general properties, interface tracking option was chosen as ‘free surface or sharp interface’ and flow mode was set to be ‘incompressible or limited compressibility’. Flow-3D enables different type of fluids to be designated. As it is supposed to be, water at 20˚C was defined for simulations. Any other options were left as default.

4.2.3 Mesh Detail

It is a predictable fact that water volume far behind from the spillway has almost no influence on discharge under radial gate. For the sake of computational efficiency, area of interest in the numerical model was restricted to the vicinity of the approach channel. In addition, half of the domain was taken into consideration as flow conditions would be perfectly symmetrical in the model. In other words, one of the mirror image pairs of the domain was analyzed, which is generated by a cut plane intersecting the crest at its midpoint. The details can be seen in Figure 4.2. Dimensions of the reduced domain were selected arbitrarily in the first place, but their validity is confirmed in Chapter 4.2.6.

Whole mesh structure is composed of three separate blocks, one of which is located around the pier and the others are responsible for flow in the chute channel. Mesh Block 3 is a nested block defined in the region where the radial gate is placed within the Mesh Block 2. Its task is to help more precise investigation of flow since properties of flow changes abruptly while entering the gate opening. This region necessitates further mesh refinement. So, two different grid sizes are used: 5 mm in the nested block and 10 mm in rest of the system, which can be referred as fine and coarse mesh resolution. As the name implies, finer meshes result in better accuracy thanks to the enhancement of rendering process. On the other hand, coarse cells give rise to less computationally intensive simulations and thus improve overall run times. For these reasons, an optimization between two standpoints is a must.

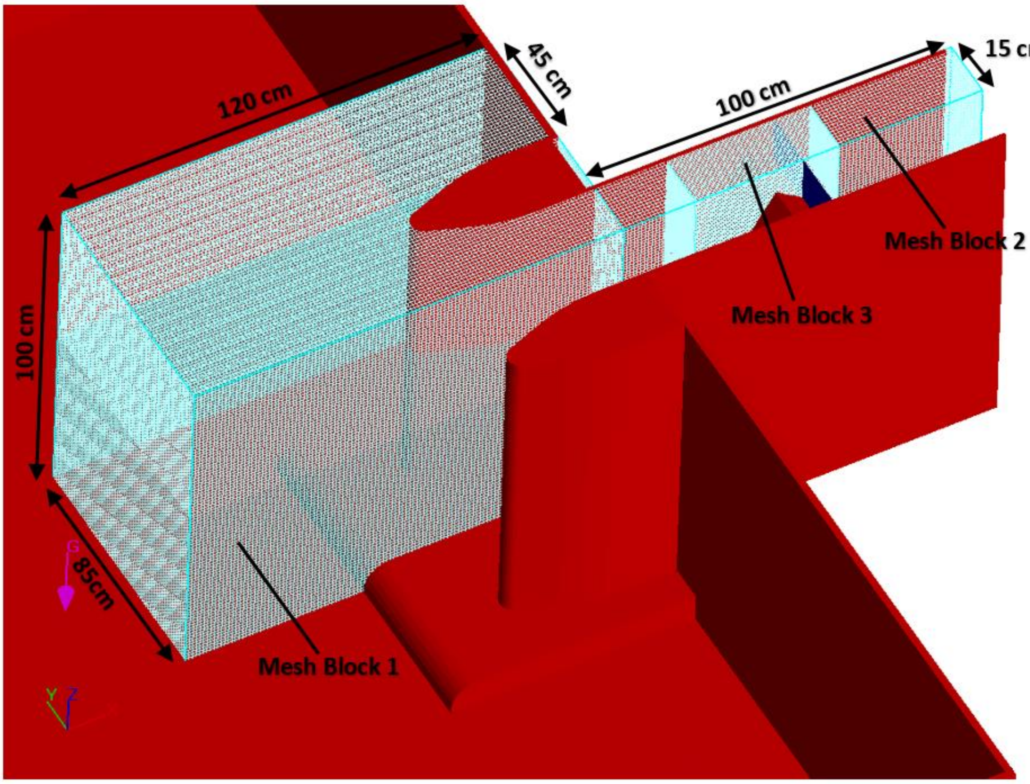

Figure 4.2 Mesh Detail of the 3D Models

Another point of view is necessity of good alignment between grid cells of containing and nested block (i.e., Mesh Block 2 and 3 in our case). Grid size ratio of the adjacent mesh blocks must preferably be two in aligned manner to help overall accuracy of data transferred between them. Also, proper intersection between mesh cells and block geometry is essential to minimize errors due to surface rendering.

4.2.4 Boundary and Initial Conditions

Aim of the boundary conditions is to maintain continuative motion of flow in the domain during simulations. Flow-3D offers various boundary types such as 'Wall', 'Symmetry', 'Outflow', 'Specified Pressure', 'Specified Velocity', 'Volume Flow Rate' etc. Only the ones used in the simulation models will be explained in this subheading.

In the experiments, hydraulic head was measured keeping discharge in the system constant by valve operation. Conversely, in the numerical models, corresponding flow rate was determined by fixing upstream water head. The software in fact allows the execution of the model in the same manner with the experiment. However, working with discharge condition is quite challenging as it differs with gate opening, which requires initial estimation of discharge before running simulation. Instead, the other scenario is independent of any configuration of the current model.

Elevation of water surface in each model were set to be 85 cm, 75 cm, 65 cm, 60 cm, 55 cm, 50 cm, 45 cm and 40 cm, respectively from the datum plane 25 cm below the spillway apex. This implies active head on the crest will be 25 cm less than surface elevation (e.g., for Z_{res}=85 cm, H_c=60 cm). First two stages could be considered as maximum and design head, which is consistent with that of the physical model. Last two stages were only able to be simulated in the models in which the gate opening satisfies orifice type of flow at those levels.

Inlet flow is controlled by 'Specifying Pressure' either with fluid fraction or fluid elevation options. With stagnation pressure check option, fluid elevation is interpreted as total upstream hydraulic head in the program. By referring to Figure 4.5 and Figure 4.6, it is clear that streamlines are coming into the entrance channel from axial as well as lateral directions. Hence, both Plane 1 and Plane 2 depicted in Figure 4.3 were set to be upstream control where fluid elevation is specified with stagnation pressure. Plane 3 is cutting plane. It was selected as 'Symmetry', which enables the selected plane to pretend identical flow conditions on both sides.

No downstream control is needed as supercritical flow will be exiting the domain: Downstream effects will not be able to propagate towards upstream. This condition could be achieved by two alternative ways: The first one is simply selecting 'Outflow', and the second method is to set fluid fraction to be zero on the related planes. So, Plane 4 and Plane 5 were activated with the latter option. Remaining outer boundary planes are of no importance since they do not interact with streamlines and were left as symmetry condition. Also, no data concerning surface roughness was entered to the program: It is interpreted as zero by default.

A flux surface was placed just downstream of the gate lip where finer mesh resolution exists. Its function is to compute physical quantities of fluid flux passing through it. Flux surface is acting like a gauge measuring total hydraulic head, mass and volume flow rate, wetted area, pressure force exerted on it and so on.

Initial condition within the mesh structure is another requisite for realistic behavior of the numerical model. For this, initial water volume with hydrostatic pressure was designated in the domain until just in front of the radial gate. This setup lets the system operate as gated flow. Otherwise, water entering the system will immediately be leaving from the opening without contacting the gate.

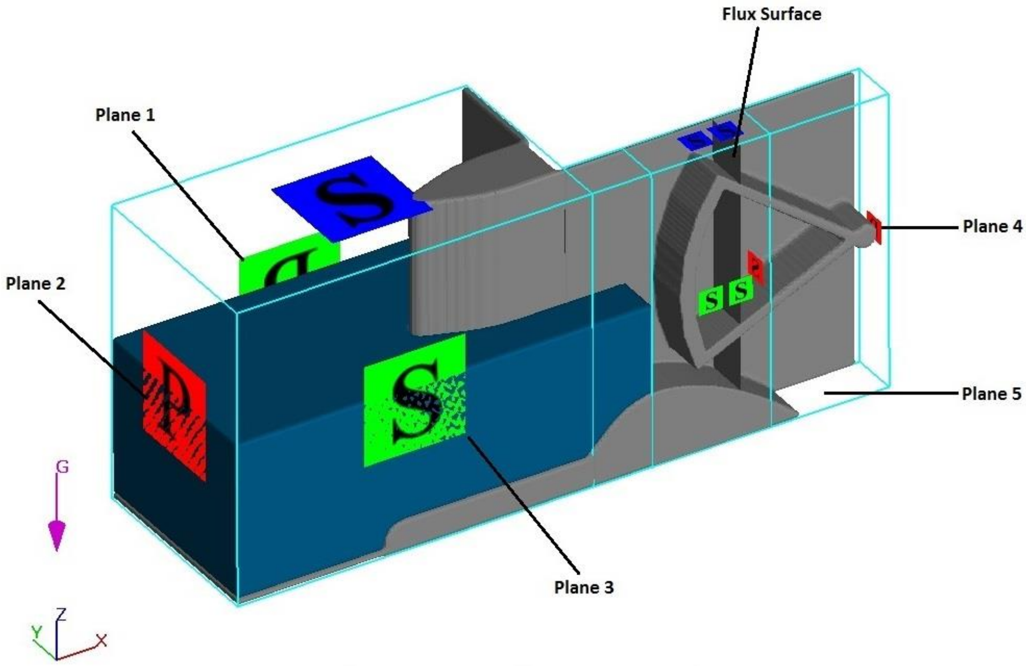

Figure 4.3 Initial and Boundary Conditions

4.2.5 Duration of Simulations

In the numerical models, discharge was measured when the system reached steady-state condition. So, there is not a fixed simulation time. It considerably varies with water head, gate opening as well as boundary conditions. As being similar to the experiments, when hydraulic head rises and gate opening becomes narrow, simulations require more time for flow rate to become totally stable. One way to understand the time when the execution reaches this phase is stabilization of the total volume in the domain. That is, at steady-state phase, total volume in the system is not changing depending on time since inlet and outlet flow are perfectly balanced.

Involving all the 2D and the 3D models, running times are between minimum 15 s, at *d*=14 cm and H_c=25 cm, and maximum 110 s, at *d*=3 cm and H_c=60 cm. After volume oscillation stops, discharge data was recorded by averaging last two readings provided by the flux surface. The obtained data was multiplied by two to get final result as only half of the domain is simulated.

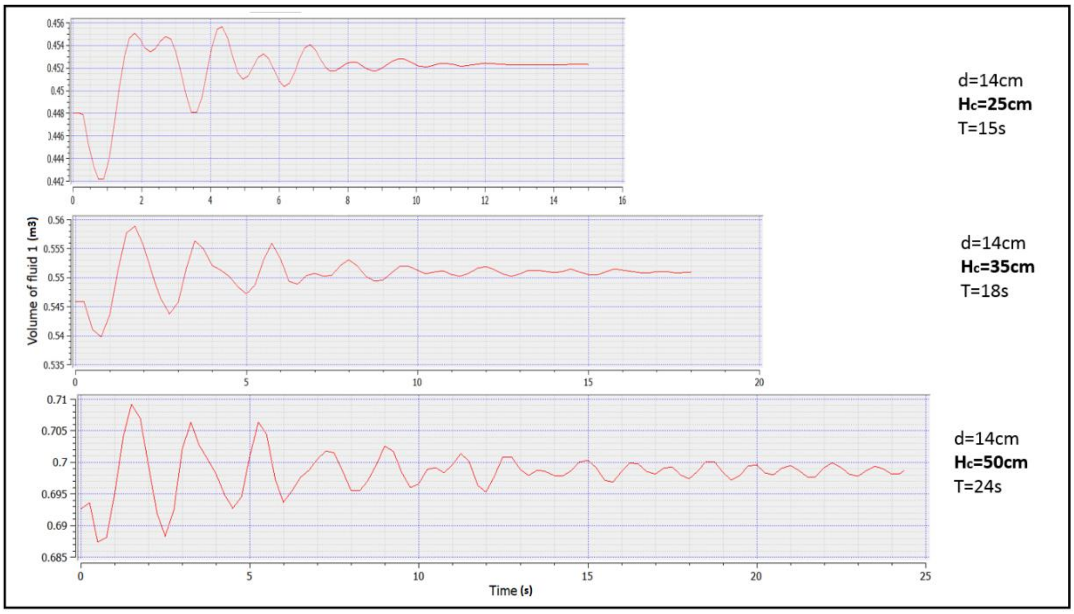

Figure 4.4 A Sample of Simulation Durations and Volume Change in the Domain

4.2.6 Effect of Reservoir Configuration

So far, reduced size of the experimental domain has been addressed. Investigation of actual setup is essential to see whether assumptions made are reasonable or not. For this aim, three additional reservoir configurations, d=12 cm and Z_{res}= 60 cm for all, were tested individually.

Firstly, in order to see symmetry impact, half-sized domain was doubled. Boundary and initial conditions were rearranged accordingly. No slight difference was observed when the discharge found is divided by half.

Secondly, a dead volume with 50 cm depth was attached under Mesh Block 1 with same length, width and also same cell size. Interestingly, this configuration increased computational effort drastically even though similar result with a negligible increase in discharge (0.5%) was obtained.

Thirdly, the numerical model was simulated with real reservoir dimensions of the experimental setup (i.e., with the model in Figure 4.1). Fourth mesh block containing Mesh Block 1 and having 20 mm cells was fit in the pool. Upstream boundary condition, for this time, was only defined to the backmost plane in order to mimic the experimental setup in which inlet flow is supplied from back side of the reservoir. Likewise, no considerable change was observed.

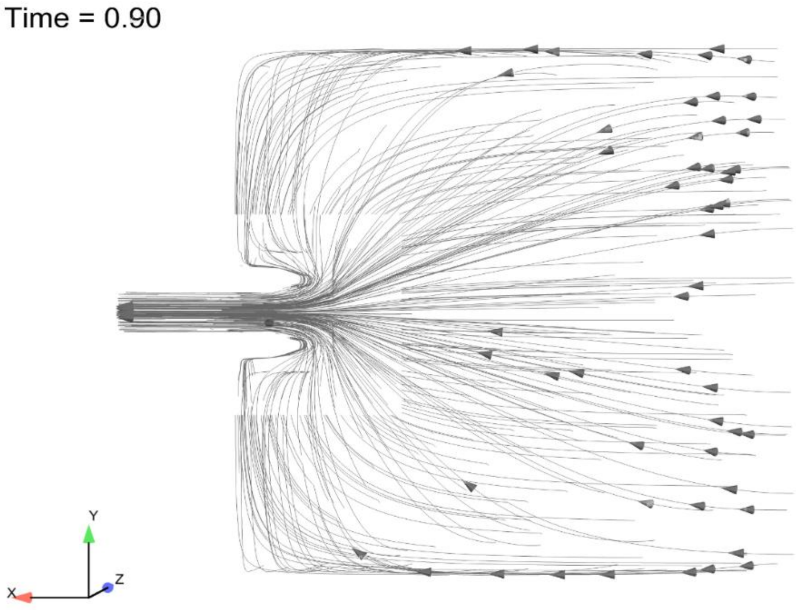

Figure 4.5 Representation of Streamlines at t=0.90s

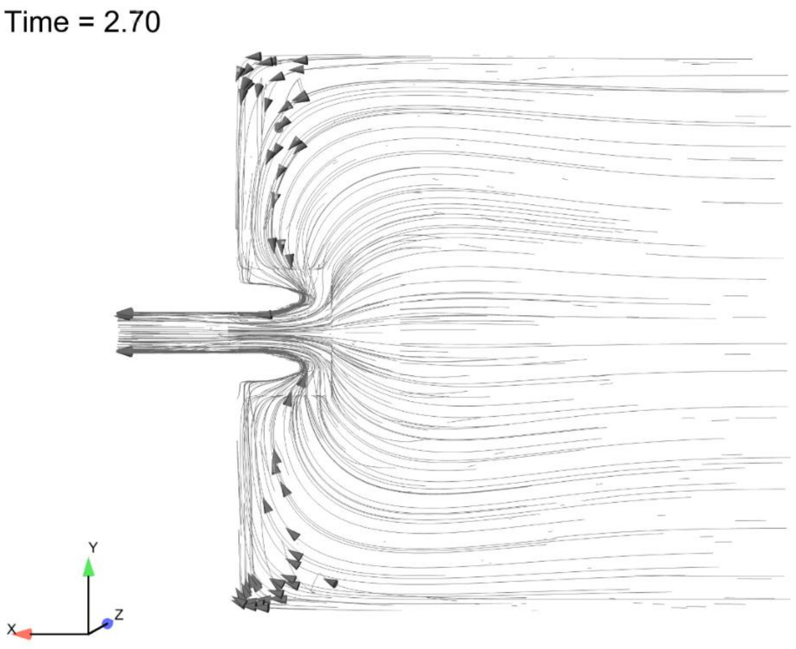

Figure 4.6 Representation of Streamlines at t=2.70s

4.3 Two-Dimensional Analysis

4.3.1 General Information on the 2D Models

3D simulations take pretty long processing time despite the reservoir manipulation and also take up large space on the hard drive. This handicap does not give much opportunity to examine discharge on different configurations of the radial gate and spillway geometry. For this reason, the 3D models were converted to 2D by taking one-centimeter slice of the spillway excluding the piers and the reservoir. That is, only approach and upstream part of the chute channel are considered as depicted in Figure 4.7. 2D and 3D numerical models have typically two main hydraulic differences in our case: Firstly, total upstream head in the 3D models was defined far behind compared to the 2D models. Secondly, contraction effect due to piers and sidewalls are simply neglected in 2D analyzes.

Graphical comparison of some 2D and 3D simulation results can be viewed in Chapter 5.2. Their results completely agree with each other at *d*=7 cm, 12 cm and 14 cm, and small discrepancies occurs at *d*=5 cm and *d*=10 cm, which are likely to be mesh-dependent errors. To this respect, it can be concluded that there is not noticeable flow variation along the crest line because of the aforementioned factors. This might arise from use of pointed-nosed piers in the model, which have experimentally zero or little negative constriction effect. In case of presence of rounded piers, the scenario might be different. On the whole, uniformity of flow between sidewalls is a valid assumption for our case. To make better use of computer sources and time, it was decided to continue with the two-dimensional analyzes.

In the 2D models, total upstream head was controlled only with the backmost boundary plane extending to the endpoint of the imaginary piers. Lateral planes were set to be in symmetric condition, and rest of the boundary conditions are kept same with that of the 3D models.

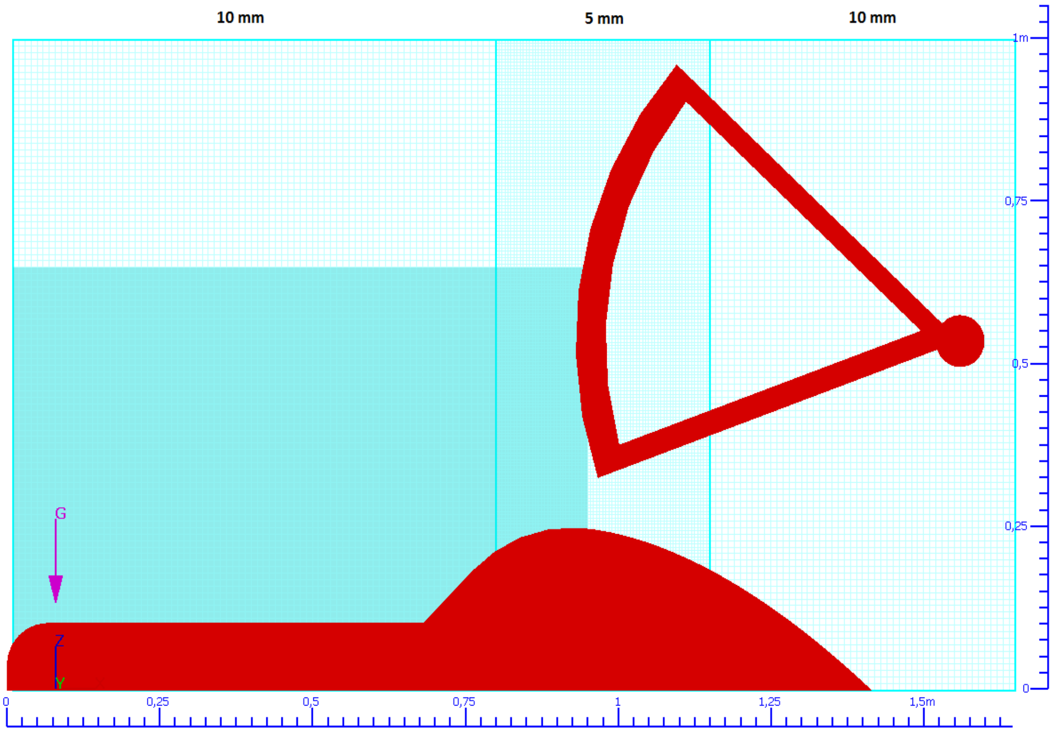

Figure 4.7 Mesh Details of the 2D Numerical Model

General form of mesh structure is more or less same with that of three-dimensional numerical solution: Mesh Block 1 was removed. Size of Mesh Block 2 and 3 were reduced to one-centimeter in the lateral direction. Unit discharges found at the end of simulations were multiplied with 30 to find the total volume flow rate.

4.3.2 Effect of Gate Position

In practice, there is no exact location where radial gate must be installed. Location of the gate seat might be planned right over the crest point as well as at the downstream face of the spillway like in the studied model. In order to investigate the discharge variation in these configurations, some manipulations on the gate location were performed on the 2D model. The original gate location was shifted to upstream direction on the horizontal axis until the gate lip touches the apex in fully closed situation. Then, the trunnion point was moved to downstream direction by half and one and a half of the initially shifted distance. Gate positions in these mentioned cases were respectively named as T1, T2, T3 and T4 from upstream to downstream. T3 represents the gate position in the first place. The distances among trunnion points are equal, 6.7 cm, but the location of the gate seat with respect to the crest differs because of curved shape of spillway. So, their relative horizontal distances to the crest are denoted as X_s, and it is 0 cm, 7.26 cm, 15.42 cm and 25.17 cm for T1, T2, T3 and T4, respectively.

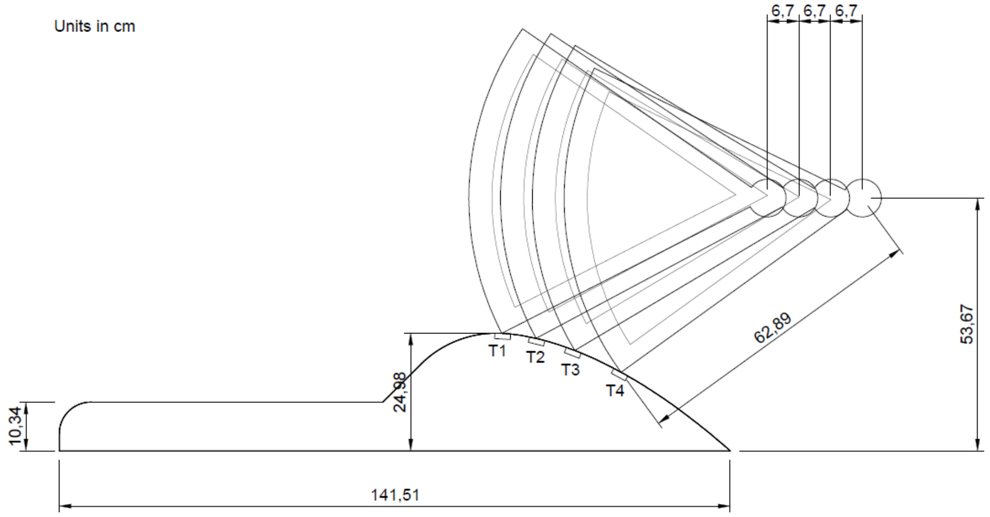

Figure 4.8 Illustrative Sketch of Gate Positions and Dimensions

As a result of simulations of each case at all gate openings, it was observed that there is a systematic increase in discharge as the gate seat is shifted from the spillway apex towards downstream. This fact is consistent with general knowledge in the literature including USACE (1977), but the mechanism is more clearly revealed in this study. This phenomenon mostly stems from gradual increment in effective head, and little contribution might be due to enhancement of curvilinearity of flowlines. It should be noted that no certain ratio exists among the increase in discharges for different configurations, but there is a trend (Figures 4.9, 4.10 and 4.11).

Although planning the radial gate at far downstream seems advantageous in terms of improvement of discharge capacity, there are a few hydraulic limitations related to it: Such configurations considerably suppress design head since level of upper gate lip moves down. Also, it reduces capability of continuing gated flow conditions at lower stages. For instance, in Figure 4.9, T4 position lets flow separate from the gate (free flow) at the stage where the others can still be operated as partially opened. As a reminder, this work does not deal with the transient head, but the example was just put as a finding of the numerical solutions.

Figure 4.9 Discharge Variation Depending on Gate Position at d=14 cm

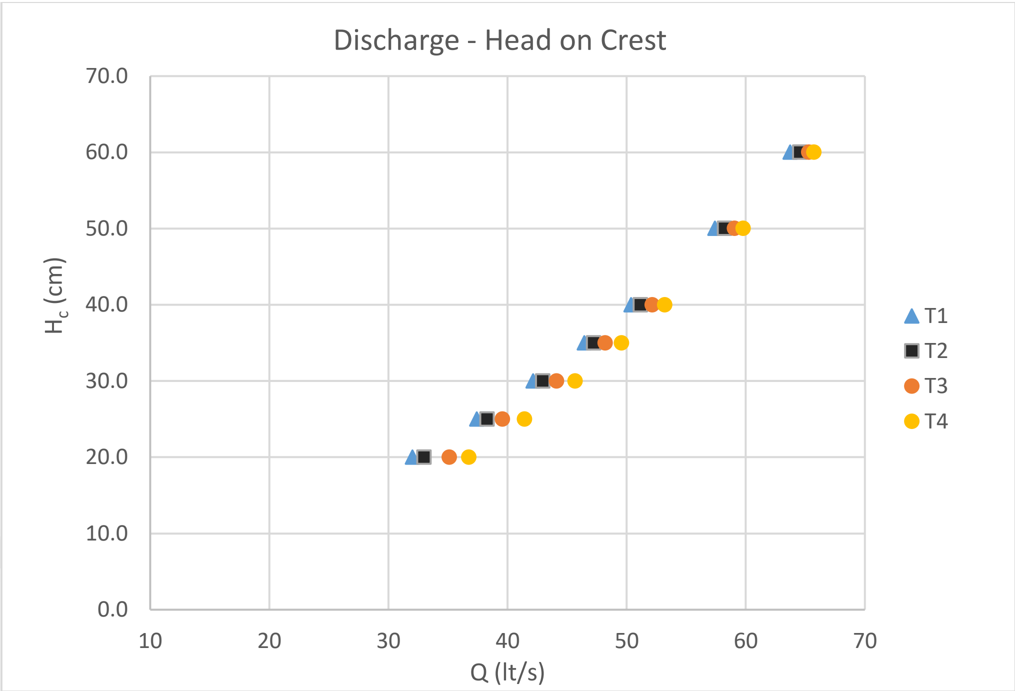

Figure 4.10 Discharge Variation Depending on Gate Position at d=9 cm

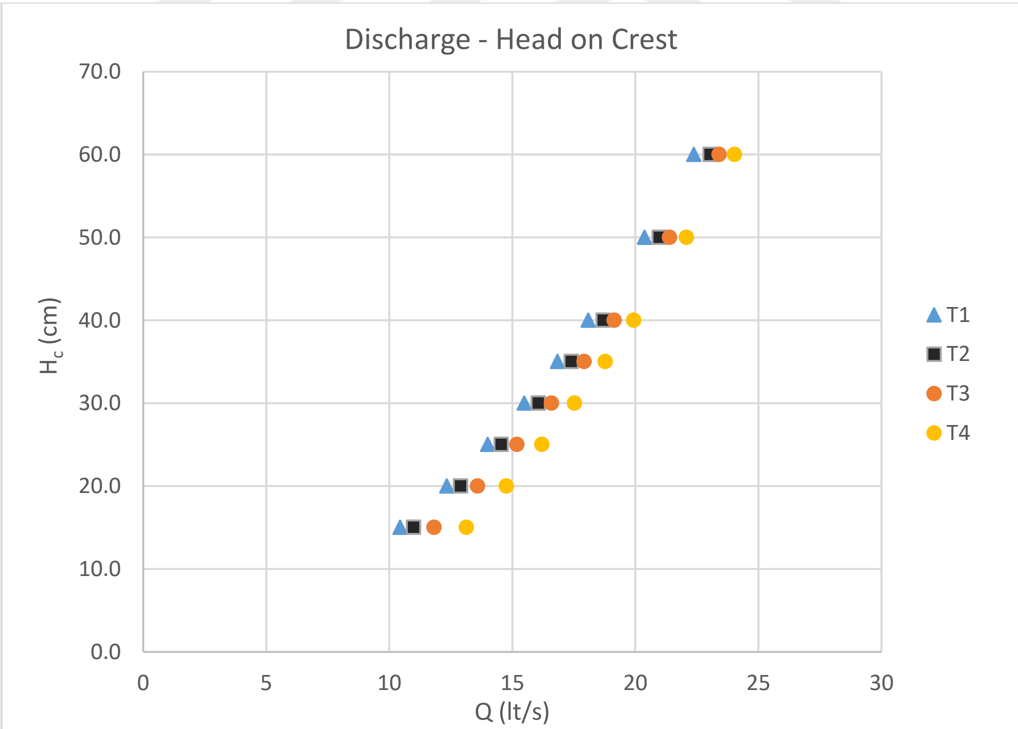

Figure 4.11 Discharge Variation Depending on Gate Position at d=4 cm

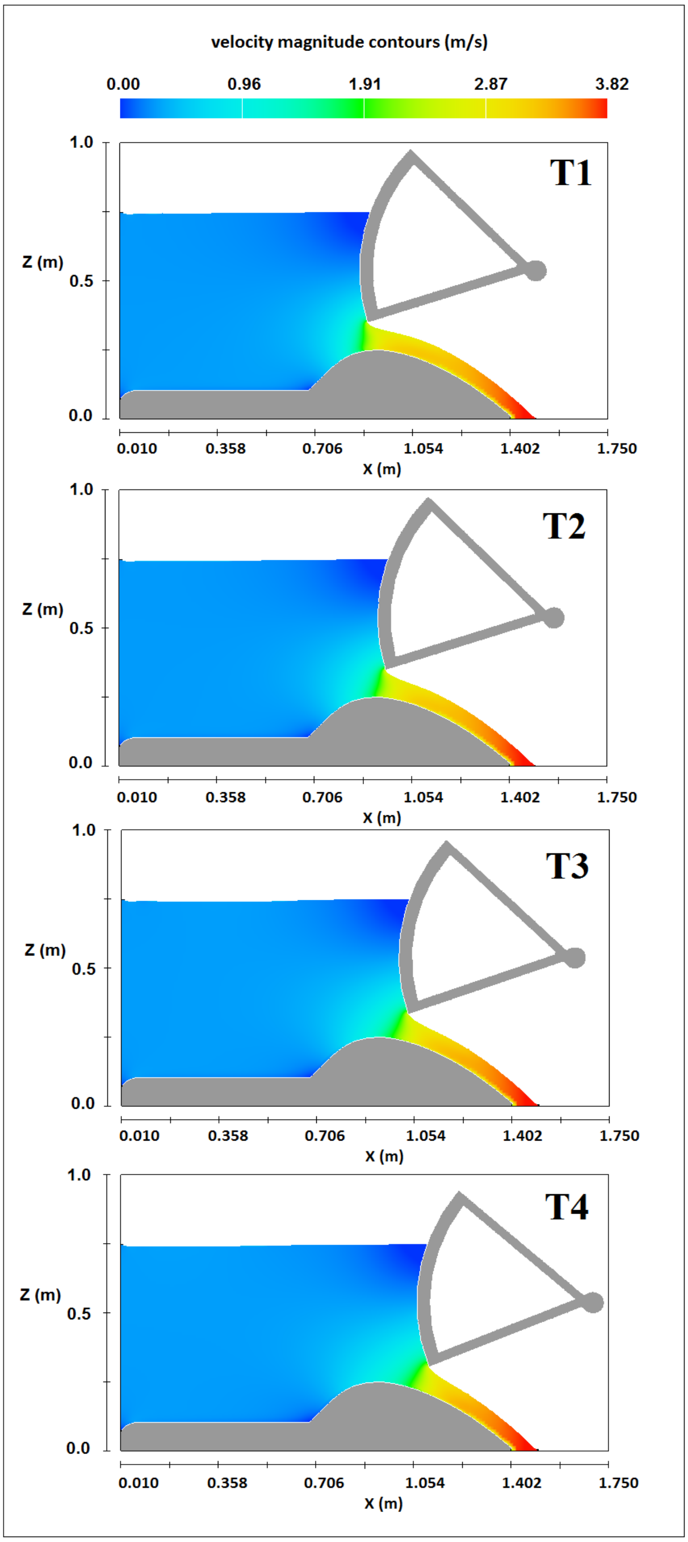

Figure 4.12 Velocity Magnitude Contours of T1, T2, T3 and T4 at the Design Head (d=10cm)

4.3.3 Effect of Spillway Geometry

Spillway geometry is another factor having influence on contraction ratio of water jet and thus discharge capacity. Despite the use of USBR crest type in our model, there are various spillway profiles in practice. In this study, no detailed investigation of geometry effect has been conducted, but one additional design was addressed to present the changes in the discharge under same hydraulic conditions.

Ogee-shaped crests are composed of three main sections: upstream weir face, upstream quadrant and downstream quadrant, whose shapes change based on selected design criteria. Geometric features of the studied spillway was explained in Chapter 3.1.1. An alternative geometry was designed according to USACE by which downstream part of the weir is defined with Equation 4.1. Radii of curvatures are prescribed as $R_1=0.5H_d$, as $R_2=0.2H_d$, and $R_3=0.04H_d$. Its design criteria does not allow to make modifications on upstream inclination of weir and only valid for vertical slopes.

$$\frac{y}{H_d} = 0.50\left(\frac{x}{H_d}\right)^{1.85}, \qquad for\ x > 0 \tag{4.1}$$

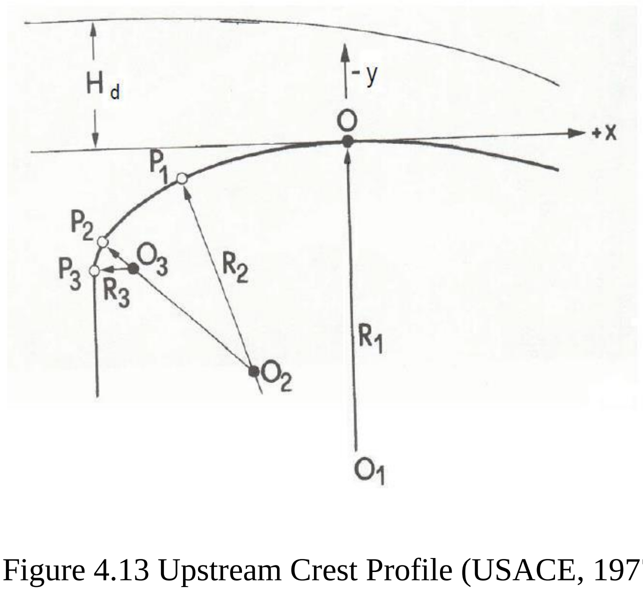

Figure 4.13 Upstream Crest Profile (USACE, 1977)

Table 4.1 Origin of Curvatures and Transition Point Locations (USACE, 1977)

Point	O_1	O_2	O_3	P_1	P_2	P_3
x/H_d	0	-0.105	-0.242	-0.175	-0.276	-0.2818
y/H_d	0.5	0.219	0.136	0.032	0.115	0.136

Design must be performed based on design head of the prototype, then converted to model scale on a CAD program. So, by considering the actual design head, H_d=15m, R_1, R_2 and R_3 are found to be 7.5 m, 3 m and 0.6 m respectively. Equation 4.1 yields $y=0.0500371x^{1.85}$ leading to a little milder slope than USBR. The other quantities are tabulated below:

Table 4.2 Station Coordinates of the Upstream Quadrant of the Alternative Design

Point	O_1	O_2	O_3	P_1	P_2	P_3
x(m)	0	-1.575	-3.63	-2.625	-4.14	-4.227
y(m)	7.5	3.285	2.04	0.48	1.725	2.04

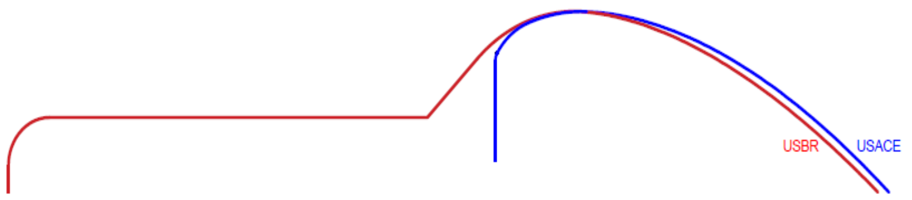

Figure 4.14 Crest Profiles According to USBR and USACE Design Criteria

Consequently, roughly 1%-2% change in discharge has emerged from several gate configurations on the alternative spillway with the same hydraulic conditions. Simulation results will be discussed in Chapter 5.4.

4.3.4 Grid Dependency

Grid cells were initially refined on the basis of comparison of numerical and experimental data. As a result, cell size of 5 mm at the vicinity of the gate opening and 10 mm at the outer fields were found be optimal. However, numerical solutions necessitate mesh sensitivity analysis to obtain consistent results not changing depending on further grid refinement. For this aim, grid cells in Mesh Block 3 in one of the 2D models were replaced with 4 mm. Accordingly, 8 mm cells were used in the rest of the domain to conform to 4 mm cells. Same procedure was repeated with 3 mm cells as a third case. Lastly, the nested block with 5 mm cells was removed from the original meshing domain to show performance of 10 mm cells solely on the discharge estimation.

Two random gate openings, d=5 cm and d=10 cm, were analyzed. By referring to Figure 4.15 and Figure 4.16, 10 mm cells seem inconvenient for the both cases. Other grids sizes result in close clustering of the discharge values with same head: There are around 1% underestimation or overestimation of discharge with 5 mm cells in comparison of the smaller ones. The errors found are acceptable because there is no increasing or decreasing trend depending on the mesh refinement. Even if the entire mesh structure, without changing cell size, is shifted a couple of millimeters in the x-direction, such errors may appear due to the changes in rendering process of sharp corners. Therefore, small discrepancies are unavoidable unless extremely fine cells are used, which boost computational effort exponentially. Elapsed times for a 90 seconds simulation, for H_c=60 cm and d= 5 cm, are roughly 0.5, 2, 4 and 7.5 hours for 10 mm, 5 mm, 4 mm and 3 mm cells, respectively with dual Intel® Xeon® E5-2650 processor. In connection with this, file size considerably increases upon refining of grids. As far as both computational efficiency and accuracy are concerned, simulations with 5 mm cells around the gate opening seem reasonable.

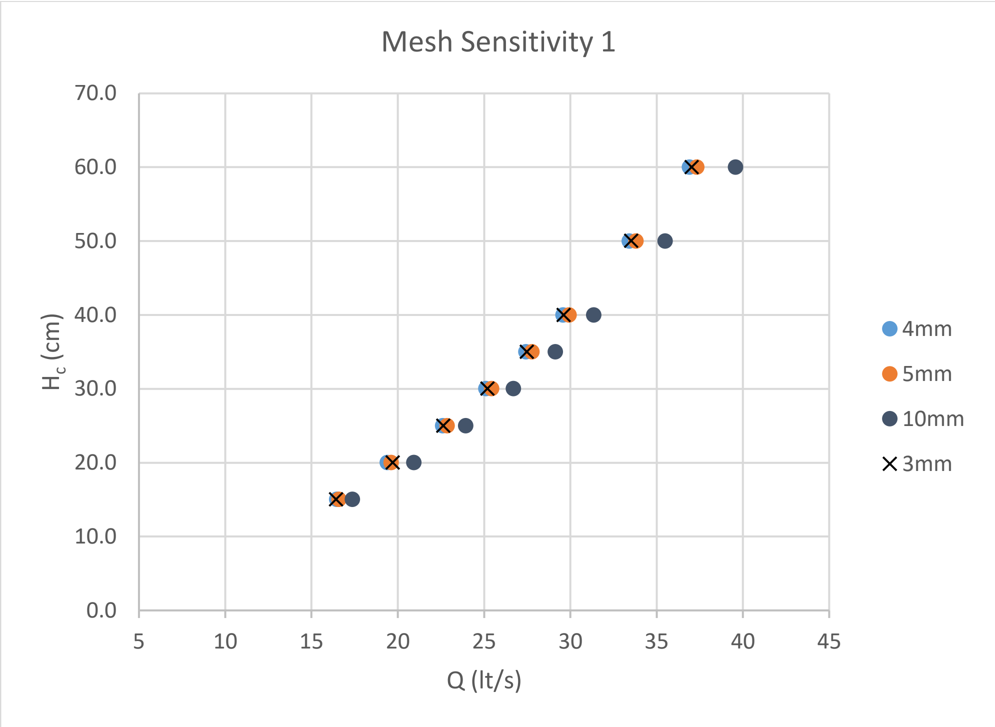

Figure 4.15 Mesh Sensitivity Analysis at d=5 cm (T1 Case)

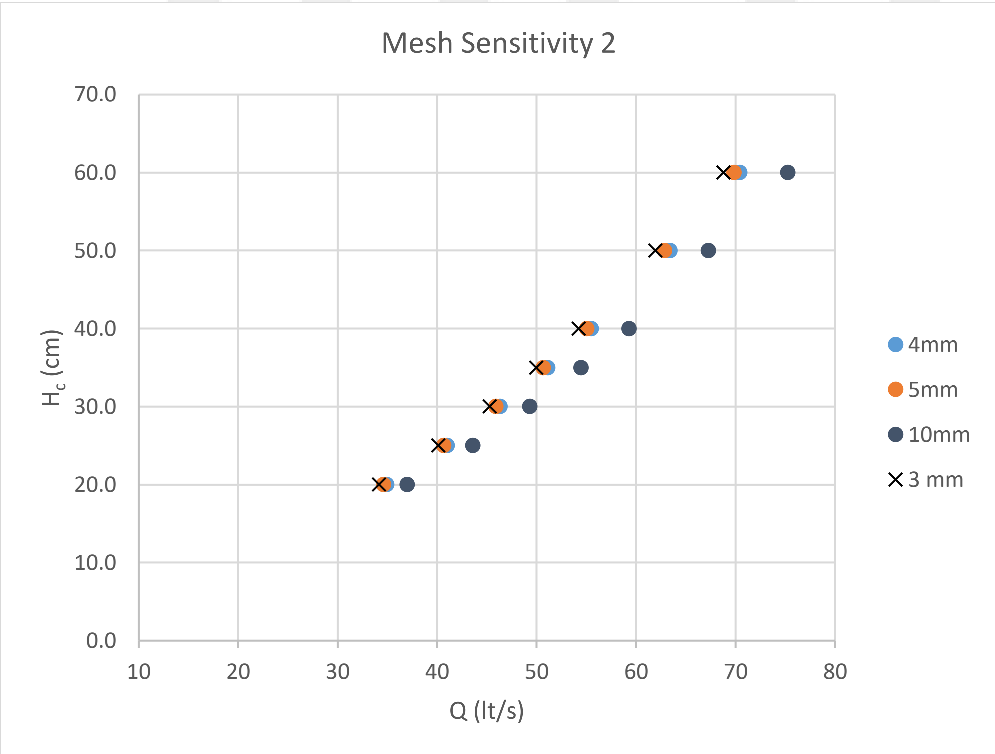

Figure 4.16 Mesh Sensitivity Analysis at d=10 cm (T1 Case)

4.3.5 Model-Scale Effect

All discharge investigations in this work have been conducted with the dimensions of the experimental model. However, in reality, model results probably will not reflect the truth when converted to prototype discharges. This is mainly caused by more distinctive viscous effect and surface tensions accompanied to the model even if scaled properly. In open channel problems, flow characteristic is mainly driven by body and gravitational forces. Similarity of ratio of these forces. i.e., Froude number, between the model and the prototype is required for calculation of corresponding velocity, flow rate, operation duration etc. from one to another. On the other hand, Reynolds number. ratio of body forces to viscous forces, diminishes upon the scaling, which means more turbulent flow in the prototype becomes less turbulent in the model.

$$(Fr)_{model} = (Fr)_{prototype}$$

$$\frac{V_m}{\sqrt{gL_m}} = \frac{V_p}{\sqrt{gL_p}} \tag{4.2}$$

$$\frac{V_m}{V_p} = \sqrt{\frac{L_m}{L_p}} = \sqrt{L_r} \tag{4.3}$$

$$Q_r = V_r A_r \tag{4.4}$$

$$\frac{Q_m}{Q_p} = \frac{V_m}{V_p}\frac{A_m}{A_p} \quad , \quad \frac{A_m}{A_p} = \left(\frac{L_m}{L_p}\right)^2 = (L_r)^2 \tag{4.5}$$

$$\frac{Q_m}{Q_p} = \sqrt{L_r} * (L_r)^2 \ , \ L_r = \frac{1}{30} \tag{4.6}$$

$$Q_p = 30^{2.5} Q_m$$

$$Q_p = 4925.5 Q_m \tag{4.7}$$

In above equations, L_r, A_r and V_r are length, area and velocity scale ratios, respectively. In order to observe scaling effect in our case, some of the 2D numerical models were simulated with the actual size of the prototype. Mesh sizes and grid cells were modified accordingly (e.g., 5 mm cells correspond to 150 mm in actual dimensions). Surprisingly, no apparent viscous effect comes forward when discharges were converted to each other with Equation 4.7 (Figs. 4.17 and 4.18). This is in fact an unexpected outcome. Some deviations must be visible practically. One explanation to this may be incapability of RNG turbulence model with computation of maximum turbulent mixing length dynamically. To see whether this problem originates from the RNG model or not, two extra turbulence models, Large Eddy Simulation (LES) and Laminar, were tested for the model with 12 cm gate opening and the corresponding prototype dimensions. Despite very small variation in discharge compared to RNG, no scaling effect was observed again. In addition to this, numerical model with another gate opening was simulated at 1/100 scale, in which viscous effect is expected to be far more prominent. However, the results do not change even though Reynolds number falls below 10^4 in this scenario. Related tables and graphs are attached in the Appendices. Based on these observations, it was concluded that Flow-3D somehow does not detect scaling effect independent of turbulence models and scale ratio.

$$R_e = \frac{V D_h}{\nu} \tag{4.8}$$

$$V = \frac{q}{d} \tag{4.9}$$

Equation 4.8 gives Reynolds number. Normally, D_h represents hydraulic depth that is four times of hydraulic radius in pressurized conduits. In our case, it was replaced with vertical gate opening, d, which can be considered as a meaningful parameter in 2D models. Average velocity, V, is simply found by dividing unit discharge, q, to vertical gate opening, and ν is kinematic viscosity, whose value for water is $1.035*10^{-6}$ at 20˚C.

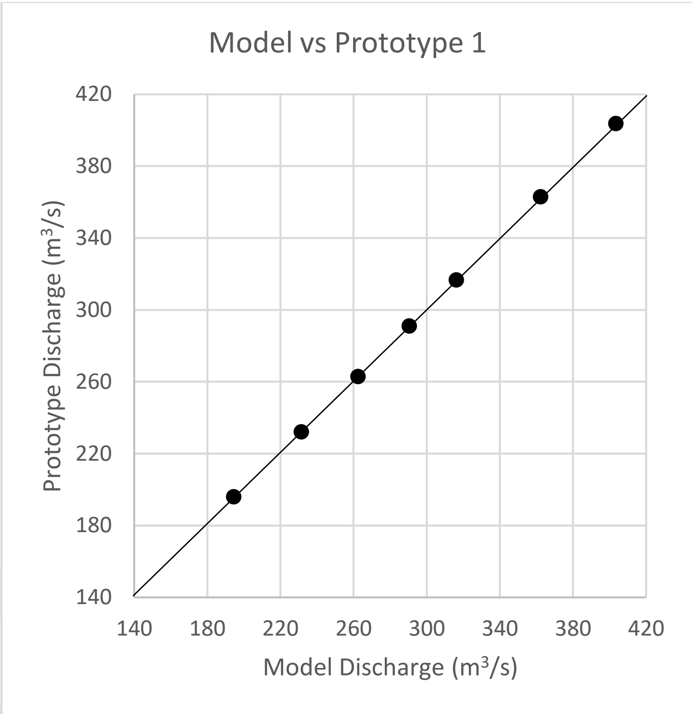

Figure 4.17 Comparison of Model and Prototype Discharges (d=12 cm & T1 Case)

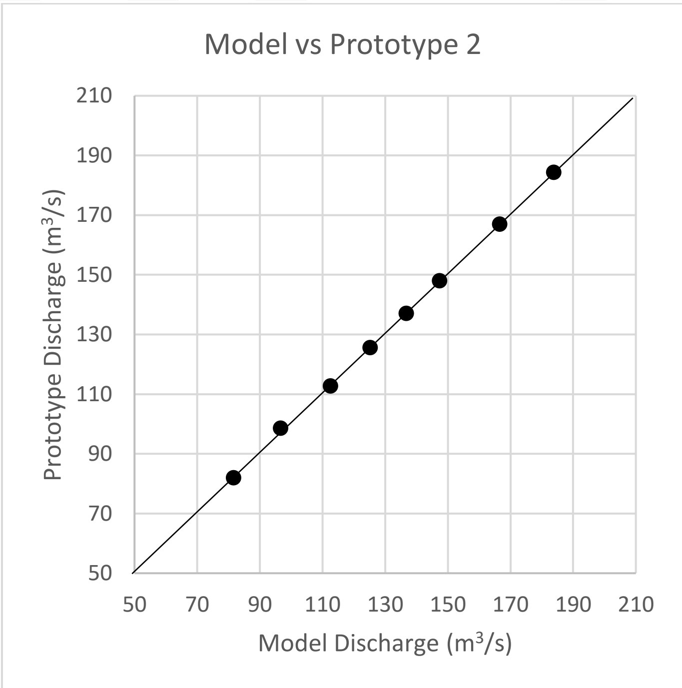

Figure 4.18 Comparison of Model and Prototype Discharges (d=5 cm & T1 Case)

Table 4.3 Model Discharges and Reynolds Numbers (d=12 cm)

Model (d=0.12 m) - RNG					*Converted Discharge (m^3/s)*	*Re*
	Z_{cr} (m)	Z_{res} (m)	H_c (m)	Q (m^3/s)		
T1	0.25	0.85	0.60	0.08190	***403.40***	263 768
	0.25	0.75	0.50	0.07356	***362.32***	236 908
	0.25	0.65	0.40	0.06417	***316.07***	206 667
	0.25	0.60	0.35	0.05895	***290.36***	189 855
	0.25	0.55	0.30	0.05325	***262.28***	171 498
	0.25	0.50	0.25	0.04698	***231.40***	151 304
	0.25	0.45	0.20	0.03945	***194.31***	127 053

Table 4.4 Prototype Discharges and Reynolds Numbers (d=360 cm)

Prototype (d=3.6 m) - RNG					*Re*
	Z_{cr} (m)	Z_{res} (m)	H_c (m)	Q (m^3/s)	
T1	7.5	25.5	18.0	***403.80***	43 349 436
	7.5	22.5	15.0	***363.00***	38 969 404
	7.5	19.5	12.0	***316.77***	34 006 441
	7.5	18.0	10.5	***291.03***	31 243 156
	7.5	16.5	9.0	***262.86***	28 219 002
	7.5	15.0	7.5	***232.16***	24 923 242
	7.5	13.5	6.0	***195.99***	21 040 258

Table 4.5 Model Discharges and Reynolds Numbers (d=5 cm)

Model (d=0.05 m) - RNG					*Converted Discharge (m^3/s)*	*Re*
	Z_{cr} (m)	Z_{res} (m)	H_c (m)	Q (m^3/s)		
T1	0.25	0.85	0.60	0.03732	***183.82***	120 193
	0.25	0.75	0.50	0.03381	***166.53***	108 889
	0.25	0.65	0.40	0.02993	***147.42***	96 393
	0.25	0.60	0.35	0.02777	***136.78***	89 436
	0.25	0.55	0.30	0.02543	***125.26***	81 900
	0.25	0.50	0.25	0.02286	***112.60***	73 623
	0.25	0.45	0.20	0.01962	***96.64***	63 188
	0.25	0.40	0.15	0.01658	***81.66***	53 398

Table 4.6 Prototype Discharges and Reynolds Numbers (d=150 cm)

Prototype (d=1.5 m) - RNG					*Re*
	Z_{cr} (m)	Z_{res} (m)	H_c (m)	Q (m^3/s)	
T1	7.5	25.5	18.0	***184.35***	19 790 660
	7.5	22.5	15.0	***167.01***	17 929 147
	7.5	19.5	12.0	***148.05***	15 893 720
	7.5	18.0	10.5	***137.10***	14 718 196
	7.5	16.5	9.0	***125.58***	13 481 481
	7.5	15.0	7.5	***112.80***	12 109 501
	7.5	13.5	6.0	***98.64***	10 589 372
	7.5	12.0	4.5	***81.99***	8 801 932

CHAPTER 5

ANALYSIS OF RESULTS

5.1 Outline of the Numerical Data

In the previous chapter, two-dimensional model was simulated at four gate positions, each of which has 12 different gate openings at various water levels. Three-dimensional model was only simulated with the same configuration of the experimental setup at five randomly selected gate openings. Results of these numerical solutions are presented in Tables 5.1 and 5.2. Total number of the 3D simulations are 34 and the 2D simulations are 498, which involve mesh sensitivity analyzes, model-scale effect and the other analyzes as well. All of them are referred in this thesis under the related topics.

Data of the 2D simulations are presented with H_c values whereas data of the 3D simulations are on the basis of effective head, which is more common parameter for gated discharge in the literature. The reason why head above the crest is considered in the 2D simulations is that effective heads vary with gate position and openings, which leads to complexity in point of comparison of large data sets. Effective head, *H*, in the numerical models are calculated by subtracting elevation of center of net gate openings, *h'*, from elevation of free water surface whereas head over the crest is simply 25 cm less than reservoir elevation independent of any gate configuration ($H = Z_{res} - h'$ & $H_c = Z_{res} - Z_{cr}$).

This work covers investigations of upstream heads leading to stable orifice flow. Transition region, where free flow suddenly turns into gated flow without any change of discharge, discussed by Mazumdar and Roy (1997) was not handled since transient head for this zone is different for rising and falling reaches. This situation may not be possible to be observed numerically. Blank cells in Table 5.1 indicate that free flow takes places in corresponding opening and water head. Actual transition heads were not investigated since it needs further investigation of various factors.

Table 5.1 Discharge data of the 2D Numerical Solutions

T1	Q (lt/s)											
Hc (cm)	d=3cm	d=4cm	d=5cm	d=6cm	d=7cm	d=8cm	d=9cm	d=10cm	d=11cm	d=12cm	d=13cm	d=14cm
60	22.38	29.25	36.90	43.62	50.64	56.55	63.72	69.84	76.13	81.90	87.60	93.39
50	20.37	26.54	33.41	39.45	45.78	51.06	57.42	62.85	68.99	73.56	78.63	83.82
40	18.09	23.52	29.57	34.83	40.29	44.78	50.37	55.05	60.17	64.17	68.49	72.84
35	16.83	21.85	27.42	32.28	37.29	41.46	46.44	50.67	55.22	58.95	62.82	66.75
30	15.48	20.06	25.11	29.49	33.99	37.98	42.15	45.90	49.82	53.25	56.64	60.00
25	14.00	18.08	22.59	26.43	30.36	33.81	37.41	40.65	43.85	46.98	49.71	52.53
20	12.34	15.86	19.58	22.98	26.27	28.98	32.01	34.62	37.35	39.45		
15	10.44	13.29	16.46	18.93								

T2	Q (lt/s)											
Hc (cm)	d=3cm	d=4cm	d=5cm	d=6cm	d=7cm	d=8cm	d=9cm	d=10cm	d=11cm	d=12cm	d=13cm	d=14cm
60	23.04	29.85	37.29	43.92	50.94	58.80	64.53	70.53	77.58	83.43	89.16	95.55
50	20.97	27.12	33.93	39.78	46.08	53.10	58.23	63.57	69.81	74.97	79.95	85.74
40	18.69	24.06	30.06	35.19	40.65	46.74	51.15	55.80	61.08	65.49	69.75	74.64
35	17.40	22.41	27.93	32.64	37.65	42.75	47.22	51.45	55.86	60.21	63.72	68.46
30	16.05	20.61	25.62	29.88	34.38	39.09	42.96	46.71	50.64	54.48	57.54	61.71
25	14.55	18.63	23.10	26.86	30.83	34.89	38.28	41.55	45.09	48.63	50.91	55.32
20	12.90	16.44	20.28	23.47	26.79	30.41	32.99	35.50	38.61	42.30		
15	10.99	13.93	17.01	19.54								

T3	Q (lt/s)											
Hc (cm)	d=3cm	d=4cm	d=5cm	d=6cm	d=7cm	d=8cm	d=9cm	d=10cm	d=11cm	d=12cm	d=13cm	d=14cm
60	23.40	30.51	37.68	44.76	51.42	58.53	65.30	71.67	77.70	83.58	91.50	96.48
50	21.39	27.84	34.26	40.74	46.65	53.04	59.04	64.74	70.11	75.33	82.32	86.79
40	19.14	24.87	30.54	36.24	41.40	46.95	52.14	56.55	61.68	66.00	72.06	75.87
35	17.91	23.22	28.47	33.75	38.52	43.56	48.20	52.71	57.00	60.99	66.30	69.90
30	16.59	21.48	26.28	31.05	35.34	39.87	44.10	48.15	51.90	55.44	60.30	63.24
25	15.18	19.58	23.85	28.14	31.92	35.91	39.57	43.05	46.29	49.41	53.28	56.79
20	13.59	17.48	21.21	24.86	28.05	31.47	35.12	37.47	40.80	43.80		
15	11.82	15.07	18.18	21.14								

T4	Q (lt/s)											
Hc (cm)	d=3cm	d=4cm	d=5cm	d=6cm	d=7cm	d=8cm	d=9cm	d=10cm	d=11cm	d=12cm	d=13cm	d=14cm
60	24.02	31.68	39.54	45.60	52.68	58.83	65.73	71.92	78.42	84.54	91.77	97.56
50	22.08	29.02	36.24	41.67	48.09	53.58	59.79	65.31	71.10	76.80	82.98	88.11
40	19.93	26.16	32.58	37.35	42.96	47.82	53.19	57.99	62.97	67.65	73.14	77.49
35	18.77	24.57	30.54	34.98	40.17	44.64	49.56	53.94	58.50	62.76	67.71	71.67
30	17.53	22.89	28.42	32.49	37.17	41.19	45.66	49.57	53.67	57.47	61.89	65.43
25	16.20	21.15	26.10	29.75	33.92	37.47	41.42	44.86	48.42	51.75	55.95	60.00
20	14.75	19.10	23.55	26.70	30.30	33.38	36.75	39.90	43.50			
15	13.13	17.66	20.69	23.33								

Table 5.2 Discharge data of the 3D Numerical Solutions

	h' (cm)	Z_{res} (cm)	H (cm)	Discharge (lt/s)
d=5cm	25.23	85	59.77	38.50
	25.23	75	49.77	35.34
	25.23	65	39.77	31.47
	25.23	55	29.77	27.06
	25.23	50	24.77	24.58
	25.23	40	14.77	18.67
d=7cm	26.57	85	58.43	51.74
	26.57	75	48.43	46.96
	26.57	65	38.43	41.61
	26.57	60	33.43	38.64
	26.57	50	23.43	31.98
	26.57	45	18.43	28.14
d=10cm	28.51	85	56.49	70.78
	28.51	75	46.49	63.68
	28.51	65	36.49	56.24
	28.51	60	31.49	52.00
	28.51	55	26.49	47.42
	28.51	50	21.49	42.44
	28.51	45	16.49	37.02
d=12cm	29.71	85	55.29	83.29
	29.71	75	45.29	75.02
	29.71	65	35.29	65.74
	29.71	60	30.29	60.25
	29.71	50	20.29	49.10
d=14cm	30.90	85	54.10	97.18
	30.90	75	44.10	87.24
	30.90	65	34.10	76.20
	30.90	60	29.10	70.01
	30.90	55	24.10	63.44
	30.90	50	19.10	56.36
	30.90	47	16.10	54.10

.

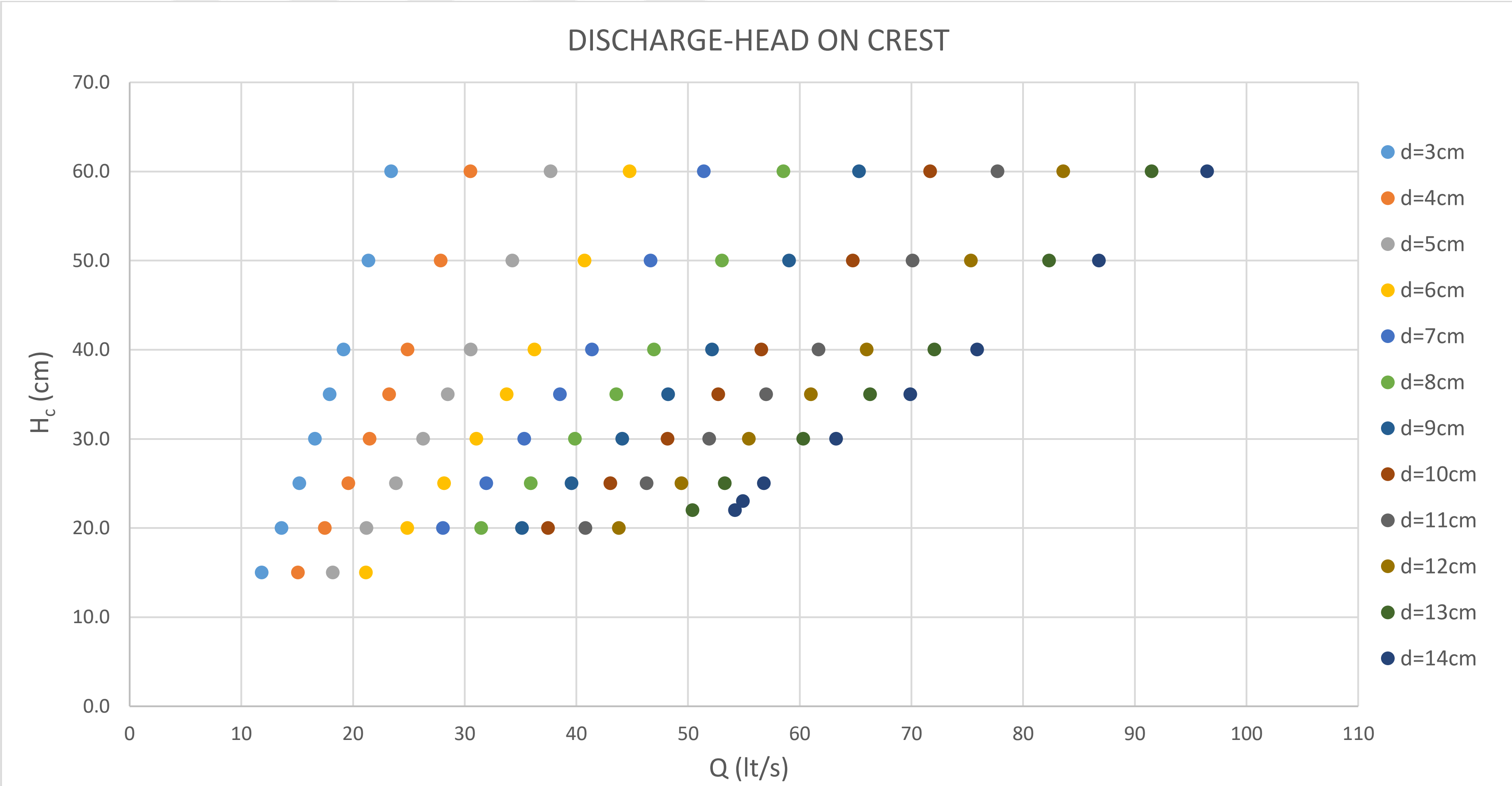

Figure 5.1 2D Numerical Results for Original Gate Position (T3)

5.2 Comparison of the Numerical and the Experimental Data

In this section, firstly, the 2D and the 3D numerical data are compared among themselves (Figs. 5.2 and 5.3), and then experiment data and numerical data are compared with each other (Figs. 5.4 and 5.5). Comparison graphs are based on effective heads and presented with randomly selected gate openings. Some additional numerical data not shown in Table 5.1 (H_c=12 cm for d=5 cm and H_c=47 cm and 48 cm for d=14 cm) were added to the last two graphs to widen the range of comparison. As can be seen from the first two graphs, the 3D and the 2D results agree with each other at the desired level, whose specific reason was explained in Chapter 4.3.1. Also, agreement of the numerical results in both dimensions with the laboratory observations are satisfactory. Small deviations of experimental data at higher stages might arise from the leakage problem discussed in Chapter 3.2.2. Furthermore, the results in Fig. 5.5 demonstrates that general discharge-head trend in upper stages starts to change its direction at very small upstream heads.

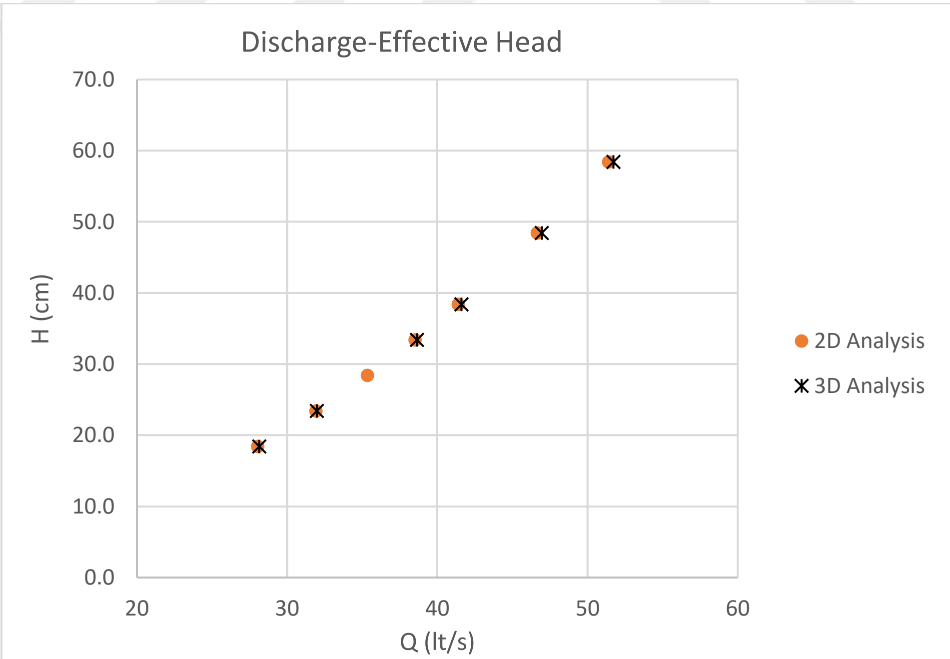

Figure 5.2 Comparison of the 2D and the 3D Numerical Results at d=7 cm

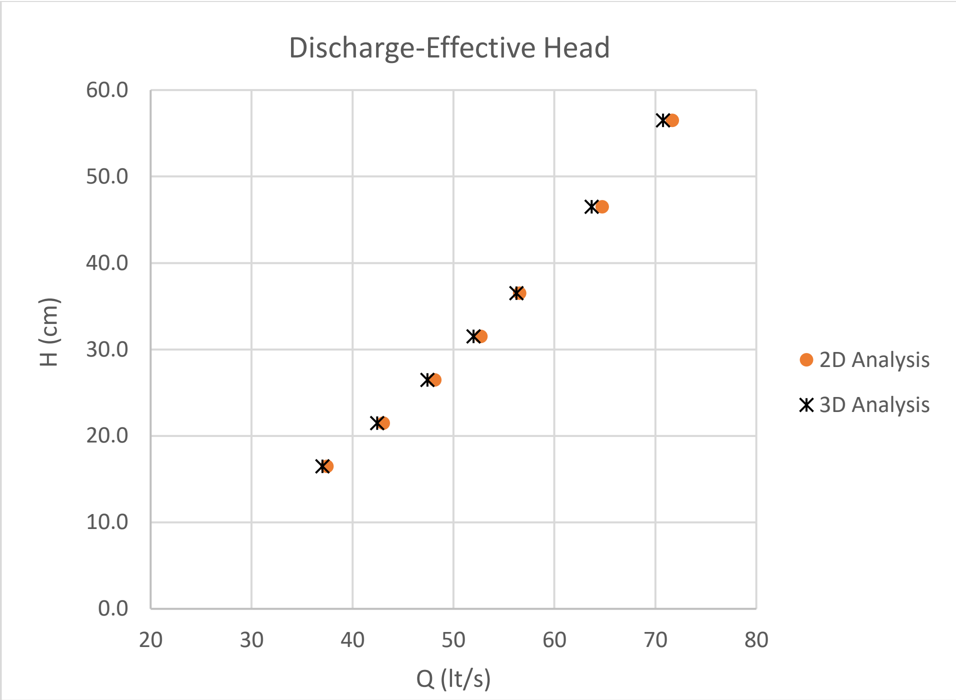

Figure 5.3 Comparison of the 2D and the 3D Numerical Results at d=10 cm

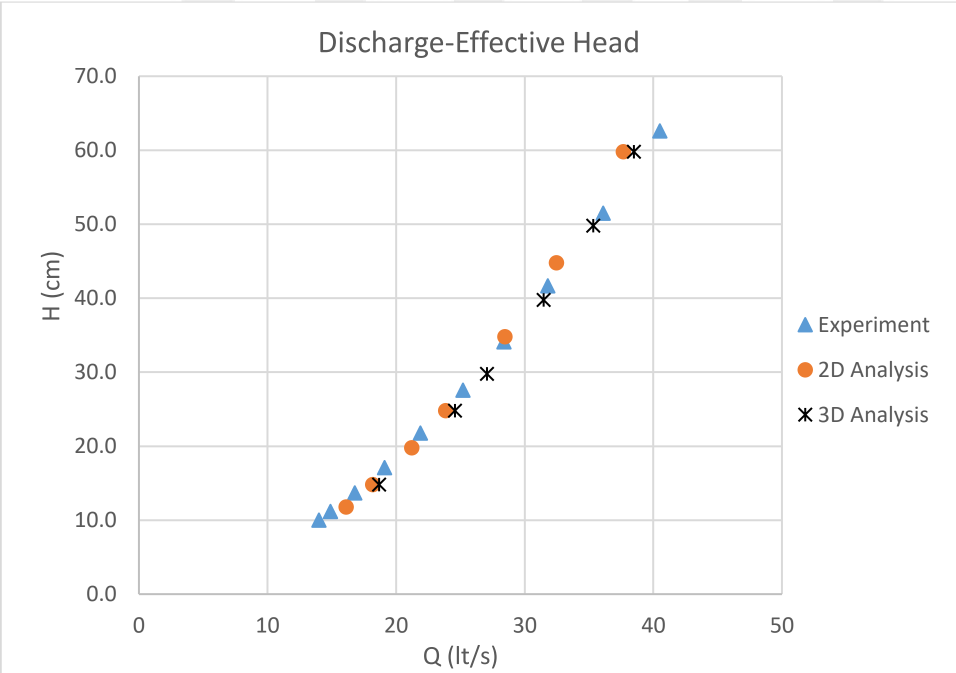

Figure 5.4 Comparison of the Numerical and the Experimental Results at d=5 cm

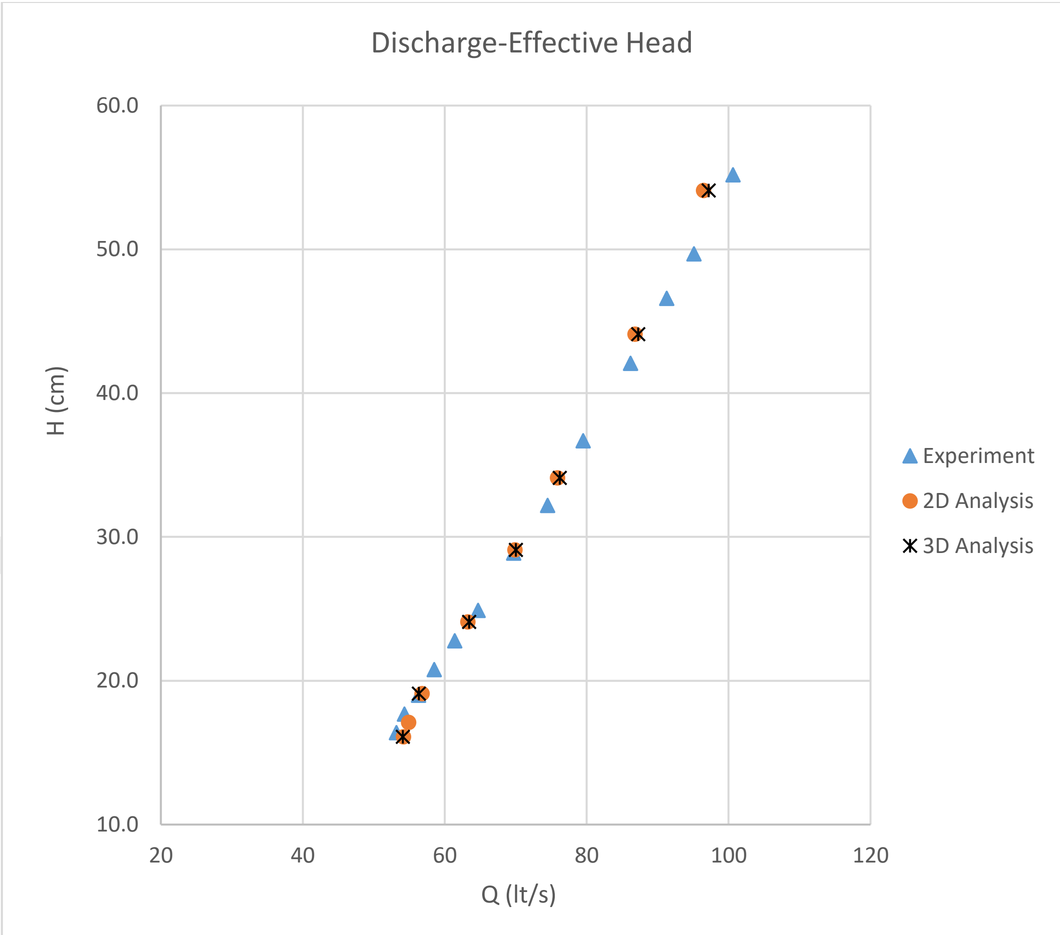

Figure 5.5 Comparison of the Numerical and the Experimental Results at d=14 cm

5.3 Derivation of New Discharge Equation

In the previous sections, it was revealed how gate position, crest geometry and water head influences characteristic of discharge under radial gates. As a result of the findings, a novel discharge formula was derived from the available data. For this, total 48 data set including 383 data acquired from the 2D numerical solutions were used. Data belonging to the experiments and the 3D simulations were excluded from the derivation since they were only utilized in the stage of comparison or verification of the 2D simulations. Also, the new equation is created on the basis of the original spillway geometry, which was designed with UBSR specification, even if effect of another crest shape was investigated.

$$C_g = \frac{Q}{dL\sqrt{2gH_c}} \tag{5.1}$$

The above formula is the modified version of the orifice equation. Its notation was described previously. General form of it is similar to the one suggested by USACE (1977) for gated spillways; however, it differentiates in several aspects. Instead of using effective head and net gate opening, head over the crest and vertical gate opening were preferred. The reason is to make discharge computation independent of changes in effective head because of the position of the gate. This effect is implicitly included in the coefficient, C_g, and thus, it eases complexity of the calculation due to effective head. Vertical gate opening is substituted into the equation for another reason. Its aim was to observe change in discharge passing through same vertical cross-sectional opening area in case of different gate positions. On the other hand, net gate opening is geometrically complicated and difficult to keep identical for all gate configurations. Under these considerations, C_g is not compatible with the definition of discharge coefficient given in the literature. Instead, gate factor would be more appropriate term.

First step for a new equation is to determine proper notation. The figure below shows the parameters and their notation in the current study.

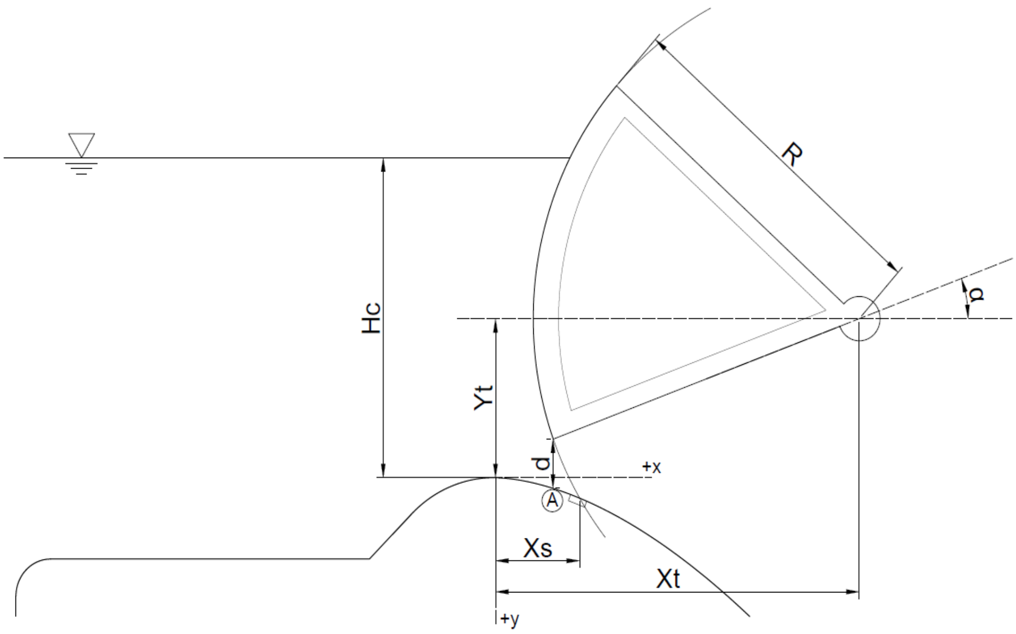

Figure 5.6 Descriptive Sketch

By using Equation 5.1, gate factors were calculated from the discharge values in Table 5.1 and presented in Table 5.3.

As can be inferred from Table 5.3, gate factor systematically reduces as water head above the crest falls, and vertical gate opening increases. This finding is quite consistent with the variation of discharge coefficients proposed by USBR (1960) for T1 situation. Gate factor also gradually goes up while the gate is shifted in downstream direction. Even if some exceptions are encountered at the small openings of T3 and T4 cases, where the gate seat is considered away from the crest, general trends enable a new equation to be derived easily.

Table 5.3 Radial Gate Factors for Different Gate Positions

T1	Cg (CFD)										
Hc (cm)	d=3cm	d=4cm	d=5cm	d=6cm	d=7cm	d=8cm	d=9cm	d=10cm	d=11cm	d=12cm	d=13cm	d=14cm
60	0.7246	0.7103	0.7169	0.7062	0.7027	0.6866	0.6877	0.6784	0.6723	0.6630	0.6545	0.6480
50	0.7225	0.7060	0.7110	0.6996	0.6959	0.6791	0.6789	0.6687	0.6673	0.6523	0.6436	0.6371
40	0.7173	0.6995	0.7035	0.6905	0.6847	0.6659	0.6658	0.6549	0.6507	0.6361	0.6267	0.6189
35	0.7134	0.6946	0.6974	0.6842	0.6774	0.6590	0.6562	0.6444	0.6384	0.6247	0.6145	0.6063
30	0.7087	0.6888	0.6898	0.6751	0.6669	0.6521	0.6432	0.6304	0.6221	0.6095	0.5984	0.5886
25	0.7021	0.6800	0.6797	0.6627	0.6525	0.6358	0.6254	0.6116	0.5997	0.5890	0.5753	0.5645
20	0.6918	0.6669	0.6586	0.6442	0.6312	0.6093	0.5982	0.5823	0.5711	0.5529		
15	0.6757	0.6451	0.6392	0.6126								

T2	Cg (CFD)										
Hc (cm)	d=3cm	d=4cm	d=5cm	d=6cm	d=7cm	d=8cm	d=9cm	d=10cm	d=11cm	d=12cm	d=13cm	d=14cm
60	0.7460	0.7249	0.7244	0.7110	0.7069	0.7140	0.6965	0.6851	0.6851	0.6753	0.6662	0.6630
50	0.7438	0.7214	0.7221	0.7055	0.7004	0.7063	0.6884	0.6764	0.6753	0.6648	0.6544	0.6516
40	0.7411	0.7155	0.7152	0.6977	0.6908	0.6950	0.6761	0.6638	0.6605	0.6492	0.6383	0.6342
35	0.7376	0.7124	0.7103	0.6918	0.6840	0.6795	0.6672	0.6543	0.6458	0.6381	0.6233	0.6218
30	0.7348	0.7077	0.7038	0.6840	0.6746	0.6711	0.6556	0.6416	0.6323	0.6236	0.6079	0.6054
25	0.7297	0.7007	0.6951	0.6735	0.6626	0.6561	0.6399	0.6251	0.6167	0.6097	0.5892	0.5945
20	0.7232	0.6913	0.6822	0.6579	0.6437	0.6393	0.6165	0.5971	0.5903	0.5929		
15	0.7113	0.6762	0.6606	0.6324								

T3	Cg (CFD)										
Hc (cm)	d=3cm	d=4cm	d=5cm	d=6cm	d=7cm	d=8cm	d=9cm	d=10cm	d=11cm	d=12cm	d=13cm	d=14cm
60	0.7577	0.7409	0.7320	0.7246	0.7135	0.7107	0.7048	0.6962	0.6861	0.6766	0.6837	0.6690
50	0.7587	0.7406	0.7291	0.7225	0.7091	0.7055	0.6980	0.6889	0.6782	0.6680	0.6738	0.6591
40	0.7589	0.7396	0.7266	0.7185	0.7035	0.6981	0.6892	0.6727	0.6670	0.6543	0.6594	0.6440
35	0.7592	0.7382	0.7241	0.7153	0.6998	0.6924	0.6810	0.6703	0.6590	0.6463	0.6485	0.6342
30	0.7595	0.7376	0.7219	0.7108	0.6934	0.6845	0.6730	0.6613	0.6480	0.6346	0.6371	0.6196
25	0.7613	0.7364	0.7176	0.7056	0.6860	0.6753	0.6615	0.6477	0.6331	0.6195	0.6166	0.6093
20	0.7619	0.7350	0.7135	0.6969	0.6740	0.6616	0.6563	0.6302	0.6238	0.6139		
15	0.7651	0.7316	0.7060	0.6841								

T4	Cg (CFD)										
Hc (cm)	d=3cm	d=4cm	d=5cm	d=6cm	d=7cm	d=8cm	d=9cm	d=10cm	d=11cm	d=12cm	d=13cm	d=14cm
60	0.7777	0.7693	0.7682	0.7382	0.7310	0.7143	0.7094	0.6986	0.6925	0.6843	0.6857	0.6769
50	0.7831	0.7720	0.7712	0.7390	0.7310	0.7126	0.7069	0.6949	0.6878	0.6810	0.6792	0.6697
40	0.7903	0.7780	0.7751	0.7405	0.7301	0.7111	0.7030	0.6898	0.6810	0.6706	0.6693	0.6584
35	0.7956	0.7811	0.7767	0.7414	0.7298	0.7096	0.7003	0.6859	0.6763	0.6651	0.6623	0.6510
30	0.8026	0.7860	0.7807	0.7437	0.7293	0.7072	0.6968	0.6808	0.6701	0.6578	0.6539	0.6419
25	0.8124	0.7955	0.7853	0.7460	0.7290	0.7047	0.6924	0.6749	0.6622	0.6488	0.6475	0.6448
20	0.8269	0.8031	0.7922	0.7484	0.7280	0.7018	0.6868	0.6711	0.6651			
15	0.8498	0.8573	0.8035	0.7550								

From the literature and this study, it is explicit fact that the most significant parameter for the discharge coefficient is the ratio of the gate opening to the water head regardless of the existence of different geometrical definitions for these variables. For this reason, alternative versions of this relationship such as d/H_c, H_c/d, square root of d/H_c etc. were also tested so as to obtain the best correlation with the gate factor. Consequently, in T1 scenario, third degree polynomial fitting was satisfied at the desired level (Figure 5.7) with the values provided in Table 5.4.

Table 5.4 $(d/H_c)^{0.5}$ Values

Hc (cm)	d=3cm	d=4cm	d=5cm	d=6cm	d=7cm	d=8cm	d=9cm	d=10cm	d=11cm	d=12cm	d=13cm	d=14cm
60	0.224	0.258	0.289	0.316	0.342	0.365	0.387	0.408	0.428	0.447	0.465	0.483
50	0.245	0.283	0.316	0.346	0.374	0.400	0.424	0.447	0.469	0.490	0.510	0.529
40	0.274	0.316	0.353	0.387	0.418	0.447	0.474	0.500	0.524	0.548	0.570	0.591
35	0.293	0.338	0.378	0.414	0.447	0.478	0.507	0.534	0.560	0.585	0.609	0.632
30	0.316	0.365	0.408	0.447	0.483	0.516	0.548	0.577	0.605	0.632	0.658	0.683
25	0.346	0.400	0.447	0.490	0.529	0.565	0.600	0.632	0.663	0.693	0.721	0.748
20	0.387	0.447	0.500	0.547	0.591	0.632	0.670	0.707	0.741	0.774		
15	0.447	0.516	0.577	0.632								

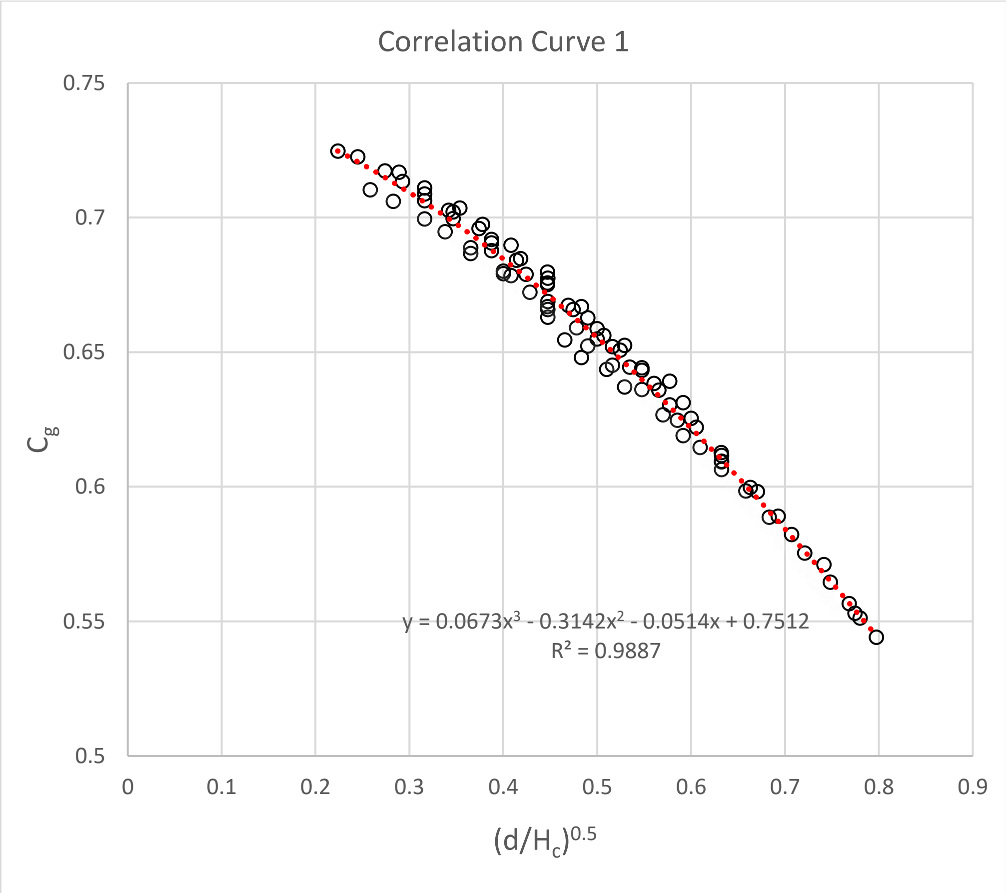

Figure 5.7 Gate Factors of T1 Configuration

For T1:

$$C_g = 0.0673\left(\sqrt{\frac{d}{H_c}}\right)^3 - 0.3142\left(\sqrt{\frac{d}{H_c}}\right)^2 - 0.0514\left(\sqrt{\frac{d}{H_c}}\right) + 0.7512 \qquad (5.2)$$

R^2 on Figure 5.7 is a statistical tool called coefficient of determination to measure how well regression model represents scattered data. As its value gets closer to one, statistical power of model enhances provided that no overfitting occurs, and with R^2=0.9887, above equation seems pretty reasonable. The gate factors for T1 case were recalculated with Equation 5.2 and presented in Table 5.5.

Validity of $(d/H_c)^{0.5}$ values in Equation 5.2 ranges from 0.2 to 0.8. Numerical analyzes show that free flow takes place if d/H_c is simply much higher than 0.64. As *d* gets smaller, the regression equation reaches its constant value, 0.7512, asymptotically. To see actual behavior of C_g values as d/H_c approaches to zero, two additional numerical simulations (*d*=1 cm and *d*=2 cm for H_c=60 cm) with much finer grid sizes (2 mm) were performed. As a result, C_g values were found to be 0.786 and 0.746 respectively for *d*=1 cm and *2* cm whereas our polynomial equation yields 0.739 and 0.732, respectively, which means it is not able to predict the sharp change in gate factors. In Figure 2.1, USBR (1960) also discovered that when d/H_c goes below 0.1, discharge coefficient starts to increase drastically. So, this region needs further experimental and numerical investigation, and the suggested equation should not be used outside of the given interval of validity.

In the next stage of formulation, the optimized results in Table 5.5 were divided to the corresponding gate factors of the other gate configurations (i.e., same head and opening of T2, T3 and T4) to obtain increase rates of discharge. The reason why optimized values are used rather than original T1 values is to eliminate additional errors that will be introduced by the second stage of derivation. Increase ratios found are presented in Table 5.6

Table 5.5 Recalculated Gate Factors for T1 Scenario

T1	Cg (Optimized)											
Hc (cm)	d=3cm	d=4cm	d=5cm	d=6cm	d=7cm	d=8cm	d=9cm	d=10cm	d=11cm	d=12cm	d=13cm	d=14cm
60	0.7247	0.7181	0.7118	0.7057	0.6997	0.6938	0.6881	0.6824	0.6769	0.6714	0.6660	0.6606
50	0.7207	0.7130	0.7057	0.6985	0.6915	0.6847	0.6780	0.6714	0.6649	0.6585	0.6522	0.6460
40	0.7149	0.7057	0.6967	0.6881	0.6796	0.6714	0.6633	0.6554	0.6475	0.6398	0.6323	0.6248
35	0.7109	0.7005	0.6905	0.6808	0.6714	0.6622	0.6531	0.6442	0.6355	0.6269	0.6184	0.6100
30	0.7057	0.6938	0.6824	0.6714	0.6606	0.6501	0.6398	0.6297	0.6198	0.6100	0.6004	0.5909
25	0.6985	0.6847	0.6714	0.6585	0.6460	0.6338	0.6218	0.6100	0.5985	0.5872	0.5760	0.5650
20	0.6881	0.6714	0.6554	0.6398	0.6248	0.6100	0.5956	0.5815	0.5677	0.5541		
15	0.6714	0.6501	0.6297	0.6100								

Table 5.6 Ratio of Gate Factors of T2&T3&T4 to Recalculated Gate Factors of T1

T2/T1	Cg Ratio of T2 to T1												Average
Hc (cm)	d=3cm	d=4cm	d=5cm	d=6cm	d=7cm	d=8cm	d=9cm	d=10cm	d=11cm	d=12cm	d=13cm	d=14cm	Ratio
60	1.0295	1.0205	1.0106	1.0069	1.0059	1.0398	1.0127	1.0099	1.0190	1.0187	1.0178	1.0231	**1.0179**
50	1.0295	1.0219	1.0156	1.0084	1.0066	1.0400	1.0141	1.0115	1.0119	1.0192	1.0168	1.0229	**1.0182**
40	1.0332	1.0230	1.0166	1.0103	1.0089	1.0438	1.0155	1.0136	1.0151	1.0206	1.0184	1.0247	**1.0203**
35	1.0339	1.0256	1.0186	1.0112	1.0097	1.0311	1.0168	1.0154	1.0116	1.0214	1.0143	1.0256	**1.0196**
30	1.0368	1.0274	1.0203	1.0132	1.0115	1.0292	1.0192	1.0176	1.0165	1.0231	1.0159	1.0285	**1.0216**
25	1.0393	1.0304	1.0226	1.0163	1.0155	1.0319	1.0233	1.0221	1.0283	1.0351	1.0241	1.0531	**1.0285**
20	1.0454	1.0366	1.0358	1.0213	1.0198	1.0493	1.0306	1.0254	1.0337	1.0722			**1.0370**
15	1.0527	1.0482	1.0334	1.0322									**1.0416**

T3/T1	Cg Ratio of T3 to T1												Average
Hc (cm)	d=3cm	d=4cm	d=5cm	d=6cm	d=7cm	d=8cm	d=9cm	d=10cm	d=11cm	d=12cm	d=13cm	d=14cm	Ratio
60	1.0456	1.0431	1.0211	1.0261	1.0154	1.0350	1.0248	1.0262	1.0206	1.0205	1.0445	1.0324	**1.0296**
50	1.0501	1.0490	1.0254	1.0327	1.0190	1.0388	1.0282	1.0301	1.0162	1.0241	1.0469	1.0346	**1.0329**
40	1.0580	1.0574	1.0328	1.0405	1.0276	1.0485	1.0351	1.0272	1.0251	1.0285	1.0521	1.0406	**1.0395**
35	1.0642	1.0627	1.0383	1.0455	1.0330	1.0507	1.0379	1.0403	1.0322	1.0346	1.0554	1.0460	**1.0451**
30	1.0717	1.0708	1.0466	1.0529	1.0397	1.0498	1.0463	1.0490	1.0418	1.0411	1.0646	1.0526	**1.0522**
25	1.0843	1.0830	1.0558	1.0647	1.0514	1.0621	1.0577	1.0590	1.0556	1.0517	1.0718	1.0794	**1.0647**
20	1.1013	1.1021	1.0832	1.0818	1.0678	1.0859	1.0972	1.0823	1.0924	1.1103			**1.0904**
15	1.1322	1.1339	1.1045	1.1167									**1.1218**

T4/T1	Cg Ratio of T4 to T1												Average
Hc (cm)	d=3cm	d=4cm	d=5cm	d=6cm	d=7cm	d=8cm	d=9cm	d=10cm	d=11cm	d=12cm	d=13cm	d=14cm	Ratio
60	1.0733	1.0831	1.0715	1.0454	1.0403	1.0403	1.0315	1.0298	1.0301	1.0322	1.0476	1.0447	**1.0475**
50	1.0839	1.0934	1.0847	1.0563	1.0505	1.0494	1.0413	1.0391	1.0306	1.0440	1.0553	1.0512	**1.0566**
40	1.1017	1.1122	1.1018	1.0724	1.0663	1.0679	1.0560	1.0534	1.0465	1.0542	1.0679	1.0638	**1.0720**
35	1.1153	1.1245	1.1138	1.0836	1.0772	1.0767	1.0672	1.0645	1.0594	1.0646	1.0778	1.0737	**1.0832**
30	1.1324	1.1411	1.1318	1.1017	1.0936	1.0845	1.0833	1.0800	1.0773	1.0792	1.0927	1.0905	**1.0990**
25	1.1571	1.1698	1.1554	1.1256	1.1173	1.1083	1.1072	1.1036	1.1042	1.1015	1.1255	1.1422	**1.1265**
20	1.1953	1.2043	1.2028	1.1619	1.1534	1.1518	1.1481	1.1525	1.1647				**1.1705**
15	1.2577	1.3288	1.2570	1.2324									**1.2690**

Average of the ratios were calculated for each water head for all the gate positions in the rightmost columns in Table 5.6, and thus, ratio fluctuation in 12 gate openings were reduced to a single value. It can be inferred from the above table that the average ratio always grows as water head falls, and the growth becomes almost exponential in case the gate is designed farther from the crest (See Figure 5.8). This phenomenon can be explained by the ascending amount of change between the values of effective head and head over the crest. Since gate factor implicitly includes this difference, its effect becomes more pronounced numerically under the mentioned conditions.

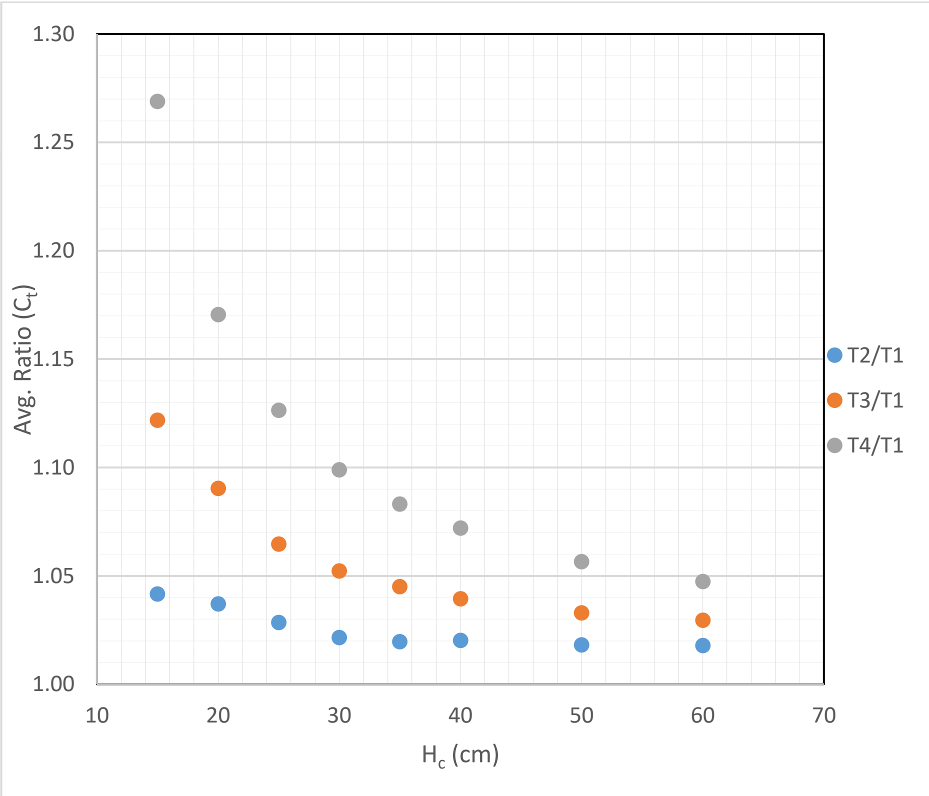

Figure 5.8 Water Head vs Average Ratio Graph

The average ratio is denoted by C_t. As seen in Figure 5.8, it rises as the gate is being shifted from upstream to downstream along with the drop in the head. Second non-dimensional parameter is possible to be generated based on these trends. For this, simply ratio of the horizontal distance between apex of the crest and the gate seat, X_s, to head above the crest, H_c, was considered, and its relationship with the average ratios was tested. Results are presented below:

Table 5.7 X_s/H_c vs Average Ratio

H_d=50cm	X_s (cm)	H_c (cm)	X_s/H_c	Avg.Ratio
T2 (Xs/Hd=0.15)	7.26	60	0.1210	1.0179
	7.26	50	0.1452	1.0182
	7.26	40	0.1815	1.0203
	7.26	35	0.2074	1.0196
	7.26	30	0.2420	1.0216
	7.26	25	0.2904	1.0285
	7.26	20	0.3630	1.0370
	7.26	15	0.4840	1.0416
T3 (Xs/Hd=0.31)	15.42	60	0.2570	1.0296
	15.42	50	0.3084	1.0329
	15.42	40	0.3855	1.0395
	15.42	35	0.4406	1.0451
	15.42	30	0.5140	1.0522
	15.42	25	0.6168	1.0647
	15.42	20	0.7710	1.0904
	15.42	15	1.0280	1.1218
T4 (Xs/Hd=0.50)	25.17	60	0.4195	1.0475
	25.17	50	0.5034	1.0566
	25.17	40	0.6293	1.0720
	25.17	35	0.7191	1.0832
	25.17	30	0.8390	1.0990
	25.17	25	1.0068	1.1265
	25.17	20	1.2585	1.1705
	25.17	15	1.6780	1.2690

Only using the range of values in Table 5.7 second degree polynomial fitting with R^2=0.9968 is possible; however, it intersects with y-axis at 1.0079, which causes discontinuity between T1 and T2 cases and thus requires a conditional equation. Therefore, the regression equation was forced to have y- intercept with 1.0 to solve this problem (Figure 5.9). As a result, third degree polynomial correlation with almost same statistical power (R^2=0.9966) was achieved. The new parameter can now be used as a product of the previous one. This situation might be arranged as in Equation 5.2. It should be remarked that the range of validity for relative gate seat position, X_s/H_d, in Equation 5.5 is between 0 and 0.5.

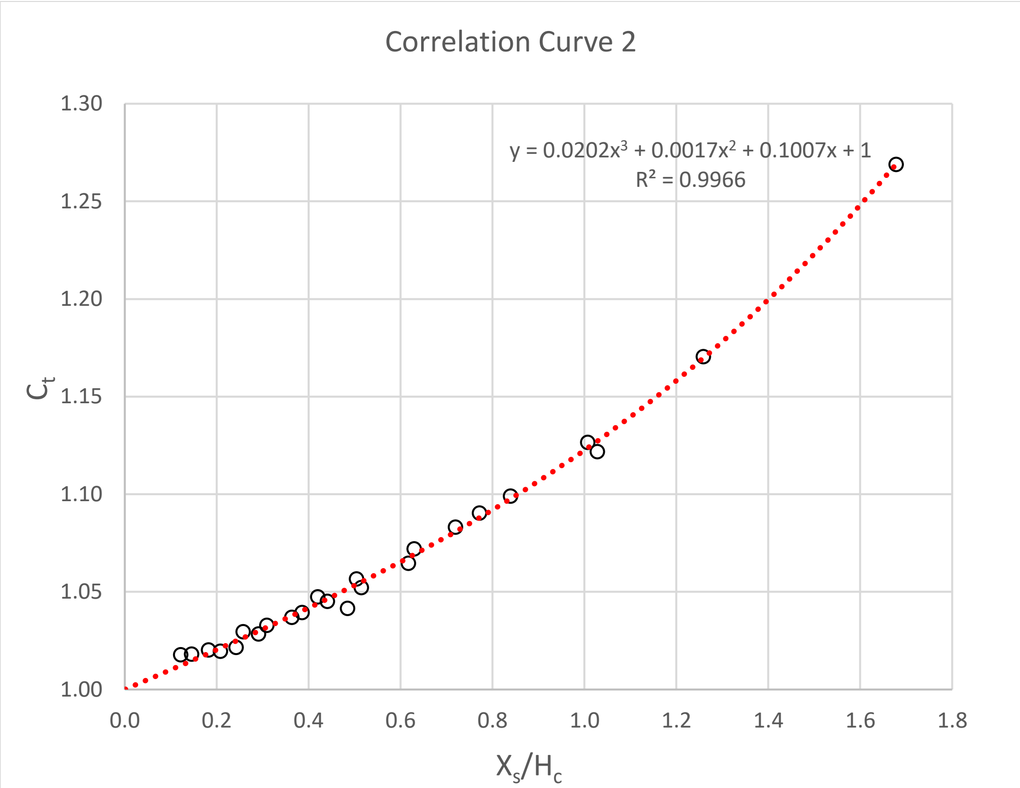

Figure 5.9 X_s/H_c vs Average Ratio Graph

$$Q = C_g C_t d L \sqrt{2 g H_c} \tag{5.3}$$

$$C_g = 0.0673\left(\frac{d}{H_c}\right)^{1.5} - 0.3142\left(\frac{d}{H_c}\right) - 0.0514\left(\frac{d}{H_c}\right)^{0.5} + 0.7512 \tag{5.4}$$

$$C_t = 0.0202\left(\frac{X_s}{H_c}\right)^{3} + 0.0017\left(\frac{X_s}{H_c}\right)^{2} + 0.1007\left(\frac{X_s}{H_c}\right) + 1.000 \tag{5.5}$$

where C_g is gate factor derived based on T1 case, and C_t is correction of C_g due to different gate positions. By using equations above, discharge under radial gates can easily be computed on an Excel sheet just knowing d and H_c variables together with X_s, which is a constant design parameter. Note that when X_s=0 in Equation 5.5, the equation yields its constant value, 1.0, which corresponds to T1 case.

5.4 Error Percentages of the Suggested Equation

After deriving a new discharge formula, its performance was tested by comparing its results with real numerical data. For this, absolute errors were calculated for each numerically found data with Equation 5.6.

$$Absolute\ Error = \left|\frac{Q_{calc} - Q_{cfd}}{Q_{cfd}}\right| * 100 \quad (5.6)$$

where Q_{calc} is result of proposed equation, and Q_{cfd} is that of numerical solution. The table including all error percentages was attached in the Appendices. Following table is a summary showing average errors corresponding to each head.

Table 5.8 Average Errors at Different Gate Configurations

H_c (cm)	T1 (%)	T2 (%)	T3 (%)	T4 (%)
60	0.81	0.69	0.68	1.77
50	0.68	0.68	0.69	1.73
40	0.62	0.63	0.76	1.74
35	0.55	0.57	0.67	1.71
30	0.48	0.57	0.68	1.71
25	0.49	0.70	0.68	1.68
20	0.49	0.95	0.74	1.46
15	0.83	0.88	0.58	1.77
Mean	**0.60**	**0.69**	**0.69**	**1.70**
Std. Dev.	**0.40**	**0.55**	**0.59**	**1.09**

Mean absolute errors (MAE) for T1, T2, T3 and T4 cases are 0.60%, 0.69%, 0.69% and 1.70%, respectively. MAE of the new formula is quite satisfactory when compared to methods in the literature. Slight increment in MAE at T4 case arises from the change in flow characteristics at limit conditions. Normally, the general trend shows that gate factors gradually reduce as head drops. Interestingly, at small gate openings of T4 and T3 configurations (*d*=3, 4, 5 and 6 cm for T4 and *d*=3 cm for T3), the trend is totally reversing, and the gate factor starts to increase from top to bottom. This unexpected behavior leads the equation to make relatively poor estimates at given situations and affects the MAE negatively. To inform designer, a constrain preventing this effect might be developed. It is inferred from the simulations that quantity of X_s/d varies from 0 to 8.4, and the mentioned effect appears when X_s/d is greater than approximately five. Values exceeding this limit too much may result in divergency from the formula.

As previously stated, the formulation was on the basis of data belonging to the spillway designed with USBR specification. So, MAE needs further investigations in case of geometrical changes in the crest. For this purpose, the suggested equation was tested on USACE crest type designed in Chapter 4.3.3. Parameters, d, H_c and X_s were arbitrarily chosen to create a meaningful sample, and eight simulations were performed accordingly. Details and absolute errors were tabulated below. The new MAEs found are still satisfactory and more acceptable in that USBR spillway design would not be practically possible for all the time.

Table 5.9 Comparison of the Simulation Results of USACE Design with the Suggested Equation

Simulation No.	d (cm)	H_c (cm)	X_s (cm)	Q_{cfd} (lt/s)	Q_{calc} (lt/s)	Abs. Error (%)
1	8	50	0	53.58	52.51	2.00
2	8	25	0	33.18	33.68	1.51
3	14	60	0	92.34	95.20	3.10
4	14	40	0	71.97	73.51	2.14
5	10	60	14.81	70.47	72.02	2.20
6	10	50	14.81	63.60	65.01	2.22
7	5	50	14.81	35.25	34.16	3.08
8	5	20	14.81	21.49	21.10	1.80

5.5 Geometric Derivation of Vertical Gate Opening

In design or operation stage of radial gate, determination of vertical gate opening could not be comfortable because of geometric complexities. Therefore, it has to be associated with more concrete parameter like rotation angle of the gate (α). By referring to Figure 5.6, the procedure below shows steps of its derivation:

For 0.1< X_s/H_d :

General form of downstream weir equation:

$$\frac{y}{H_d} = K\left(\frac{x}{H_d}\right)^n \tag{5.7}$$

It can be rearranged by leaving y on the left-hand side:

$$y = K\, H_d^{1-n}\, x^n \tag{5.8}$$

d can be expressed as the difference between the distance from point A in Figure 5.6 to the horizontal datum line and vertical projection of the radius, from the gate lip to the rotation axis.

$$d = Y_t + y - R\sin\alpha \tag{5.9}$$

By substituting Eqn. 5.8 to Eqn. 5.9, we get:

$$d = Y_t + K\, H_d^{1-n}\, x^n - R\sin\alpha \tag{5.10}$$

x is defined by subtraction of horizontal projection of the gate radius from the distance between the crest and the trunnion point:

$$x = X_t - R\cos\alpha \tag{5.11}$$

By plugging Eqn. 5.11 into Eqn. 5.10, final form of the relationship is obtained:

$$d = Y_t + K\, H_d^{1-n}\, (X_t - R\cos\alpha)^n - R\sin\alpha \tag{5.12}$$

Min(α)=0 and Max(α) is found by equating *d* to zero:

$$Y_t + K\, H_d^{1-n}\, (X_t - R\cos\alpha_{max})^n = R\sin\alpha_{max} \tag{5.13}$$

Numerical Example:

Following lengths were directly measured from AutoCAD software for USACE spillway (K=0.5, n=1.85 and H_d=50cm) to determine whether the derived relationship yields satisfactory result or not.

d =10 cm

α=18.44°

Y_t=28.69 cm

X_t=69.35 cm

R=62.89 cm

d=28.69+0.5*$50^{-0.85}$ *(69.35-62.89*cos $(18.44))^{1.85}$-62.89*sin (18.44) =9.998 cm

With two decimal figures, 0.02% error is achieved for the selected example. In case of four decimal figures, the error is found as 0.01%. So, leaving two figures after decimal point is good enough provided that the inputs are measured meticulously.

For X_s/H_d =0:

$$d \cong Y_t - R\ sin\alpha \tag{5.14}$$

Elevation difference between gate lip and apex of the spillway might be used in calculation of small gate openings. However, as previously stated, d is the distance from the gate lip point to its vertical projection point on the spillway surface (i.e., point A in Figure 5.6). It is independent of crest point wherever gate seat is located. When X_s/H_d=0, point A coincides with upstream of spillway face, and as the gate is being lifted, it shifts more in the upstream direction. In this context, at greater openings, divergence from Equation 5.14 will be more evident. To prevent this, if possible, designer should alternatively create d versus α table using a CAD program. Operator may use this relationship table for the sake of better control of discharge.

To conserve computational accuracy, the suggested discharge formula needs some restrictions. Otherwise, unexpected outcome might emerge depending on violating domain of this study. To this end, intervals of the meaningful dimensionless parameters are attached to give preliminary idea for interested users before commencing computation.

Table 5.10 Constrains of the Suggested Equation

Parameter	X_s/H_c	X_s/d	X_s/H_d	d/H_c	α	C_g	C_t
Min.	0	0	0	0.05	17˚	0.55	1.00
Max.	1.68	8.38	0.50	0.56	34˚	0.72	1.27

5.6 Comparison of Empirical Equations with the Novel Equation

In the last stage of this work, the suggested equation was compared to a couple of empirical equations to understand the progress made. Since methods of USBR (1960) and USACE (1977) were widely utilized in the design processes, their performance was tested against the new one. Two gate configurations, T1 and T3, and three gate openings, 5 cm, 10 cm and 14 cm, were randomly chosen. Unfortunately, both of the old methods were not able to be compared in the same case due to disagreement of their constraints. For instance, the method of USBR is only valid for which radial gate is seated on crest (i.e., T1 case). Although USACE offers a discharge coefficient rating curve for this situation, it stipulates minimum lip angles to be 83˚. However, maximum lip angle in the studied model is 76˚. Extrapolation of the curve is possible, but it was not preferred for the sake of accuracy of the work. This problem stems from the fact that USACE used a single laboratory model to develop the rating curve. Most probably, trunnion point in the model was designed lower than that of the studied model, which allows greater lip angles. In this context, lip angle is not a convenient parameter without involving additional restrictions to the formula. For other gate positions, minimum lip angle has to be equal to or greater than 50˚, which is satisfied at 10 cm and 14 cm gate openings of T3 scenario.

By referring to Figure 2.1 and Figure 2.2, calculation was done with the following equations:

USBR (1960):

$$Q = \frac{2}{3}\sqrt{2g}CL_{eff}\left(H_1^{\frac{3}{2}} - H_2^{\frac{3}{2}}\right) \tag{5.15}$$

H_1 and H_2 are in terms of total head but may be treated as net head as velocity head is negligibly small. Effective crest length is calculated with the following expression:

$$L_{eff} = L_{net} - 2\left(N_pK_p + K_a\right)H_c \tag{5.16}$$

in which K_a and K_p contraction coefficients due to abutments and piers, respectively. N_p indicates number of piers. The respective model does not include abutments and has pointed-nosed piers whose contraction effect is assumed to be zero; that is, net crest width is same with effective width.

USACE (1977):

$$Q = CL_{net}D\sqrt{2gH_{eff}} \tag{5.17}$$

Details of the calculation for each method can be seen in Table 5.11 and Table 5.12. In Figure 2.1, *d* is replaced with *d** so as not to cause confusion with the gate opening, *d*, specially defined for this work. These quantities are not exactly same as previously clarified.

Consequently, unlike the consensus in the literature, USBR (1960) yields close results to the numerical solution and the new equation for selected cases (*d*=5 cm and *d*=10 cm for T1). This may be related to the fact that discharge on USBR crest type is investigated in this study. However, it is unable to show the same performance at different gate positions and crest shapes according to various researches done together with the current one. On the other hand, method of USACE (1977) does not seem adequate to estimate flow rate precisely, and this may not only arise from the mentioned reason, but also their design criteria require a USACE type of crest.

Table 5.11 Comparison Table for USBR (1960)

	USBR							Novel Formula				Numeric Sol.	
	d* (cm)	H1(cm)	H2=H1-d*	d*/H1	C	L_{eff} (cm)	Q(lt/s)	Hc (cm)	Cg*Ct	Xs (cm)	Q(lt/s)	H (cm)	Gauge (lt/s)
d=5cm	4.97	60	55.03	0.08	0.718	30	35.96	60	0.712	0	36.63	60	36.90
	4.97	50	45.03	0.10	0.713	30	32.46	50	0.706	0	33.15	50	33.41
	4.97	40	35.03	0.12	0.708	30	28.63	40	0.697	0	29.28	40	29.57
	4.97	35	30.03	0.14	0.706	30	26.58	35	0.691	0	27.14	35	27.42
	4.97	30	25.03	0.17	0.702	30	24.31	30	0.682	0	24.83	30	25.11
	4.97	25	20.03	0.20	0.699	30	21.89	25	0.671	0	22.30	25	22.59
	4.97	20	15.03	0.25	0.693	30	19.14	20	0.655	0	19.47	20	19.58
	4.97	15	10.03	0.33	0.684	30	15.95	15	0.630	0	16.21	15	16.46
d=10cm	9.87	60	50.13	0.17	0.702	30	68.30	60	0.682	0	70.24	60	69.84
	9.87	50	40.13	0.20	0.699	30	61.51	50	0.671	0	63.09	50	62.85
	9.87	40	30.13	0.25	0.693	30	53.78	40	0.655	0	55.08	40	55.05
	9.87	35	25.13	0.29	0.689	30	49.49	35	0.644	0	50.65	35	50.67
	9.87	30	20.13	0.33	0.684	30	44.84	30	0.630	0	45.83	30	45.90
	9.87	25	15.13	0.40	0.678	30	39.73	25	0.610	0	40.53	25	40.65
	9.87	20	10.13	0.50	0.666	30	33.75	20	0.582	0	34.56	20	34.62

Table 5.12 Comparison Table for USACE (1977)

	USACE						Novel Formula				Numeric Sol.	
	β°	D (cm)	C	L (cm)	H_{eff} (cm)	Q (lt/s)	Hc (cm)	Cg*Ct	Xs (cm)	Q(lt/s)	H (cm)	Gauge (lt/s)
d=10cm	57.33	9.67	0.671	30	56.49	67.02	60	0.700	15.42	72.09	60	71.67
	57.33	9.67	0.671	30	46.49	60.80	50	0.693	15.42	65.09	50	64.74
	57.33	9.67	0.671	30	36.49	53.86	40	0.682	15.42	57.29	40	56.55
	57.33	9.67	0.671	30	31.49	50.04	35	0.674	15.42	53.00	35	52.71
	57.33	9.67	0.671	30	26.49	45.89	30	0.664	15.42	48.35	30	48.15
	57.33	9.67	0.671	30	21.49	41.33	25	0.651	15.42	43.27	25	43.05
	57.33	9.67	0.671	30	16.49	36.21	20	0.633	15.42	37.60	20	37.47
d=14cm	62.77	13.64	0.673	30	54.10	92.09	60	0.678	15.42	97.71	60	96.48
	62.77	13.64	0.673	30	44.10	83.14	50	0.667	15.42	87.68	50	86.79
	62.77	13.64	0.673	30	34.10	73.11	40	0.650	15.42	76.47	40	75.87
	62.77	13.64	0.673	30	29.10	67.54	35	0.638	15.42	70.26	35	69.90
	62.77	13.64	0.673	30	24.10	61.46	30	0.623	15.42	63.52	30	63.24
	62.77	13.64	0.673	30	19.10	54.72	25	0.603	15.42	56.10	25	56.79

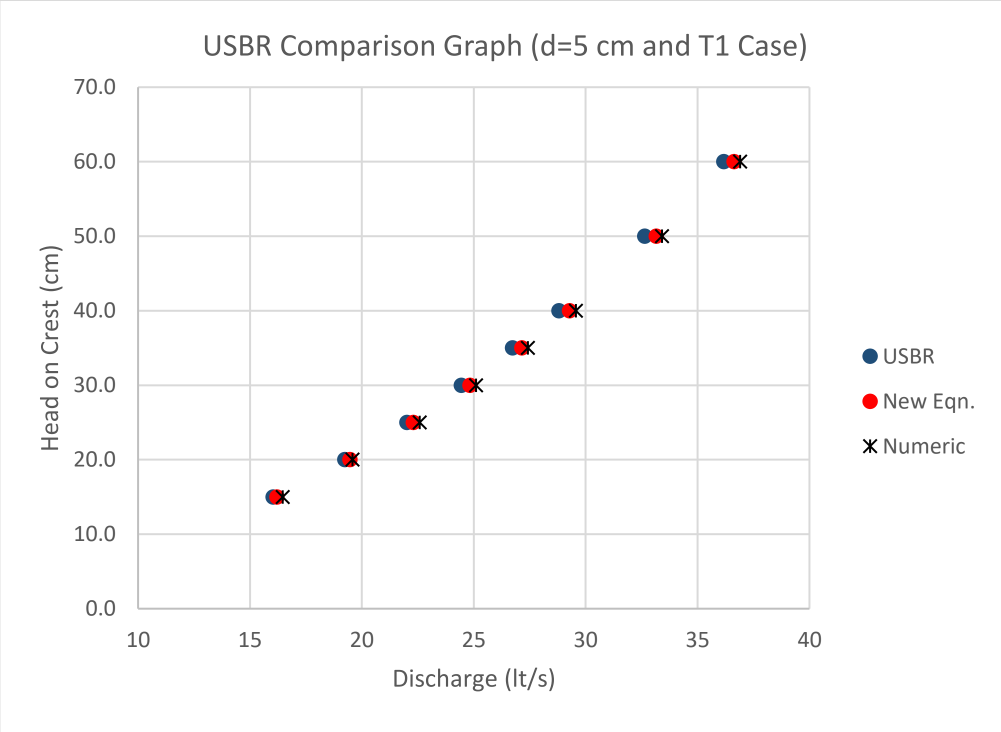

Figure 5.10 Comparison of USBR and the Suggested Equation

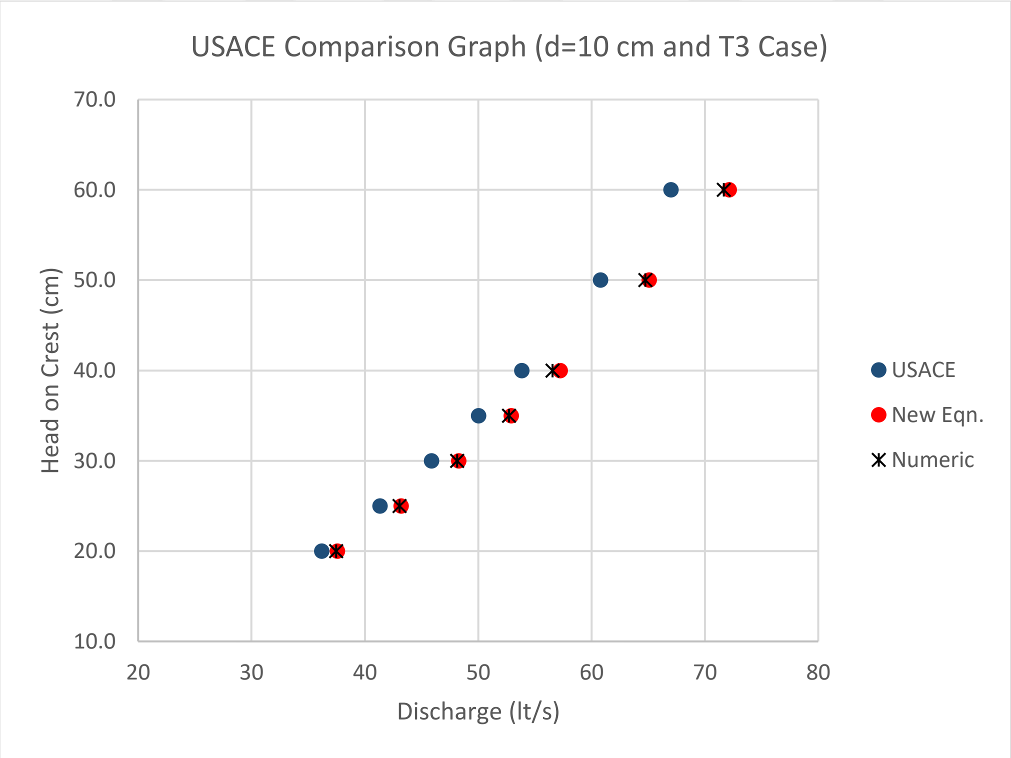

Figure 5.11 Comparison of USACE and the Suggested Equation

CHAPTER 6

CONCLUSIONS

The point of departure of this work was the problem of poor discharge estimation of widely used empirical equations on radial-gated spillways. As a research method, actual discharge was experimentally and numerically determined for a variety of gate configurations and upstream heads. On the basis of the findings listed below, a new discharge equation involving three independent and meaningful parameters, H_c, X_s and d, was developed from a set of data obtained numerically. Experimental results were excluded from the derivation since they are limited in number and belong only to the original setup. At the end, a sample discharge calculation was made with old empirical formulas and the novel equation, and more satisfactory results with lower error percentage were obtained with the new formula as a result of their comparison with numerical solutions.

Findings:

1) Experimentally and numerically found discharges on the radial-gated spillway are consistent with each other.

2) $(d/H_c)^{0.5}$ is a significant parameter according to the numerical investigation, and discharge coefficient can be formulated with only this number in case the gate seat is at apex of the spillway.

3) As the radial gate is shifted towards downstream, flow rate gradually increases provided that total upstream head and vertical gate opening remain same, which can also be mathematically expressed.

4) In case of the third article, gated flow turns into free flow at relatively upper stages.

5) Results of the two-dimensional and the three-dimensional numerical analyzes agree with each other (Pointed-nosed piers are considered). Therefore, solely 2D models of radial -gated spillway is favorable for numerical computation of discharge.

6) USACE (1977) is an inadequate method since its significant parameter, β, is strongly dependent upon elevation of the trunnion point whereas USBR (1960) is not valid when gate seat is planned at slightly downstream.

7) Turbulence models programmed on Flow-3D are not able to predict scale effect: It interprets the model and the prototype in the same way (RNG, LES and Laminar were tested).

Future Studies

1) Effect of spillway geometry should be investigated in detail by modifying inclination of upstream weir and downstream slope individually. An additional correction factor may be introduced to Equation 5.3.

2) Discharge characteristic at transition region and transient head should be determined at different geometric conditions.

3) Combination of several gates and asymmetrical flow conditions do not take place in this study and should be studied in future.

It is strongly advised that designer should be aware of the limitations of the discharge equation selected from the literature and choose the appropriate one suitable to handled radial gate-spillway configuration. Otherwise, it is no surprising to get erroneous discharge values. The suggested equation is subjected to some constraints as well and should be implemented accordingly.

REFERENCES

U.S. Bureau of Reclamation (USBR). (1960). Design of small dams, U.S. Government Printing Office, Washington, D.C.

U.S. Army Engineer Waterways Experiment Station. (1977). Hydraulic Design criteria (Vol. 1).

U.S. Army Engineer Waterways Experiment Station. (1977). Hydraulic Design criteria (Vol. 2).

U. S. Bureau of Reclamation (USBR). (1987). Design of Small Dams, United Stated Department of the Interior, 3rd Edition, Washington DC.

Sinniger R. O. and Hager W. H. (1989). Constructions Hydrauliques, Presses Polytechnique Romanades, pp 197-201

Mazumdar, S. K., and Roy, I. D. (1997). Orifice flow in a gated spillway. ISH Journal of Hydraulic Engineering, 3(2), 44-52.

Hussain, S., Hussain, A. and Ahmad, Z. (2014). Discharge characteristics of orifice spillway under oblique approach flow. Vol (39). pp. 9-18

Schohl, G. (2016). Discharge Correlations for Spillways with Radial Gates. In B. Crookston & B. Tullis (Eds.), Hydraulic Structures and Water System Management. 6th IAHR International Symposium on Hydraulic Structures, Portland, OR, 27-30 June (pp. 641-651). doi:10.15142/T3410628160853 (ISBN978-1-884575-75-4).

Shayan, H. K., Farhoudi, J., Aminpour, Y., Seyedzadeh, A., Roshan, R. and Vatankhah, A. (2017). Effective parameters for calculating the discharge of spillway with radial gates at large dams. doi:10.3217/978-3-85125-564-5-042.

Haktanır, T., and Khalaf, M. A. (2020). Discharge Coefficients for Radial-Gated Ogee Spillways by Laboratory Data and by Design of Small Dams. Teknik Dergi, 32(4).

Wikimedia Foundation. (2021, April 27). Tainter gate. Wikipedia. https://en.wikipedia.org/wiki/Tainter_gate.

Sayın, B. (2018, January 23). Lower Kaleköy Dam and Hydroelectric Power Plant [Pdf]. ANKARA: TEMELSU.

Tokyay, N. D. (2019). Middle East Technical University CE 473 Lecture Notes. Lecture.

Electromagnetic flow meter. Q&T Instrument Co.,Ltd. (2019). https://www.qtinstrument.com/product/electromagnetic-flow-meter.

APPENDICES

A. Error Percentages of the Suggested Equation

T1	Absolute Error (%)											
Hc (cm)	d=3cm	d=4cm	d=5cm	d=6cm	d=7cm	d=8cm	d=9cm	d=10cm	d=11cm	d=12cm	d=13cm	d=14cm	Average
60	0.02	1.10	0.71	0.07	0.43	1.05	0.05	0.59	0.68	1.27	1.75	1.96	0.81
50	0.24	1.00	0.75	0.16	0.63	0.82	0.13	0.40	0.36	0.96	1.34	1.40	0.68
40	0.33	0.88	0.96	0.36	0.74	0.83	0.37	0.08	0.48	0.59	0.88	0.94	0.62
35	0.35	0.85	0.98	0.49	0.89	0.47	0.47	0.02	0.45	0.35	0.63	0.61	0.55
30	0.43	0.73	1.06	0.54	0.94	0.30	0.53	0.11	0.36	0.09	0.33	0.39	0.48
25	0.51	0.68	1.23	0.63	1.00	0.33	0.57	0.25	0.21	0.31	0.12	0.09	0.49
20	0.54	0.68	0.50	0.67	1.02	0.13	0.43	0.12	0.59	0.22			0.49
15	0.64	0.77	1.48	0.42									0.83

T2	Absolute Error (%)											
Hc (cm)	d=3cm	d=4cm	d=5cm	d=6cm	d=7cm	d=8cm	d=9cm	d=10cm	d=11cm	d=12cm	d=13cm	d=14cm	Average
60	1.66	0.28	0.54	0.46	0.19	1.63	0.00	0.83	0.01	0.63	1.19	0.87	0.69
50	1.67	0.29	0.83	0.47	0.18	1.63	0.07	0.72	0.09	0.52	1.14	0.59	0.68
40	1.75	0.44	0.78	0.44	0.20	1.62	0.08	0.55	0.16	0.38	0.89	0.33	0.63
35	1.58	0.40	0.74	0.50	0.24	0.50	0.04	0.55	0.49	0.33	1.31	0.18	0.57
30	1.59	0.47	0.63	0.59	0.36	0.73	0.01	0.59	0.45	0.25	1.21	0.02	0.57
25	1.41	0.63	0.52	0.70	0.41	0.52	0.07	0.50	0.05	0.82	0.68	2.12	0.70
20	1.27	0.79	0.30	0.93	0.72	0.98	0.26	1.08	0.20	3.00			0.95
15	0.76	1.09	0.23	1.43									0.88

T3	Absolute Error (%)											
Hc (cm)	d=3cm	d=4cm	d=5cm	d=6cm	d=7cm	d=8cm	d=9cm	d=10cm	d=11cm	d=12cm	d=13cm	d=14cm	Average
60	1.82	0.52	0.20	0.06	0.06	0.20	0.20	0.61	1.25	1.85	0.02	1.36	0.68
50	1.98	0.65	0.13	0.25	0.25	0.14	0.22	0.56	1.16	1.72	0.12	1.13	0.69
40	2.01	0.75	0.25	0.38	0.38	0.04	0.12	1.34	0.99	1.73	0.26	0.91	0.76
35	2.01	0.70	0.21	0.40	0.40	0.07	0.35	0.57	0.92	1.50	0.22	0.66	0.67
30	1.99	0.76	0.27	0.35	0.35	0.20	0.30	0.46	0.90	1.42	0.58	0.61	0.68
25	2.05	0.75	0.13	0.37	0.37	0.18	0.35	0.55	0.91	1.18	0.28	1.01	0.68
20	1.75	0.62	0.07	0.11	0.11	0.31	1.27	0.39	0.99	1.80			0.74
15	1.07	0.18	0.55	0.52	0.52								0.57

T4	Absolute Error (%)											
Hc (cm)	d=3cm	d=4cm	d=5cm	d=6cm	d=7cm	d=8cm	d=9cm	d=10cm	d=11cm	d=12cm	d=13cm	d=14cm	Average
60	2.71	2.54	3.26	0.20	0.07	1.41	1.26	1.99	2.05	2.43	1.40	1.90	1.77
50	3.02	2.67	3.59	0.40	0.32	1.24	1.06	1.80	1.87	1.89	1.19	1.65	1.73
40	3.28	3.03	3.91	0.66	0.48	0.94	0.87	1.57	1.66	2.00	0.99	1.44	1.74
35	3.43	3.07	3.91	0.75	0.56	0.86	0.80	1.51	1.56	1.87	0.91	1.28	1.71
30	3.49	3.11	4.05	0.92	0.57	0.91	0.79	1.52	1.52	1.79	0.78	1.04	1.71
25	3.39	3.28	3.93	0.80	0.43	1.07	0.91	1.57	1.56	1.69	0.04	1.53	1.68
20	2.67	2.21	3.23	0.00	0.38	1.68	1.45	1.36	0.16				1.46
15	0.27	3.75	0.53	2.55									1.77

B. Mesh Sensitivity Tables

Table B.1 Discharge Variation Depending on Mesh Refinement (d=5 cm)

d=5 cm (2D Analysis)				Grid Size			
				10 mm	5 mm	4 mm	3 mm
	Z_{cr} (cm)	Z_{res} (cm)	H_c (cm)	Q (lt/s)	Q (lt/s)	Q (lt/s)	Q (lt/s)
T1	25.0	85.0	60.0	39.57	37.32	36.90	37.02
	25.0	75.0	50.0	35.49	33.81	33.41	33.54
	25.0	65.0	40.0	31.35	29.93	29.57	29.61
	25.0	60.0	35.0	29.13	27.77	27.42	27.48
	25.0	55.0	30.0	26.69	25.43	25.11	25.20
	25.0	50.0	25.0	23.94	22.86	22.59	22.64
	25.0	45.0	20.0	20.92	19.62	19.38	19.71
	25.0	40.0	15.0	17.37	16.58	16.46	16.42

Table B.2 Discharge Variation Depending on Mesh Refinement (d=10 cm)

d=10 cm (2D Analysis)				Grid Size			
				10 mm	5 mm	4 mm	3 mm
	Z_{cr} (cm)	Z_{res} (cm)	H_c (cm)	Q (lt/s)	Q (lt/s)	Q (lt/s)	Q (lt/s)
T1	25.0	85.0	60.0	75.24	69.84	70.41	68.79
	25.0	75.0	50.0	67.26	62.85	63.39	61.92
	25.0	65.0	40.0	59.28	55.05	55.50	54.24
	25.0	60.0	35.0	54.45	50.67	51.12	49.95
	25.0	55.0	30.0	49.32	45.90	46.32	45.30
	25.0	50.0	25.0	43.59	40.65	41.01	40.11
	25.0	45.0	20.0	36.99	34.62	34.92	34.14
	25.0	40.0	15.0	-	-	-	-

C. Model-Scale Effect with Different Turbulence Models

Table C.1 Model Discharges and Reynolds Numbers with LES (L_r=1/30)

Model (d=0.12 m) - LES					*Converted Discharge (m^3/s)*	*Re*
	Z_{cr} (m)	Z_{res} (m)	H_c (m)	Q (m^3/s)		
T1	0.25	0.85	0.60	0.08220	***404.9***	264 734
	0.25	0.75	0.50	0.07388	***363.9***	237 939
	0.25	0.65	0.40	0.06411	***315.8***	206 473
	0.25	0.60	0.35	0.05886	***289.9***	189 565
	0.25	0.55	0.30	0.05313	***261.7***	171 111
	0.25	0.50	0.25	0.04689	***231.0***	151 014
	0.25	0.45	0.20	0.03957	***194.9***	127 440

Table C.2 Prototype Discharges and Reynolds Numbers with LES

Prototype (d=3.6 m) - LES					*Re*
	Z_{cr} (m)	Z_{res} (m)	H_c (m)	Q (m^3/s)	
T1	7.5	25.5	18.0	***405.3***	43 510 467
	7.5	22.5	15.0	***362.4***	38 904 992
	7.5	19.5	12.0	***316.2***	33 945 250
	7.5	18.0	10.5	***290.4***	31 175 523
	7.5	16.5	9.0	***262.3***	28 158 884
	7.5	15.0	7.5	***231.6***	24 863 124
	7.5	13.5	6.0	***195.3***	20 966 184

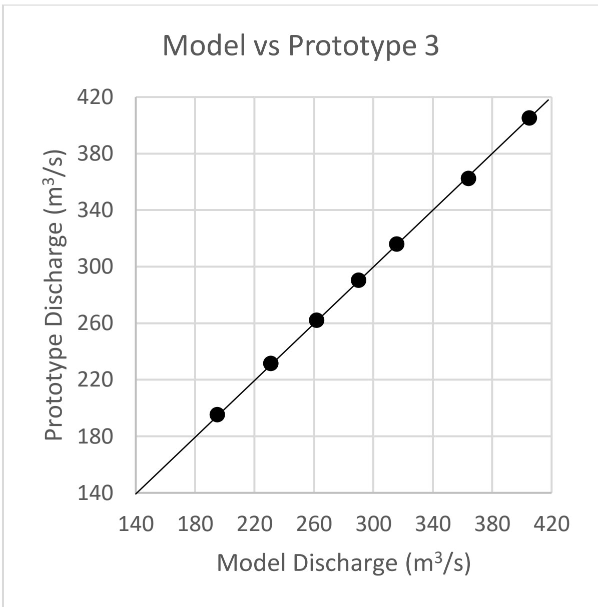

Figure C.1 Comparison of Model and Prototype Discharges with LES (L_r=1/30)

Table C.3 Model Discharges and Reynolds Numbers with Laminar (L_r=1/30)

Model (d=0.12 m) - Laminar					*Converted Discharge (m³/s)*	*Re*
	Z_{cr} (m)	Z_{res} (m)	H_c (m)	Q (m³/s)		
T1	0.25	0.85	0.60	0.08202	***404.0***	264 155
	0.25	0.75	0.50	0.07368	***362.9***	237 295
	0.25	0.65	0.40	0.06429	***316.7***	207 053
	0.25	0.60	0.35	0.05928	***292.0***	190 918
	0.25	0.55	0.30	0.05352	***263.6***	172 367
	0.25	0.50	0.25	0.04713	***232.1***	151 787
	0.25	0.45	0.20	0.03984	***196.2***	128 309

Table C.4 Prototype Discharges and Reynolds Numbers with Laminar

Prototype (d=3.6 m) - Laminar					*Re*
	Z_{cr} (m)	Z_{res} (m)	H_c (m)	Q (m³/s)	
T1	7.5	25.5	18.0	***404.1***	43 381 643
	7.5	22.5	15.0	***363.3***	39 001 610
	7.5	19.5	12.0	***317.1***	34 041 868
	7.5	18.0	10.5	***291.3***	31 272 142
	7.5	16.5	9.0	***263.1***	28 244 767
	7.5	15.0	7.5	***231.6***	24 863 124
	7.5	13.5	6.0	***196.4***	21 084 273

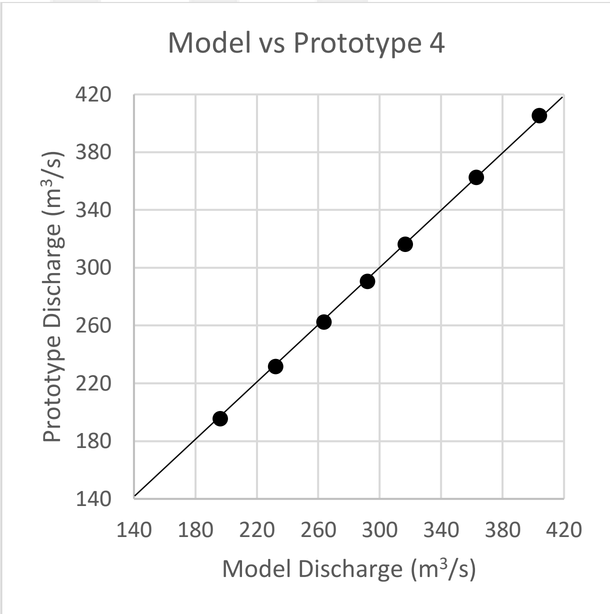

Figure C.2 Comparison of Model and Prototype Discharges with Laminar (L_r=1/30)

Table C.5 Model Discharges and Reynolds Numbers with RNG (L_r=1/100)

Model (d=0.024 m) - RNG					*Converted Discharge (m³/s)*	*Re*
	Z_{cr} (m)	Z_{res} (m)	H_c (m)	Q (m³/s)		
T1	0.075	0.255	0.180	0.002784	***278.4***	8923
	0.075	0.225	0.150	0.002512	***251.2***	8090
	0.075	0.195	0.120	0.002209	***220.9***	7114
	0.075	0.180	0.105	0.002039	***203.9***	6567
	0.075	0.165	0.090	0.001855	***185.5***	5974
	0.075	0.150	0.075	0.001663	***166.3***	5356
	0.075	0.135	0.060	0.001422	***142.2***	4580

Table C.6 Prototype Discharges and Reynolds Numbers with RNG

Prototype (d=2.4 m) – RNG					*Re*
	Z_{cr} (m)	Z_{res} (m)	H_c (m)	Q (m³/s)	
T1	7.5	25.5	18.0	***279.3***	29 983 897
	7.5	22.5	15.0	***252.1***	27 066 023
	7.5	19.5	12.0	***223.0***	23 938 808
	7.5	18.0	10.5	***206.0***	22 109 501
	7.5	16.5	9.0	***187.5***	20 128 824
	7.5	15.0	7.5	***167.0***	17 932 367
	7.5	13.5	6.0	***143.9***	15 452 496

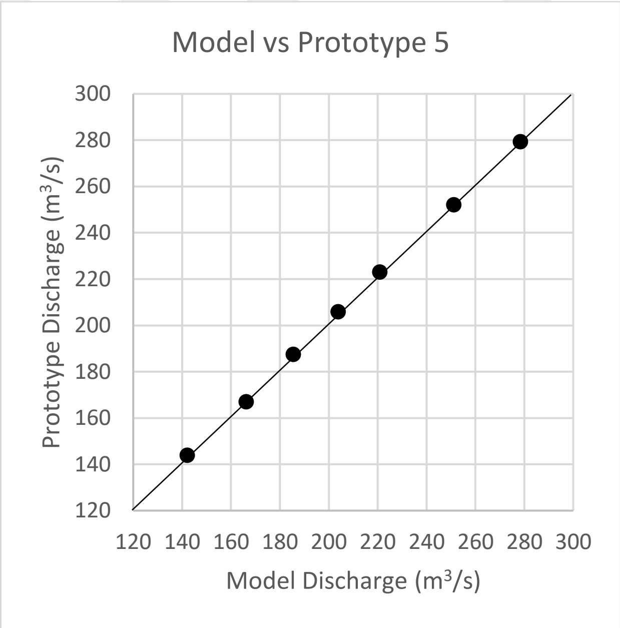

Figure C.3 Comparison of Model and Prototype Discharges with RNG (L_r=1/100)

D. Relative Position of the Gate in Different Configurations

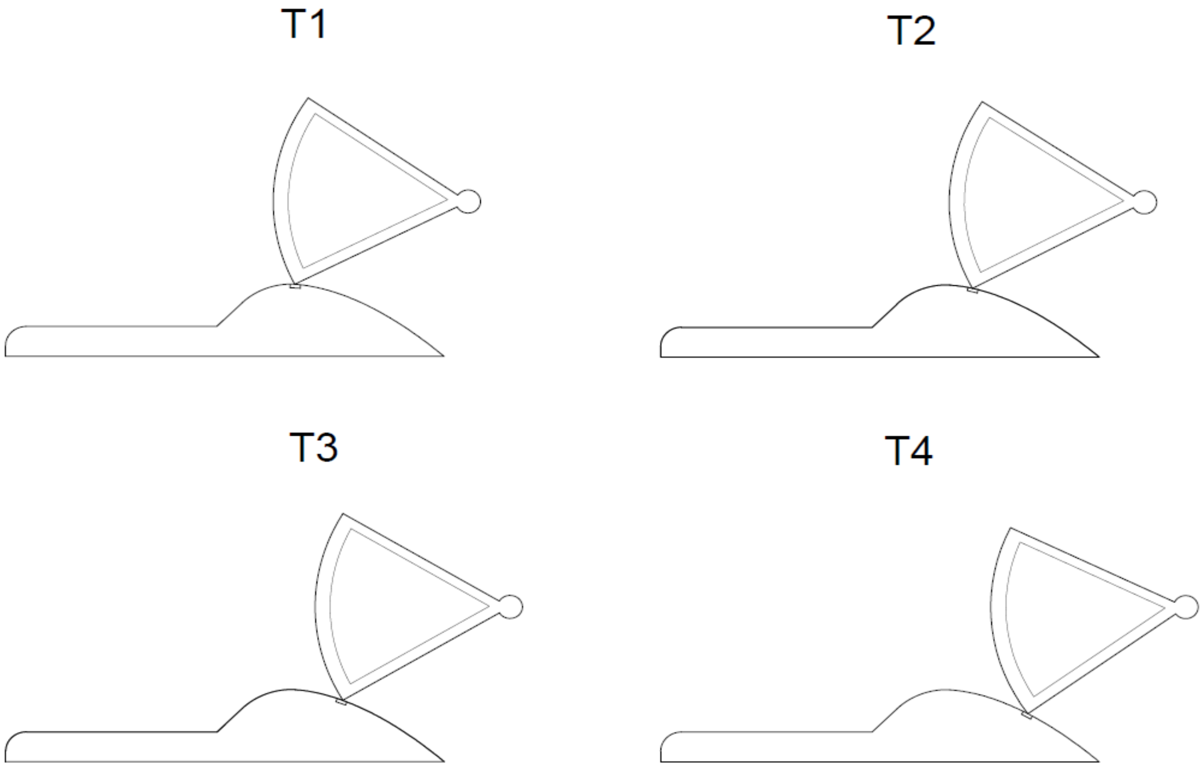

E. Numerical Results for the Other Gate Positions

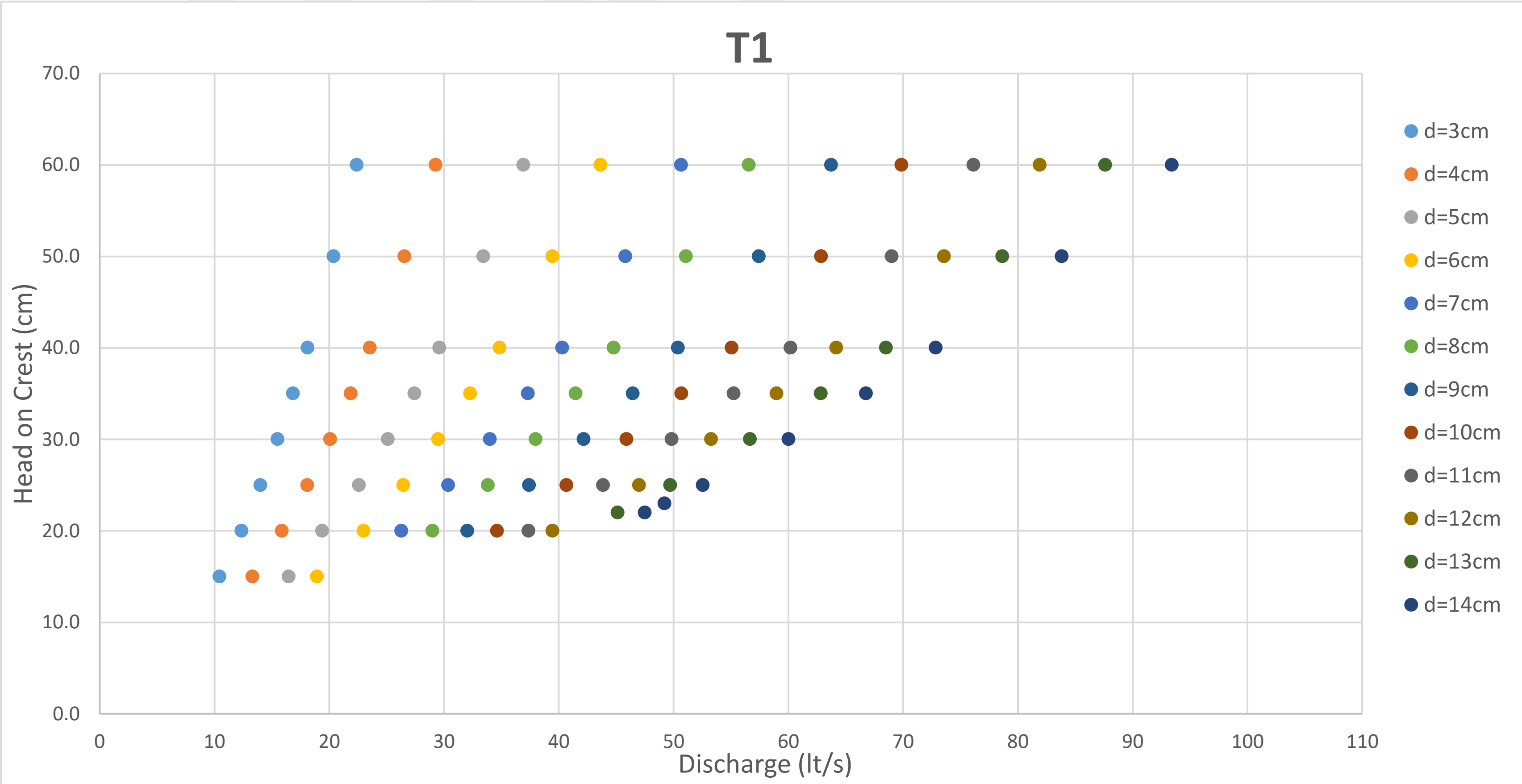

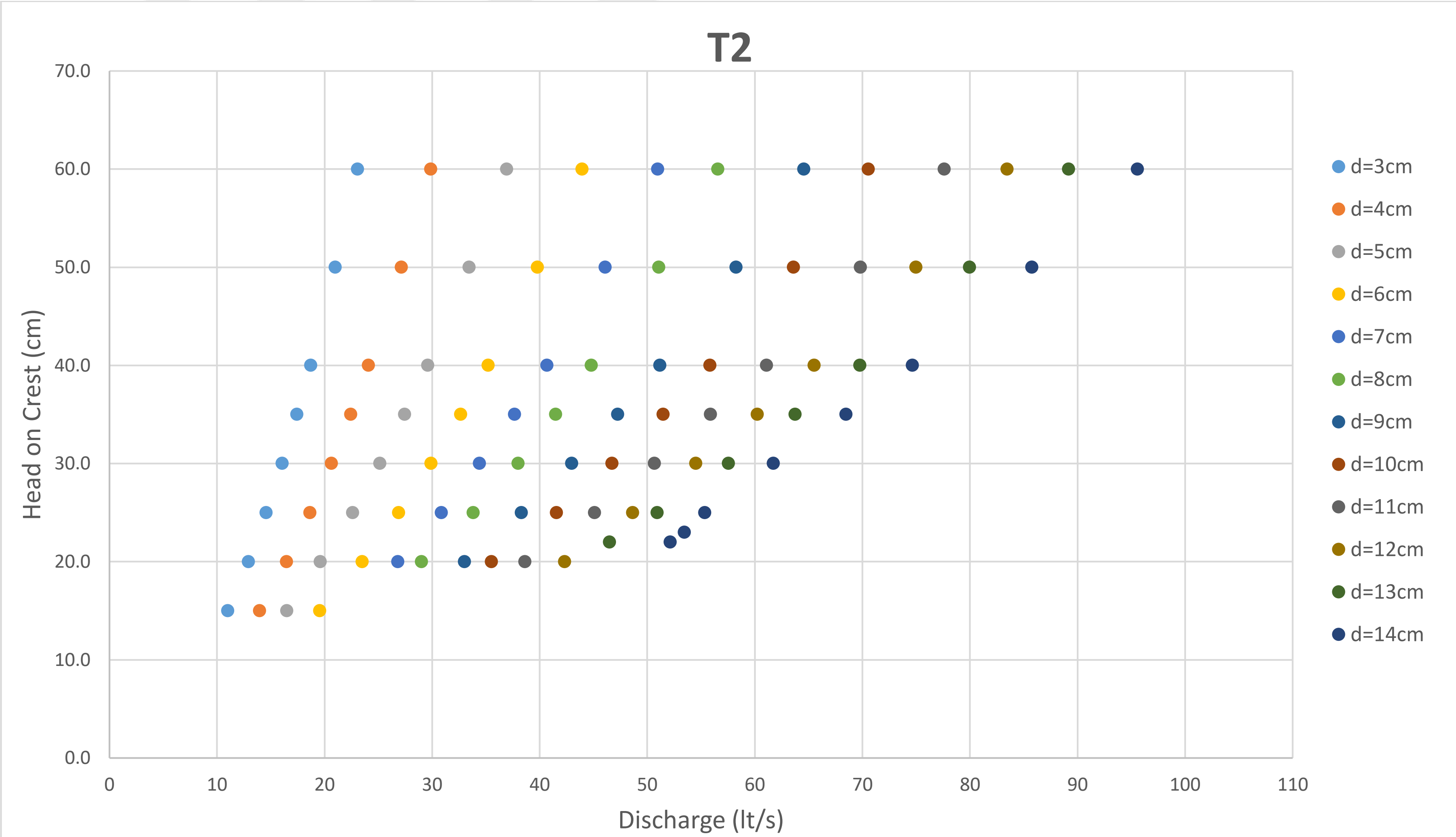
T2
Head on Crest (cm)
70.0
60.0
50.0
40.0
30.0
20.0
10.0
0.0
0
10
20
30
40
50
60
70
80
90
100
110
Discharge (lt/s)
d=3cm
d=4cm
d=5cm
d=6cm
d=7cm
d=8cm
d=9cm
d=10cm
d=11cm
d=12cm
d=13cm
d=14cm

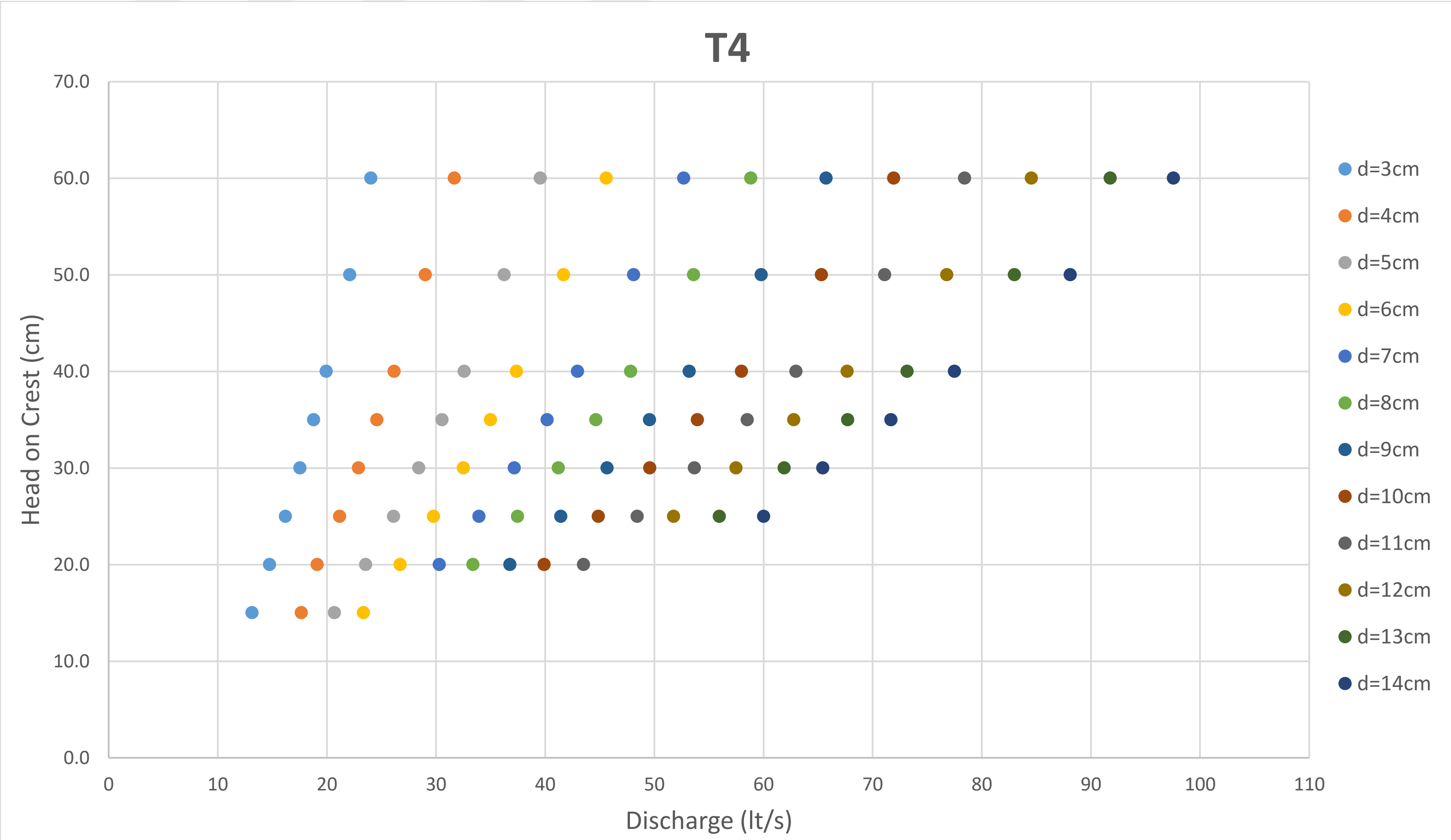
T4
Head on Crest (cm)
Discharge (lt/s)
70.0
60.0
50.0
40.0
30.0
20.0
10.0
0.0
0
10
20
30
40
50
60
70
80
90
100
110
d=3cm
d=4cm
d=5cm
d=6cm
d=7cm
d=8cm
d=9cm
d=10cm
d=11cm
d=12cm
d=13cm
d=14cm